

## TABLE OF CONTENTS

<b>Estimation of the long-term cyclical fluctuations of snow-rain floods in the Danube basin within Ukraine</b> Tetiana ZABOLOTNIA, Liudmyla GORBACHOVA, Borys KHRYSYTIUK	3
<b>Multi-annual variability of global solar radiation in the agricultural area of Lower Silesia (SW Poland) and its relationship with the North Atlantic Oscillation</b> Krystyna BRYŚ, Tadeusz BRYŚ	13
<b>Sensitivities of the Tiedtke and Kain-Fritsch Convection Schemes for RegCM4.5 over West Africa</b> Mojisola Oluwayemisi ADENIYI	27
<b>Water vapor induced airborne rotational features</b> Roman MARKS	39
<b>Learning to cope with water variability through participatory monitoring: the case study of the mountainous region, Nepal</b> Santosh REGMI, Jagat K. BHUSAL, Praju GURUNG, Zed ZULKAFI, Timothy KARPOUZOGLOU, Boris Ochoa TOCACHI, Wouter BUYTAERT, Feng MAO	49
<b>Long-term seasonal characterization and evolution of extreme drought and flooding variability in northwest Algeria</b> Kouidri SOFIANE, Megnounif ABDESSELAM, Ghenim Abderrahmane NEKKACHE	63
<b>Homogeneous regionalization via L-moments for Mumbai City, India</b> Amit Sharad PARCHURE, Shirish Kumar GEDAM	73
<b>After COP24 Conference in Katowice – the role of the Institute of Meteorology and Water Management – National Research Institute in connection of hydrological and meteorological measurements and observations with climate change adaptation actions</b> Marta BARSZCZEWSKA, Ksawery SKĄPSKI	85



## Estimation of the long-term cyclical fluctuations of snow-rain floods in the Danube basin within Ukraine

Tetiana Zabolotnia, Liudmyla Gorbachova, Borys Khrystiuk

*Ukrainian Hydrometeorological Institute, Prospekt Nauki 37, 03028 Kyiv, Ukraine, e-mail: tzabolotnia@gmail.com, gorbachova@uhmi.org.ua, khryst@uhmi.org.ua*

**Abstract.** Floods are a periodic natural phenomenon, often accompanied by negative consequences for the local population and the economy as a whole. Therefore, knowledge of the trends of maximum flow have great practical importance, because it is the basis for planning and designing various hydraulic structures, hydrological forecasting, the mapping of flood risk, etc. In this paper, we analysed the long-term cyclical fluctuations of the maximum flow of snow-rain floods of the Danube basin within Ukraine (5 large rivers, 14 medium and 5 small). The database includes time series (34 gauging stations) of the maximum discharges of the cold period from the beginning of the observations up to 2015. The methodological approaches (developed by Gorbachova) are based on the use of hydro-genetic methods – namely the mass curve, the residual mass curve, and combined graphs. The presented results illustrate that the long-term fluctuations of the maximum flow of snow-rain floods are synchronous at all study gauging stations in the Danube basin within Ukraine, but these fluctuations are not always in the synchronous phase. We found that the maximum flow of snow-rain floods in the Danube basin within Ukraine have four types of long-term fluctuations, each with a different cycle duration.

**Keywords:** cyclical fluctuations, stationarity, homogeneity, snow-rain flood, synchronicity, mountain rivers

**Submitted** 13 December 2017, **revised** 24 April 2018, **accepted** 14 November 2018

### 1. Introduction

The long-term cyclical fluctuations of streamflow mean that there are instabilities in the streamflow, characterised by alternating wet and dry phases of different durations and different degrees of deviation from the mean of the long-term flow for the review period (Pekarova et al. 2003). The periods of wet years change to dry, and vice versa. In closely located river basins, under the same climatic conditions and similar elements of the geographical landscape, the streamflow fluctuations are usually synchronous. However, as was found in our previous studies (Gorbachova, Bauzha 2012, 2013; Gorbachova, Khrystiuk 2014; Bauzha, Gorbachova 2017), in the case of the synchronous fluctuations of flow, it is often observed that there is asynchronicity in the phase of fluctuations in the various hydrological stations within the same basin.

In the study of the spatio-temporal fluctuations of water flow, a variety of methods are used. Both statistical and genetic methods are more commonly used (WMO 2009). Among the statistical methods, the most frequently used are correlation, regression, cluster, dispersion, and spectral analysis. The genetic method consists of the graphic methods that mainly include various correlation graphs, frequency of values, histograms, mass curves, double mass curves, residual mass curves, chronological

charts, and others (Chow et al. 1988). The methodical approaches to using these methods were developed by Rippl (1883), Merriam (1937), Searcy and Hardison (1960), and others. The guidelines for these methods were developed separately for each method and for solving particular problems. However, with certain graphic (hydro-genetic) methods, we can successfully carry out the assessment of the spatio-temporal fluctuations of runoff. Therefore, in this paper, the methodological approaches for the hydro-genetic methods are used. This approach was developed by Gorbachova (2014, 2015).

In this paper, the maximum flow of the cold period of the Danube River basin (Ukrainian part) was investigated. The study of the current spatio-temporal fluctuations in the dangerous phase of the hydrological regime of this river is our actual task, because snow-rain floods of varying heights repeat 3-8 times a year in the mountain rivers of the Danube basin within Ukraine. These floods are especially dangerous in the wet phase that is caused by global atmospheric circulation. In the wet phase, significant floods are observed predominantly with 3-4 and 6-8 year recurrence intervals. At the same time, Central and Western Europe also suffer from these natural disasters (Susidko, Luk'yanets 2009; Pekarova et al. 2014). Thus, such studies are important for hydrological and water

management calculations. The goal of this paper is the study of the long-term cyclicity fluctuations of maximum flow of the snow-rain floods of the Danube basin within Ukraine based on the use of hydro-genetic methods.

The main tasks of the research are as follows:

- assessment of the spatio-temporal fluctuations of the maximum flow of the snow-rain floods of the Danube Basin within Ukraine;
- analysis of the phases of cyclical fluctuations of the maximum discharges;
- assessment of the stationarity of the observation series with residual mass curves;
- estimation of the homogeneity of the observation series with the mass curves;
- analysis of the largest and smallest maximum discharge of the snow-rain floods of the Danube basin within Ukraine for a long-term period.

## 2. The study area

The Danube River is the second largest water course in Europe (after the Volga River), with a total catchment area of 817 000 km<sup>2</sup>. It is the world's most international river basin and includes the territories of 19 countries (including Romania, Hungary, Austria, Serbia, Germany, Slovakia, and Bulgaria) (Pekarova et al. 2003). The river originates in the central-western part of Europe (Schwarzwald), runs through the central part of the continent, crosses the Pannonian Depression to the confluence with the Drava, then pierces the Carpathian Mountains through the Iron Gate Gorge. Farther down, it separates the southern part of the Romanian Plain from the Prebalkan Tableland, and the eastern part of the Plain from the Dobrogea Plateau and Mountains. The last sector of the river, up to the Black Sea, encompasses the Delta area (Gastescu, Tuchiuc 2012). The Danube River has a total length of 2 857 km,

Table 1. Characteristics of rivers of the Danube River Basin

Name of river	Catchment area [km <sup>2</sup> ]	Catchment area [km <sup>2</sup> ] (within Ukraine)
Danube	817 000	32 350
Tysa	153 000	11 300
Siret	47 600	2 070
Prut	27 500	17 400
Latorytsya	7 680	4 900
Uzh	2 750	2 010

and approximately one third of its basin is mountainous. The Danube Basin can be subdivided into three main parts (the Upper, Central and Lower Danube regions), in addition to the Danube delta (Pekarova et al. 2014). Within Ukraine, the Danube River flows only in its lower part, with a length of 174 km (6% of the total length), and the catchment area is 32 350 km<sup>2</sup> (Table 1). It occupies the southern and south-eastern slopes of the Eastern Carpathians, Transcarpathia, and the southwestern outskirts of the Black Sea Lowland.

In this paper, the main rivers and their tributaries in the Danube Basin within Ukraine are investigated (Fig. 1). These are 5 large rivers (Tysa, Prut, Latorytsya, Uzh, and Cheremosh) ( $F_{basin} = 1\ 000\text{--}10\ 000\text{ km}^2$ ), 14 medium rivers (Siret, Chornyi Cheremosh, Teresva, Bilyi Cheremosh, Rika, Putyla, Turia, Borzhava, Chorniava, Vicha, Stara, Chorna Tysa, Bila Tysa, and Kosivska) ( $F_{basin} = 100\text{--}1\ 000\text{ km}^2$ ), and 5 small rivers (Iltzia, Holiatyinka, Pylypets, Studenyi, and Kamianka) ( $F_{basin} = 10\text{--}100\text{ km}^2$ ) according to the classification of the EU Water Framework Directive (2000/60/EC). Such a classification was carried out according to the area of the catchment of the river from river springs to locking post within Ukraine.

The Tysa River Basin is the largest sub-basin in the Danube Basin (Table 1). It is also the Danube's longest tributary (966 km). In the territory of Ukraine, there is the upper, mostly right bank part of the Tysa basin.

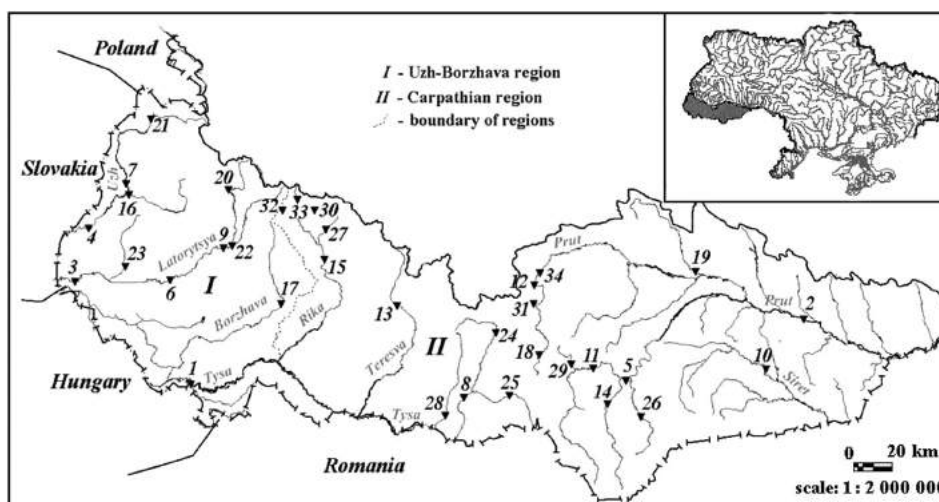


Fig. 1. Location of the 34 water gauges in the Danube basin within Ukraine (the numbering of stations is based on Table 2)

The river at the upper part is a typical mountain river. It has a narrow valley, and it sometimes looks like a gorge with relatively steep slopes. The right bank tributaries of the Tysa River cover the southern slope of the Ukrainian Carpathians. The average altitudes of these catchments within the mountains are 800-1200 m, and the average slopes are 200-400 m/km. The long-term average water discharge near Vylok village is  $207 \text{ m}^3 \text{ s}^{-1}$  (1954-2013).

The Prut River is a left tributary of the Danube (Table 1). The river springs from the northeastern slope of the Chornohora Massif at an altitude of approximately 1600 m. The basin of the Prut River, being a transboundary basin, is located in the territory of three countries (Moldova, Ukraine, and Romania). The average slope of the catchment in the upper reaches is 285 m/km, whereas it is much smaller in the lower reaches. The average meandering ratio is 2.1. The largest tributary of the Prut River is the Cheremosh River. The long-term average water discharge near Chernivtsi city is  $67.7 \text{ m}^3 \text{ s}^{-1}$  (1945-2013).

The Siret River is a left tributary of the Danube, starting from the confluence of the Bursuky and Lustun mountain sources next to Dolysnyi Shepit village in Chernivtsi Oblast (Table 1). In its upper section (to the Beregomet settlement), it is a typical mountain river, but downstream it gains submountain and lowland features with a wide valley, which is swampy in some places. The Siret flows into the Black Sea. In the upper part, it flows through the territory of Ukraine (110 km) and then Romania (596 km). The general fall is 435 m. The slope of the river is 4.4 m/km. The meandering ratio is 1.92. The long-term average water discharge near Storozhynets town is  $6.63 \text{ m}^3 \text{ s}^{-1}$  (1953-2013).

The Latorytsya River is a left tributary of the Bodrog River (tributary of the Tysa River) (Table 1). The river springs from the Ukrainian Carpathians (Eastern Carpathian Mountains) near the village Latorka. It flows from Ukraine (156.6 km) to Slovakia (31.4 km). Its slope varies from 80 m/km in the upper reaches to 0.2 m/km in the lower reaches. The long-term average water discharge near Chop town is  $35.9 \text{ m}^3 \text{ s}^{-1}$  (1957-2013).

The Uzh River is a left tributary of the Laborec River (tributary of the Latorytsya River) (Table 1). The river springs in the mountains in the northwest of Transcarpathia. It flows from Ukraine (107 km) to Slovakia (26 km). The slope of the river is 7.2 m/km. The long-term average water discharge near Uzhhorod city is  $29.3 \text{ m}^3 \text{ s}^{-1}$  (1947-2013).

The temperature regime in the Danube basin is determined mainly by the nature of the circulation of air masses and the features of the terrain. The long-term average annual air temperature within the Ukrainian part

of the basin is  $8.1^\circ\text{C}$  for the Chernivtsi weather station and  $9.6^\circ\text{C}$  for the Uzhhorod weather station. The coldest month is January, with average temperatures ranging from  $-0.3$  to  $-3^\circ\text{C}$  in the lowlands and  $-8$  to  $-9^\circ\text{C}$  at the highest points, and in some places even lower. In July, the average air temperatures rise to  $17$ - $24^\circ\text{C}$  (Pekarova et al. 2014). The long-term annual average precipitation total at the Uzhhorod weather station is 785 mm, and it is 652 mm at the Chernivtsi weather station.

The Ukrainian Carpathians are characterised by significant heterogeneity of the territory, which results in different conditions of flow formation. Thaws are observed in the mountain rivers of the Carpathians due to the unstable thermal regime and frequent transitions in the winter period from negative to positive air temperatures in December to February. During these thaws, a flow of mixed origin (from the melting of snow and liquid precipitation) is formed. In this case, high floods occur, which are characterised by the highest water discharges per year in the long-term period. Sometimes, such floods become catastrophic and threaten not only the economy of the region but also human life. The Carpathians are the region with the most danger of flooding in all of Ukraine (Susidko, Luk'yanets 2009).

According to hydrological regionalisation by the intra-annual distribution of the flow, the Tysa, Prut and Siret Rivers within Ukraine belong to two hydrological regions, namely the Uzh-Borzhava and Carpathian regions (Gorbachova 2015). For the rivers of the Carpathian region (the upper reaches of the Tysa River to the Rika River, including the Prut and Siret rivers), the wet period lasts from March to July, the autumn period is characterised by floods, and winter is characterised by the smallest discharges in the year. The rivers of the Uzh-Borzhava region are characterised by intense floods in the cold period of the year. Thus, the lowest discharges are observed from August to October.

### 3. Methodology and data

Available and reliable flood observation data help to improve understanding of flood processes and associated changes in flood characteristics and regimes (Hall et al. 2015). The analysis of the cyclicity of water flow depends on the availability of long-term observation data. The longer the duration of the observation series, the more it is possible to reliably determine the decrease and increase in the phases of cyclic fluctuations of water flow for each river.

This study of the long-term fluctuations of the maximum flow of snow-rain floods is conducted at 34 gauging

Table 2. List of selected water gauges along the Danube River Basin within Ukraine

No.	River	Water gauge	Catchment area [km <sup>2</sup> ]	Study period
1	Tysa	Vylok village	9140	1954-2015
2	Prut	Chernivtsi city	6890	1895-1911, 1919-1924, 1926-1935, 1945-2015
3	Latorytsya	Chop town	2870	1957-2015
4	Uzh	Uzhhorod city	1970	1947-2015
5	Cheremosh	Usteriky village	1500	1958-2015
6	Latorytsya	Mukachevo town	1360	1947-2015
7	Uzh	Zaricheve village	1280	1947-2015
8	Tysa	Rahiv city	1070	1947-2015
9	Latorytsya	Svaliava town	680	1962-2015
10	Siret	Storozhynets town	672	1953-2015
11	Chorny Cheremosh	Verhovyna village	657	1958-2015
12	Prut	Yaremche town	597	1950-2015
13	Teresva	Ust-Chorna village	572	1949-1976, 1978-1982, 1986-2015
14	Bilyi Cheremosh	Yablunytzia village	552	1958-2015
15	Rika	Mizhhiria village	550	1946-2015
16	Turia	Simer village	464	1958-2015
17	Borzhava	Dovhe village	408	1947-2015
18	Prut	Tatariv village	366	1959-2015
19	Chorniava	Lyubkivtsi village	333	1985-1989, 1991, 1993-1997, 1999-2007, 2009-2015
20	Latorytsya	Pidpolozzia village	324	1947-2015
21	Uzh	Zhornava village	286	1952-2015
22	Vicha	Nelipyne village	241	1958-2015
23	Stara	Zniatseve village	224	1952-2015
24	Chorna Tysa	Yasinia village	194	1956-2015
25	Bila Tysa	Luh village	189	1955-2015
26	Putyla	Putyla village	181	1963-1993, 1996-2015
27	Rika	Verhnii Bystryi village	165	1954-1994, 1999-2015
28	Kosivska	Kosivska Poliana village	122	1963-2015
29	Iltsia	Iltsi village	86.1	1959-2015
30	Holiatynka	Maidan village	86	1956-1994, 1999-2015
31	Prut	Vorohta village	48.3	1978-2015
32	Pylypets	Pylypets village	44.2	1956-2015
33	Studenyi	Nyzhnii Studenyi village	25.4	1954-1994, 1999-2015
34	Kamianka	Dora village	18.1	1946-2015

stations situated in the Danube River basin within Ukraine. The maximum discharges in the cold period are analysed in the study. The cold period is characterized by a steady decrease in air temperature below 0°C. During this period, the floods are of mixed origin, namely snow-rain (Kosovets et al. 2005). The maximum discharge data of the cold period are obtained from the archive of the Central Geophysical Observatory of Ukraine. The analyses are carried

out for the data series at all stations from the beginning of the observations to 2015 inclusive. The period of observation of these water bodies is from 27 (Chorniava River – Liubkivtsi village) to 104 (Prut River – Chernivtsi city) years (Table 2).

In terms of the hydro-genetic analysis, including concepts such as change and variability, the homogeneity and stationarity of the hydrological series were defined.

The homogeneity of the time series is the absence of unidirectional changes of the hydrological characteristic (this refers to one genetic series: floods, rain floods, etc.) over time against the backdrop of its variability due to long-term cyclical fluctuations. The stationarity of the time series is the constancy of average value hydrological characteristic over time if the time series has at least one full closed cycle (dry and wet phase) of long-period fluctuations. The change of the time series is the unilateral deviation from a straight line of the hydrological characteristic, which is in such a state that the hydrological characteristic moves to a new quality, due to the state of factors that are formed by the hydrological characteristic or human activities. The variability of the time series is a temporary deviation from a straight line of the hydrological characteristic that is in such a state that the hydrological characteristic acquires a new quality only for a period. In the case of long-term cyclical fluctuations, this period can last for decades; but at the same time, the hydrological characteristic from time to time returns to its “old” state. This same scenario is relevant for short-term cyclical fluctuations, but the period is much shorter and is usually considered to be a few years.

The assessment of the homogeneity and stationarity of the hydrological series necessitated the following:

- In the hydrological series, there is a need to restore the gaps in observations and bring them to a long time period, thus allowing the tracing of the temporal dynamics of hydrological characteristics over a longer time interval.
- The homogeneity of the hydrological characteristic over time is researched with a mass curve.
- The stationarity of the hydrological characteristic is researched with a residual mass curve.

To clarify the results obtained (if necessary), other hydro-genetic methods and approaches can be used (the analysis of meteorological factors of the runoff formation, the combined graphics, etc.)

For the assessment of the homogeneity of the observation series, the mass curve was used. In 1883 Rippl developed the mass curve and the residual mass curve methods. Now, the mass curve is used to detect the influence of anthropogenic factors (hydraulic structures, canals) and of climate change (the presence of trends in the data series). If “jumping” on the mass curve is not found, and neither are “emissions” or unidirectional deviation, then the generation of runoff in the study area is homogeneous, and vice versa. The mass curve is defined with the following formula:

$$W = \sum_{t=1}^T w(t) \quad (1)$$

where:  $W$  – the total runoff of the river for time period  $T$ ;  $w(t)$  – the runoff of  $t$ th year.

For the assessment of the spatio-temporal fluctuations of the maximum flow of the snow-rain floods of the Danube basin within Ukraine, the residual mass curve and combined graphs were used. The analysis of the residual mass curve allows the definition of the stationarity of data series, namely the sustainability of the average value of the hydrological characteristic in the course of time. The average value of the time series is stable in the presence of at least one full closed cycle (dry and wet phase) of long-period fluctuations. The residual mass curve is defined according to (Andreyanov 1959):

$$f(t) = \frac{\sum_{t=1}^T (k(t) - 1)}{C_v} \quad (2)$$

where:  $C_v$  – the variation coefficients of runoff;  $k(t) = Q(t)/Q_0$  – the modulus coefficients;  $Q(t)$  and  $Q_0$  – the discharge of the  $t^{\text{th}}$  year and the average discharge for the period of time  $T$ .

According to Andreyanov’s formula (2), the dry and wet phases were identified. The wet phase is characterized by an increasing tendency, and the dry phase is characterized by a decreasing tendency.

Combined graphs of characteristics allow the definition of the synchrony/asynchrony of long-term fluctuations in different rivers within the one hydrologically homogeneous area. In turn, the synchronous fluctuations are indicated on the homogeneous climatic conditions for the formation of runoff.

#### 4. Results

Graphs of the mass curves and residual mass curves of the maximum flow of the snow-rain floods in the Danube Basin within Ukraine were created for 34 catchments.

The analysis of these graphs shows that the series of observations are homogeneous, because no significant points of fracture in direction (“jumpings” or unidirectional deviation) were found on any mass curves (Gorbachova, Bauzha 2012, 2013; Bauzha, Gorbachova 2017). Examples of such curves are shown in Figure 2.

Some of these may raise doubts about the homogeneity of the hydrologic characteristics, e.g., the observation series in Figure 2c. However, the shape of the sum curve is determined by the structure of the observation series, namely the presence of only phases of prolonged increase and decrease in the cyclical fluctuations (Fig. 3).

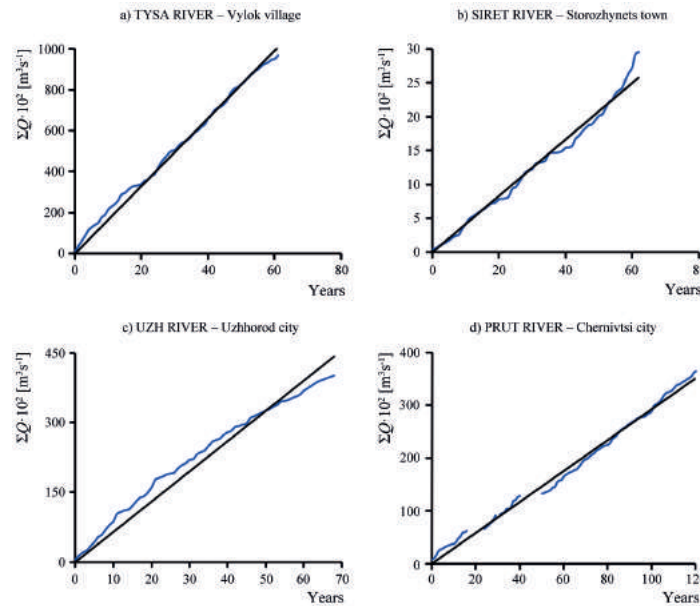


Fig. 2. Some mass curves of the maximum flow of snow-rain floods in the Danube River basin within Ukraine

Such a situation is temporary. With the extension of the duration of observations, the data series will have several phases of cyclical fluctuations. For example, the mass curve looks similar to that in Figure 2d for the gauging station Prut River – Chernivtsi city. The observation series at the gauging station Prut river – Chernivtsi city is the longest and has several decreasing and increasing phases of long-term cyclical fluctuations. The durations of full cycles are approximately 15-20 years (Fig. 3). Therefore, the observation series of the maximum flow of snow-rain floods in the Danube Basin within Ukraine are homogeneous and quasi-homogeneous.

An analysis of the stationarity of the maximum flow of snow-rain floods of the Danube River Basin and its cyclical fluctuations was carried out using the residual mass curves of the data series of 34 gauging stations. According to the analysis, these curves have similar and distinctive features in their configuration. The long-term fluctuations of the maximum flow at all gauging stations are synchronous, but they are not always in synchronous phase (Fig. 4).

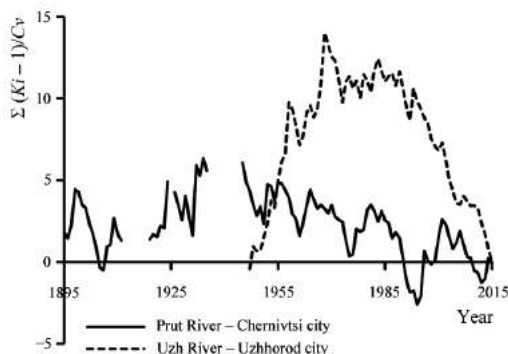


Fig. 3. The residual mass curves of the maximum flow of snow-rain floods in the Danube River basin within Ukraine

Thus, several types of cyclical fluctuations were identified (Fig. 5). The first type of long-term cyclical fluctuations includes the observations series that have only two phases: decreasing and increasing. Such fluctuations in the maximum flow of snow-rain floods are characteristic of the Uzh River. The increase phase began from the beginning of the observation and continued until 1968. The decrease phase began after 1968 and continues to this day (Fig. 5a). For some rivers in other basins, which can also be attributed to the first type of fluctuation (e.g., the Holyatynka river – Maidan village, and the Turia River – Simer village), the increasing phase continued until 1989 (Fig. 5a).

The second type of cyclical fluctuation includes the observation series, which are characterized by an increasing phase from the beginning of the observations to the end of the 1960s. After this, such phases changed to the decreasing

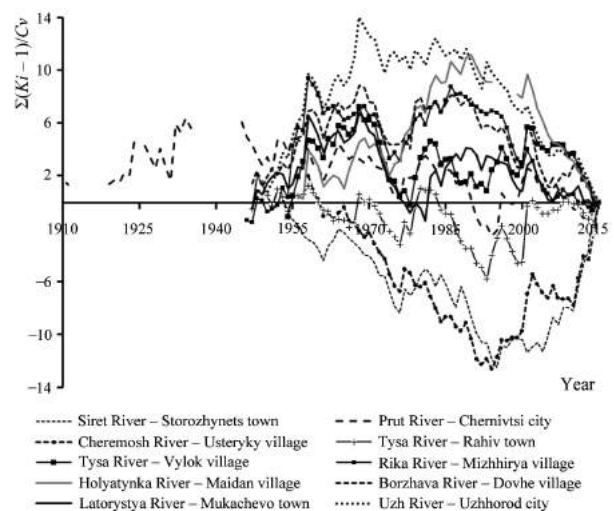


Fig. 4. Some residual mass curves of the maximum flow of snow-rain floods in the Danube River Basin within Ukraine

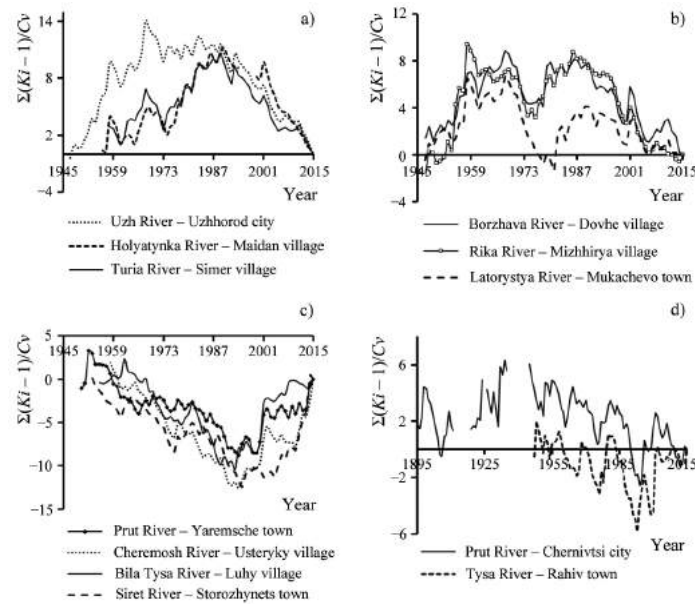


Fig. 5. Types of long-term cyclic fluctuations of the maximum flow of snow-rain floods in the Danube River Basin within Ukraine

phase, which continued until the mid-1970s. The increasing phase began again after the 1970s and continued until the mid-1980s, and it has since then changed to the decreasing phase of cyclical fluctuations. This type of fluctuation is seen in such rivers as Latorysya, Borzhava, and Rika (Fig. 5b).

The third type of fluctuations includes the rivers that, from the beginning of the observation and until the mid-1990s, are characterized by the decreasing phase. After this, the phase changed to the increasing phase, with minor variations in some years. This type of fluctuation is seen in the rivers Upper Tysa, Siret and Upper Prut (Fig. 5c).

The fourth type of fluctuations includes the rivers Tysa and Prut, which have cyclic fluctuations of 15-20 year duration. On Figure 5d, it is seen that the long-term cyclical fluctuations at the gauging stations Tysa River – Vylok village and Prut River – Chernivtsi city have synchronous and in-phase fluctuations.

Generally, the observation series of the maximum flow of snow-rain floods in the Danube Basin within Ukraine are characterised by synchronous fluctuations, which do not always have synchronous phases. It can be assumed that the differences in cyclic fluctuations are caused by factors of the underlying surface of the river basins – namely:

- 1) The mountain relief, which is significantly cut by river valleys (defines peculiar patterns of runoff formation, which manifest in the uneven distribution of precipitation, temperature and humidity in the basin).
- 2) Exposure of slopes (the windward slopes receive considerably more rainfall).
- 3) The presence of large forest areas.

Table 3 provides information on the largest and smallest maximum discharge of the cold period of the year of the 34 water gauges along the Danube River Basin

within Ukraine for long-term periods. During the study period, the largest values of the maximum discharge of snow-rain floods ( $3580 \text{ m}^3 \text{ s}^{-1}$ ) were observed for the water gauges on the Tysa River – Vylok village in 2001. This value is 2.3 times higher than the long-term average of the maximum water discharge (1954-2015). It was the largest flood over the entire observation period (historical flood), and it had catastrophic consequences because it resulted in the loss of human lives and significant economic damage (Boiko, Kulbida 2001).

In general, the maximum runoff of the cold period over the past 10 years is characterised by a decreasing trend in most of the study gauges (Fig. 5a, b, d), with the exception of some hydrological stations (Siret River – Storozhynets town, Cheremosh River – Usteryky village, Iltzia River – Iltzi village, Prut River – Yaremche town, Prut River – Tatariv village, Bila Tysa River – Luhy village, Chorny Cheremosh – Verhovyna village, Putyla River – Putyla village, and Kamianka River – Dora village) (Fig. 5c).

## 5. Conclusion

The study presents results from time-series analyses using hydro-genetic methods for maximum discharges of snow-rain floods in the Danube Basin within Ukraine. The observation series of the maximum flow have different types of long-term cyclic fluctuations. In total, four types of fluctuations were determined, and they are conditioned by the climatic and the orographic features of the research area. Each type of cyclic fluctuation is characterised by a different duration. Only for the rivers Prut and Tysa can the duration of fluctuations be reliably

Table 3. The largest and the smallest of the maximum discharge [ $\text{m}^3 \text{s}^{-1}$ ] of the cold period of the year of the Danube Basin within Ukraine for long-term periods

River	Water gauge	$Q_{\text{average}}$ [ $\text{m}^3 \text{s}^{-1}$ ]	$Q_{\text{max. cold period}}$ [ $\text{m}^3 \text{s}^{-1}$ ] (per year)	
			max	min
Tysa	Vylok village	207 (1954-2013)	3580 (2001)	302 (1973)
Tysa	Rahiv city	25.6 (1947-2013)	938 (2001)	15.4 (1987)
Chorna Tysa	Yasinia village	4.83 (1956-2013)	186 (2001)	5.50 (1963)
Bila Tysa	Luhv village	5.11 (1955-2013)	84 (2001)	5.44 (1969)
Borzhava	Dovhe village	11.0 (1947-2013)	411 (1979)	26.4 (1972)
Kosivska	Kosivska Poliana village	4.60 (1963-2013)	213 (2001)	4.48 (1984)
Teresva	Ust-Chorna village	18.3 (1949-2013)	665 (2001)	22.2 (1963)
Siret	Storozhynets town	6.63 (1953-2013)	195 (2014)	2.69 (1990)
Prut	Chernivtsi city	67.7 (1945-2013)	1316 (1932)	46.2 (1990)
Prut	Vorohta village	1.98 (1978-2013)	82.6 (2001)	2.18 (1991)
Prut	Tatariv village	8.01 (1960-2013)	126 (2001)	13 (1991)
Prut	Yaremche town	12.6 (1950-2013)	299 (1952)	10.5 (1998)
Cheremosh	Usteriky village	27.8 (1958-2013)	392 (2001)	26.3 (1991)
Bilyi Cheremosh	Yablunytzia village	9.38 (1958-2013)	120 (2001)	8.85 (1991)
Chorni Cheremosh	Verhovyna village	14.1 (1958-2013)	219 (2001)	8.05 (1991)
Iltsia	Iltsi village	1.66 (1959-2013)	51.2 (2014)	1.84 (1991)
Kamianka	Dora village	0.36 (1949-2013)	22.6 (2011)	0.17 (1946)
Putyla	Putyla village	2.57 (1963-2013)	74.4 (2012)	1.59 (1974)
Chorniava	Lyubkivtsi village	1.67 (1985-2013)	85.1 (1996)	1.21 (1991)
Latorytsya	Mukachevo town	26.4 (1962-2013)	1480 (1958)	64.1 (1972)
Latorytsya	Pidpolozzia village	9.27 (1947-2013)	537 (1958)	44.2 (2003)
Latorytsya	Svaliava town	14.7 (1962-2013)	540 (1967)	34.4 (1973)
Latorytsya	Chop town	35.9 (1957-2013)	653 (1968)	66.5 (2015)
Vicha	Nelipyne village	6.87 (1958-2013)	249 (1958)	18.6 (1973)
Stara	Zniatseve village	2.27 (1952-2013)	54.7 (1974)	9.0 (2014)
Uzh	Uzhhorod city	29.3 (1947-2013)	1680 (1958)	108 (1973)
Uzh	Zhornava village	6.63 (1952-2013)	284 (1958)	30.9 (1961)
Uzh	Zaricheve village	21.0 (1947-2013)	1210 (1958)	92.8 (1973)
Turia	Simer village	9.26 (1958-2013)	427 (1958)	22.8 (1973)
Rika	Verhnii Bystryi village	4.17 (1954-2013)	142 (1958)	16.2 (2003)
Rika	Mizhhiria village	13.7 (1946-2013)	735 (1958)	54 (1946)
Holiatynka	Maidan village	2.16 (1956-2013)	100 (1958)	7.87 (1961)
Pylypets	Pylypets village	1.44 (1958-2013)	57.1 (1958)	4.74 (2003)
Studenyi	Nyzhnii Studeniyi village	0.61 (1954-2013)	62.6 (1986)	1.54 (1961)

determined, because they have several full cycles of fluctuations. The duration of the cycles on their tributaries and the Siret River will be specified with the extension of the observation series, because such data have incomplete increase and decrease phases of long-term cyclic fluctuations. The observation series of the maximum flow of snow-rain floods in the Danube Basin within Ukraine are characterised by synchronous fluctuations, which do not always have synchronous phases. In general, the maximum runoff of the cold period over the past 10 years was

characterised by fluctuation and has a decreasing trend at most of the study gauges. Some hydrological stations are an exception. Because the results of the analysis of changes of river flow depend on the availability and length of long-term data series, there is a need to continuously carry out estimation of the long-term cyclical fluctuations of the maximum runoff of rivers. This will allow the discovery of new tendencies in fluctuations and the making of forecasts for the future, because the Danube River Basin within Ukraine is characterised by dangerous flood activity.

## Bibliography

- 2000/60/EC, Directive of the European Parliament and of the Council of 23 October 2000 establishing a framework for Community action in the field of water policy, EUR-Lex
- Andreyanov V.G., 1959, Cyclical fluctuations of annual runoff and their account at hydrological calculations, (in Russian), Proceedings of Russian State Hydrological Institute, 68, 3-49
- Bauzha T., Gorbachova L., 2017, The features of the cyclical fluctuations, homogeneity and stationarity of the average annual flow of the Southern Buh River Basin, Annals of Valahia University of Targoviste. Geographical Series, 17 (1), 5-17, DOI: 10.1515/avutgs-2017-0001
- Boiko V., Kulbida M., 2001, Hydrological analysis of high snow-rain flood in Transcarpathia in March 2001 and problems of operational forecasting, (in Ukrainian), Hydrology, Hydrochemistry and Hydroecology, 2, 272-278
- Chow V.T., Maidment D.R., Mays L.W., 1988, Applied hydrology, McGraw-Hill, 572 pp.
- Gâştescu P., Ţuchiu E., 2012, The Danube River in the Pontic sector – hydrological regime, [in:] Water resource and wetlands. Conference Proceedings, P. Gâştescu, W. Lewis Jr., P. Breţcan (eds.), Tulcea, Romania, 13-26
- Gorbachova L., 2014, Methodical approaches the assessment of the homogeneity and stationarity of hydrological observation series, (in Ukrainian), Hydrology, Hydrochemistry and Hydroecology, 5 (32), 22-31
- Gorbachova L., 2015, Place and role of hydro-genetic analysis among modern research methods runoff, (in Ukrainian), Proceedings of Ukrainian Hydrometeorological Institute, 268, 73-81
- Gorbachova L., Bauzha T.O., 2012, The reasons of the instationarity of the seasonal runoff of rivers and streams in the Rika River basin, [in:] Water resource and wetlands. Conference Proceedings, P. Gâştescu, W. Lewis Jr., P. Breţcan (eds.), Tulcea, Romania, 209-214
- Gorbachova L., Bauzha T., 2013, Complex analysis of stationarity and homogeneity of flash flood maximum discharges in the Rika River basin, Energetika, 59 (3), 167-174, DOI: 10.6001/energetika.v59i3.2708
- Gorbachova L., Khrystyuk B., 2014, Hydro-genetic methods of the analysis of the average annual runoff in the Danube basin, [in:] Proceeding of the XXVI conference of the Danubian countries on hydrological forecasting and hydrological bases of water management. Bridging the sciences – crossing borders, 22-24 September 2014, Deggendorf, Germany, 71-74
- Hall J., Arheimer B., Aronica G.T., Bilibashi A., Boháč M., Bonacci O., Borg, M., Burlando P., Castellarin A., Chirico G.B., Claps P., Fiala K., Gaál L., Gorbachova L., Gül A., Hannaford J., Kiss A., Kjeldsen T., Kohnová S., Koskela J.J., Macdonald N., Mavrova-Guirguinova M., Ledvinka O., Mediero L., Merz B., Merz R., Molnar P., Montanari A., Osuch M., Parajka J., Perdigão R.A.P., Radevski I., Renard B., Rogger M., Salinas J.L., Sauquet E., Šraj M., Szolgay J., Viglione A., Volpi E., Wilson D., Zaimi K., Blöschl G., 2015, A European Flood Database: facilitating comprehensive flood research beyond administrative boundaries, Proceedings of the International Association of Hydrological Sciences, 370, 89-95, DOI: 10.5194/piahs-370-89-2015
- Merriam C.F., 1937, A comprehensive study of the rainfall on the Susquehanna Valley, Transactions American Geophysical Union, 18 (2), 471-476
- Kosovets O.O., Kulbida M.I., Babichenko V.M. (eds.), 2005, Climatic Cadastre of Ukraine, (in Ukrainian), Central Geophysical Observatory, 85-104
- Pekarova, P., Miklanek, P., Pekar, J., 2003, Spatial and temporal runoff oscillation analysis of the main rivers of the world during the 19th–20th centuries. Journal of Hydrology, 274, 62-79, DOI: 10.1016/S0022-1694(02)00397-9.
- Pekarova P., Miklanek P., Melo M., Halmova D., Pekar J., Bacova Mitkova V., 2014, Flood marks along the Danube River between Passau and Bratislav, Veda, Slovak Committee for Hydrology, Bratislava, 102 pp.
- Rippl W., 1883, The capacity of storage reservoirs for water supply, Proceedings of the Institute of Civil Engineers, 71, 270-278. DOI: 10.1680/imotp.1883.21797
- Searcy J.K., Hardison H.C., 1960, Double-mass curves. Manual of hydrology: Part 1. General surface-water techniques, Geological Survey Water-Supply Paper 1541-B, United States Government Printing Office, 36 pp.
- Susidko M.M., Luk'yanets O.I., 2009, The Carpathians – flood danger region of Ukraine. Basin runoff forecasting system in Zakarpattia: methodical and technological basis of its components, Nika-Centre, Kyiv, 88 pp.
- WMO, 2009, Guide to hydrological practices. Volume II: Management of water resources and application of hydrological practices, WMO-No. 168, World Meteorological Organization, Geneva



## Multi-annual variability of global solar radiation in the agricultural area of Lower Silesia (SW Poland) and its relationship with the North Atlantic Oscillation

Krystyna Bryś

*Wrocław University of Environmental and Life Sciences, The Faculty of Environmental Engineering and Geodesy, Grunwaldzka 55, 50-357 Wrocław, Poland, e-mail: krystyna.brys@upwr.edu.pl*

Tadeusz Bryś

*Polish Geophysical Society, Wrocław Division, Plac Grunwaldzki 24, 50-363 Wrocław, Poland, e-mail: tbrys@o2.pl*

**Abstract.** In this paper, the long-term variability of global solar radiation in the agricultural area of Lower Silesia is analyzed based on a 56-year long (1961-2016) measurement series recorded at the Agro- and Hydro-meteorological Wrocław-Swojec Observatory (SW Poland). Yearly and monthly global radiation sums with their extreme and mean values were compared with radiation data from Warsaw (Central Poland) and Potsdam (East Germany). The dynamics of variability between consecutive months, seasons and years was also taken into account. The conducted positive trends show a significant increase in the investigated global radiation sums for Lower Silesia and also for Central Poland and the eastern part of Germany. The trends are strongly related to long-term macro-circulation changes in the North Hemisphere, particularly with the phases and sub-phases of the North Atlantic Oscillation (NAO). The relations between the investigated values of global solar radiation and these macro-circulation patterns are very complicated and they very often have an asynchronous character. The first, juvenile stage of the NAO positive phase (the 1970s and 1980s), when annual sums of global solar radiation in Wrocław-Swojec reached only the average level of about  $3\,700\text{ MJ}\cdot\text{m}^{-2}$  and warm half-year about  $2\,800\text{ MJ}\cdot\text{m}^{-2}$  respectively, was cloudy and rainy. This period was distinctly different than the advanced stage of one (the 1990's and later years) with bigger sunshine duration and smaller annual precipitation, when the adequate radiation sums amount to  $3\,900\text{--}4\,000\text{ MJ}\cdot\text{m}^{-2}$  and  $3\,000\text{--}3\,100\text{ MJ}\cdot\text{m}^{-2}$  respectively.

**Keywords:** global radiation, multi-annual variability, climate change, NAO

**Submitted** 5 February 2018, **revised** 28 August 2018, **accepted** 30 January 2019

### 1. Introduction

The increasingly widespread use of sustainable sources of clean energy, such as solar energy, which is an alternative of fossil fuels, calls for a comprehensive nationwide identification of such resources. Detailed analysis, taking into consideration the varying volume and dynamics of the resources on both a regional and local scale, is needed, particularly in the context of climate change. Such analysis is possible for the agricultural area of the Lower Silesia region due to the availability of multi-annual data obtained from measurements of global radiation. The present paper is a continuation of the previous studies of the authors (e.g. Bryś 2006, 2007, 2013, 2015, 2017; Bryś, Bryś 2002, 2003, 2007), with an attempt to determine the parameters and dynamics of the solar features of the climate of Lower Silesia based on radiation trends in Poland.

Past studies on the solar radiation variability in Poland have mainly been based on sunshine duration data (Górski, Górka 2000; Koźmiński, Michalska 2005; Kuczmarzka,

Kuczmarzka 1998; Kuczmarzka 1990; Marciniak, Wójcik 1991; Matuszko 2009, 2014; Morawska-Horawska 1985, 2002; Podstawczyńska 2003, 2007; Podogrocki, Słomka 1993). The influence of circulation and climatic conditions on these distributions was presented in detail by Paszyński and Niedźwiedz (1991), Woś (1999, 2010), Kożuchowski et al. (2000).

A similar analysis for the south-western part of Poland, particularly the Wrocław and Sudety Mts., based on atmospheric circulation, was performed by Bryś (2007), Dubicka (1994, 1998), Dubicka and Karal (1994), Dubicka and Limanówka (1994), Dubicka and Mięgała (1997), Dubicka and Pyka (2001), Dubicka et al. (1995). The relationship between the structure of solar radiation and sunshine duration in Wrocław was presented by Bryś and Bryś (2003, 2007).

The temporal variability and spatial distribution of global solar radiation in Poland based on selected stations of the Polish actinometrical network for different years from the period of 1961-1995 were analyzed in the works

of Bogdańska and Podogrocki (2000), Podogrocki (1984, 1989, 2001, 2007). The study of the annual distribution of global radiation in Wrocław and its variability in the years 1961-1980 in relation to macro-circulation weather conditions was made by Dubicka (1994). The potential solar radiation resources of the Lower Silesia (SW Poland) as a source of the so-called clean energy was analyzed by Bryś (2006). The climatic and meteorological conditions necessary for the use of solar energy in Poland were presented by Podogrocki (1989, 2007).

Over the past few decades, many studies have pointed out the change of global solar trends, together with an alternation of radiation periods. Since the 1980s, the so-called period of “dimming”, characteristic for earlier decades of the twentieth century, has been displaced by a new “brightening” radiation period (Alpert et al. 2005; Norris, Wild 2007; Ohrvil et al. 2009; Sanchez-Lorenzo et al. 2007, 2017; Stanhill 2005, 2007; Stanhill, Cohen 2001, 2005; Stjern et al. 2009; Streets et al. 2006; Wild 2009; Wild et al. 2005, 2007, 2009). The research performed in Estonia (Russak 1987, 1990; Tooming 2002) and Russia (Abakumova et al. 1996; Abakumova, Bondarenko 2008) and prove that the changes are related both with long-term trends of cloudiness (Kleniewska et al. 2016; Matuszko 2009, 2012; Ohrvil et al. 2009; Stjern et al. 2009; Warren et al. 2007; Wibig 2003, 2004; Żmudzka 2007) and changes in air transparency (Ohrvil et al. 2009; Ruckstuhl, Norris 2009; Sun, Groisman 2000; Uscka-Kowalkowska 2008a, b, 2009, 2013). A great number of research papers point to the anthropogenic genesis of these changes (Ahrens 2008; IPCC 2013; Wibig 2009), yet many other accentuate the importance of natural source factors (Bryś 2005; Bryś, Bryś 2003; Jaworowski 2003, 2007; Kondratyev, Galindo 1997; Marsz 2005, 2010; Marsz, Styszyńska 2002, 2006, 2009; Ohrvil et al. 2009; Pisek, Brazdil 2006; Soon et al 1996). In this context, the key aim of this paper is the presentation of the multi-annual variability of global solar radiation in the agricultural area of Lower Silesia on a broad spatial background, in order to provide new arguments to the discussion on the observed long-term radiation changes in Europe and the North Hemisphere.

## 2. Materials and methods

The Agro- and Hydrometeorology Wrocław-Swojec Observatory (51°07'φN, 17°10'λE, 121 m a.s.l.) is located in the eastern peripheral, agricultural part of Wrocław (formerly: Breslau). The observatory is located on the side of watershed area, under the hydrological influence of floodwaters from the Odra and Widawa rivers. Such a location facilitates the neutralization of the urban heat island (UHI)

and accentuates the frequency of winds from the WNW-NW sector (Bryś 2007a, b). Due to its location and the features of the active area, which is characteristic for agricultural land in the Silesian Lowlands, the results of actinometrical measurements conducted in this area are representative for the eastern part of Wrocław-Magdeburg Ustromtal.

Since 1961, measurements of sunshine duration ( $S$ ) and global radiation ( $K\downarrow$ ) have been collected at the height of 1.5 m above ground level, over the lawn of the observatory. Detailed characteristics in terms of the instrumental and methodological approaches used here can be found in previous papers of the authors (Bryś 2006, 2007, 2013, 2015, 2017; Bryś, Bryś 2002, 2003, 2007), which point to circulation conditions and the influence of the cyclical magnetic activity of the sun (Wolf number) on the analyzed actinometrical data.

The research is based on the revised, continuous and homogenous 56-year long measurement series (1961-2016) of global radiation (Bryś 2017). The paper presents average and extreme (monthly, annual) values and variability of the analyzed radiation flux on a seasonal and yearly basis, as such dynamic aspects play an important role in climatological analysis. The paper also includes a comparative approach to respective data from Warsaw (1961-2015), as a relatively representative area for the central part of Poland<sup>1</sup> (Bogdańska, Podogrocki 2000; Podogrocki 2007), and Potsdam (1950-2016), as representative area for the eastern part of Germany<sup>2</sup>.

## 3. Measurement results and discussion

The course of global radiation  $K\downarrow$  in the period of 1961-2016 (Fig. 1) is marked by a strong positive trend, with the wave-like variability of the moving sums of 12- and 60-month periods. It only partly corresponds to a solar cyclicity of approximately 11-12 years of length, as the influence of the multiannual variability of circulation is prevalent. It is important to contrast the cloudy and rainy period of the 1970s and 1980s, when annual sums of  $K\downarrow$  reached only the average level of approximately 3 700 MJ·m<sup>-2</sup> compared to later years with smaller annual precipitation levels (Bryś, Bryś 2002; Bryś 2017), when the adequate radiation sums amount to 3 900-4 000 MJ·m<sup>-2</sup>. It is indicative that annual sums for sunshine duration in the first period reached the average level of 1 300 hrs, followed 1 600-1 700 hrs in the next period (Bryś 2015, 2017).

The extreme annual values of  $K\downarrow$  were recorded 8 or 12 years later than the respective values obtained for sunshine

<sup>1</sup> <http://wrdc.mgo.rssi.ru>

<sup>2</sup> <http://www.klima-potsdam.de/>

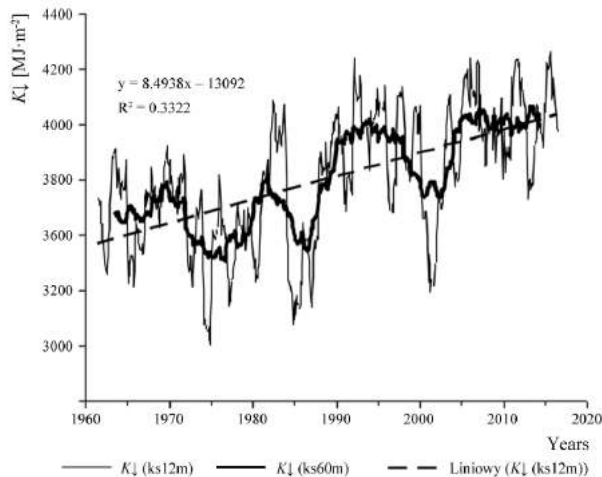


Fig. 1. The runs of 12- and 60-month (mean yearly values) moving sums (ks12m and ks60m) of global radiation  $K_{\downarrow}$  in Wrocław-Swojec in the years of 1961-2016 (Liniowy = Linear trend)

duration (Bryś 2015, 2017), which indicates the effect of circulation conditions on these differences, as well as a considerable independence of direct radiation from the global radiation. A minimum  $K_{\downarrow}$  ( $3257.3 \text{ MJ}\cdot\text{m}^{-2}$ , that is  $904.8 \text{ kWh}\cdot\text{m}^{-2}$ ) was recorded in 1974 (8 years later than the minimum  $S$ ). The first maximum ( $4246.7 \text{ MJ}\cdot\text{m}^{-2}$ , i.e.  $1179.6 \text{ kWh}\cdot\text{m}^{-2}$ ) was observed in 2015 (12 years later than the maximum  $S$ ), and the second maximum in magnitude ( $4227.1 \text{ MJ}\cdot\text{m}^{-2}$ , i.e.  $1174.2 \text{ kWh}\cdot\text{m}^{-2}$ ) in 2011 (8 years later than the maximum  $S$ ). The mean annual sum for the period (1971-2000) amounted to  $3751.6 \text{ MJ}\cdot\text{m}^{-2}$  (i.e.  $1042.1 \text{ kWh}\cdot\text{m}^{-2}$ ), while for the 50- and 56-year long periods, the sums were calculated as  $3773.6 \text{ MJ}\cdot\text{m}^{-2}$  and  $3802.9 \text{ MJ}\cdot\text{m}^{-2}$  (i.e.  $1048.2$  and  $1056.4 \text{ kWh}\cdot\text{m}^{-2}$ ), respectively.

For the purpose of determining the climate change influence on global radiation and solar energy resources in the Silesian Lowlands, it is important to consider the dynamics of radiation variability. The linear trend of global radiation in Wrocław-Swojec in the years of 1961-2016 (Fig. 1) shows a growth of annual  $K_{\downarrow}$  sums by  $407,8 \text{ MJ}\cdot\text{m}^{-2}$  (i.e.  $113.3 \text{ kWh}\cdot\text{m}^{-2}$ ) within 50 years and by  $457,7 \text{ MJ}\cdot\text{m}^{-2}$  (i.e.  $127.1 \text{ kWh}\cdot\text{m}^{-2}$ ) within 56 years.

For all seasons (Fig. 2), a significant positive trend of the 3-month sums of global radiation  $K_{\downarrow}$  can be observed. The strongest trend ( $a = 3.808$ ,  $R^2 = 0.347$ ) is recorded in spring (March-May). A weaker trend is observed in summer ( $a = 2.991$ ,  $R^2 = 0.137$ ), as the highest values of  $K_{\downarrow}$  for this season were already recorded in the first part of the 1990s. The weakest seasonal trend is characteristic for winter ( $a = 0.469$ ,  $R^2 = 0.077$ ), so but the changes are jointed with the time when the values of  $K_{\downarrow}$  are the lowest in the year.

The very significant positive trend of the  $K_{\downarrow}$  sums of the warm half-year (April-September) (Bryś 2017)

is also reached (Fig. 3). In these sums, which are of crucial importance to the values for the  $K_{\downarrow}$  yearly sums (of which they constitute on average 77.8%), as well as in the appropriate annual (Jan.-Dec.) sums, a significant increase (Bryś 2017) in values is recorded (approx.  $250 \text{ MJ}\cdot\text{m}^{-2}$  for the half-year sums) between the two circulation periods (early and advanced) of the NAO (North Atlantic Circulation) positive phase. For the target time periods of the  $K_{\downarrow}$  yearly and half-year sums (distinctly visible in the runs of the 60-month moving sums), a boundary can be seen at year 1987, between the earlier period (1961-1987) with relatively low values of these sums and the later period (1988-2016), with relatively high values of these sums. Such a division of the study period of 1961-2016 is not only induced by an evident radiation turning point, which appears in the research of actinometrical series (Bryś 2013, 2017), but also occurs in similar series of air temperature  $T_p$ , saturation deficit  $d$  and precipitation  $P$  in Wrocław (Bryś 2017). There are significant macro-circulation reasons behind this, and therefore, such a division appears also in the mean NAO indexes for the warm half-year and summer (Bryś 2017), that is, in the periods when the maximum yearly  $K_{\downarrow}$ ,  $T_p$ ,  $d$ ,  $P$  values in Wrocław are observed.

The first period includes the advanced and last stages of the negative phase of the NAO (1955-1973, or up until 1978), and the juvenile stage of the positive phase of the NAO (1974-1987, or 1979-1987). The 1974-1978 years include a turning point, and therefore it is very difficult to fix a precise time boundary between these phases (Hurrell 2017; Marsz, Styszyńska 2002, 2006). For the years of 1979-1987, an abrupt transition to recurring positive phases of the NAO is observed, occurring during the 1979/80 winter. In addition, a substantial negative phase of the pattern appeared twice, in the winters of 1984/85 and 1985/86<sup>3</sup>. The second analyzed period (1988-2016) includes the advanced stage of the positive phase of the NAO. However, the period of November 1995 to February 1996 was characterized by a return to the strong negative phase of the NAO, with later years dominated by evident positive values of the wintertime NAO.

The precise distinction of these phases and stages is not an easy task and is still the subject of research and discussion (Bryś, Bryś 2002; Marsz, Styszyńska 2002, 2006; Wibig 2000, 2001)<sup>4</sup>. Most often, the relationship between changes of the NAO and European climate are considered as teleconnections of different NAO winter patterns with continental temperature and precipitation (Hurrell 1995;

<sup>3</sup> <http://www.cpc.ncep.noaa.gov/data/teledoc/nao.shtml>

<sup>4</sup> see also: <http://www.cpc.ncep.noaa.gov/data/teledoc/nao.shtml> 2017; <https://climatedataguide.ucar.edu/climate-data/hurrell-north-atlantic-oscillation-nao-index-station-based>

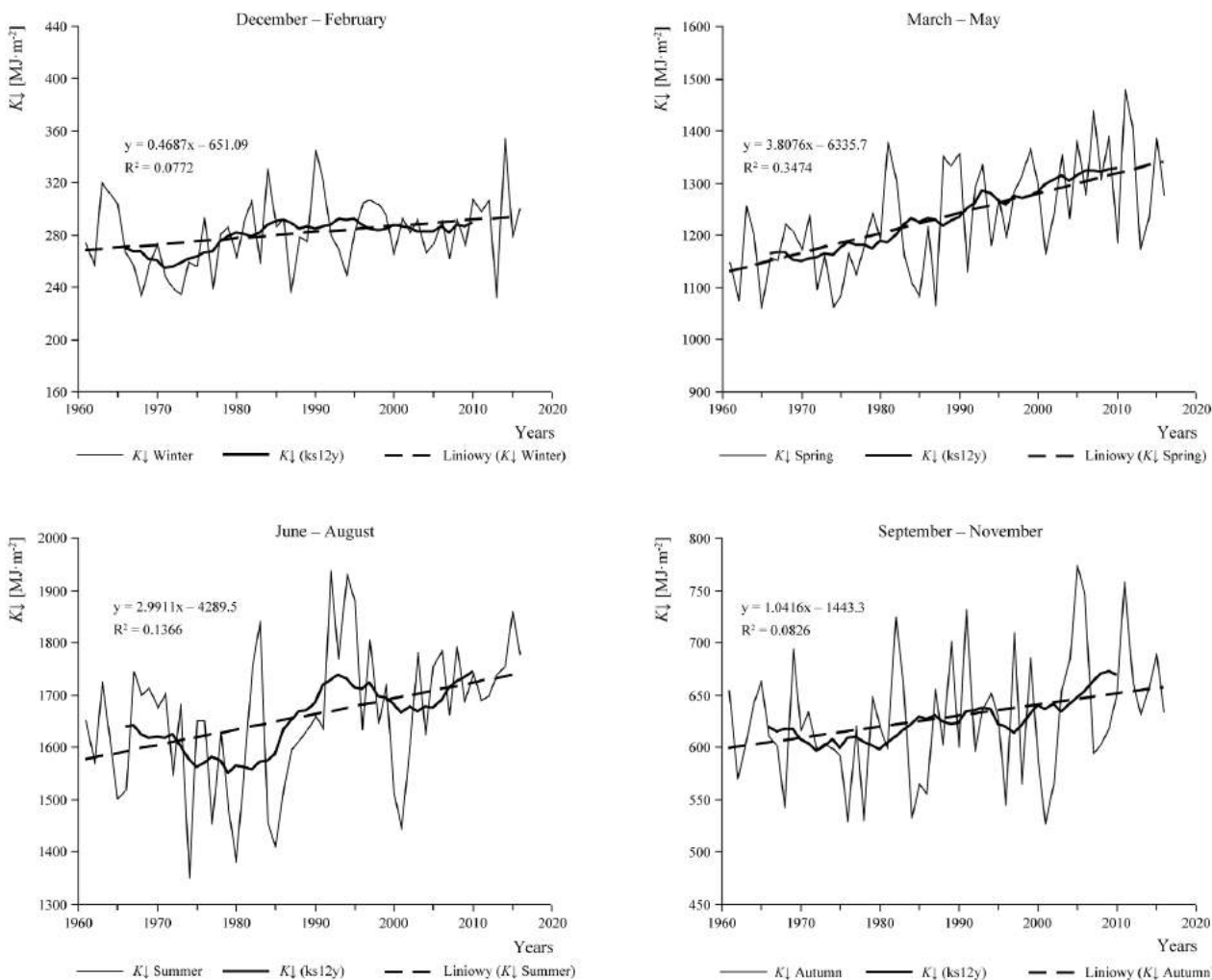


Fig. 2. The courses of seasonal (winter XII-II, spring III-V, summer VI-VIII, autumn IX-XI) sums of global radiation  $K_{\downarrow}$  and their 12-year (ks12y) moving averages in Wrocław-Swojec in the years of 1961-2016 (Liniowy = Linear trend)

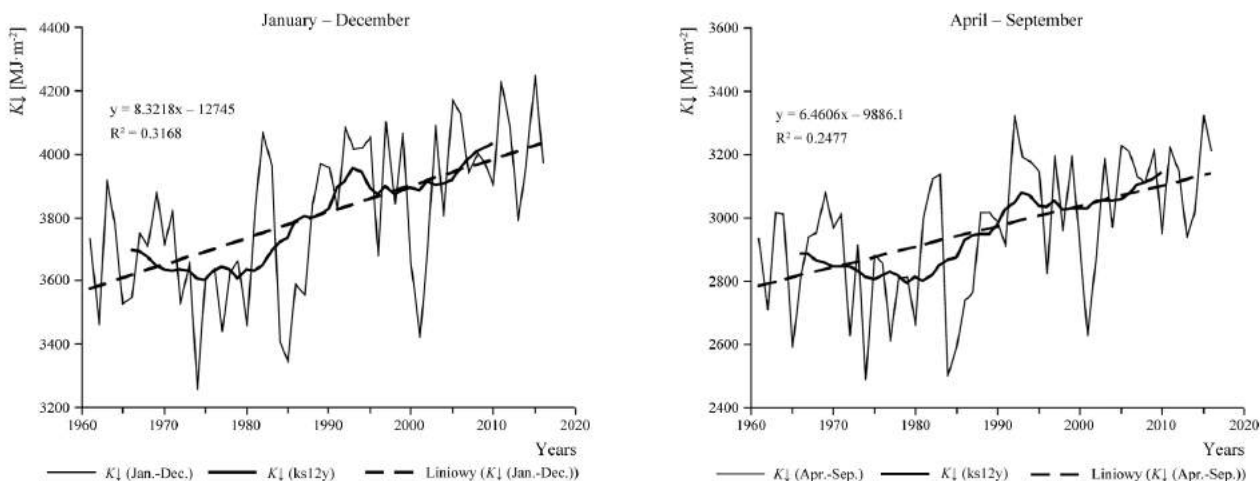


Fig. 3. The runs of annual (Jan.-Dec.) and half-year (Apr.-Sep.) sums of  $K_{\downarrow}$  and their 12-year (ks12y) moving averages in Wrocław-Swojec in the years of 1961-2016 (Liniowy = Linear trend)

Marsz 2005; Marsz, Styszyńska 2002, 2006). The problem of teleconnections between NAO and monthly sums of  $K_{\downarrow}$  in Wrocław is only considered in the earlier studies of the authors (Bryś, Bryś 2002; Bryś 2017). There exists a lack of similar studies for other areas in Poland

and Central Europe, thus the current study also takes into consideration Potsdam and Warsaw.

The courses of monthly mean values of global radiation intensity  $K_{\downarrow}$  in Wrocław-Swojec between the years 1961-2016 (Fig. 4) show that the most important trends

in the spring and summer growth of  $K\downarrow$  are found in April ( $a = 0.549$ ,  $R^2 = 0.207$ ), May ( $a = 0.619$ ,  $R^2 = 0.137$ ), and August ( $a = 0.467$ ,  $R^2 = 0.147$ ). Also significant is the positive trend for March ( $a = 0.272$ ,  $R^2 = 0.105$ ), and the increasing trend for July ( $a = 0.446$ ,  $R^2 = 0.064$ ) (with a significance of  $p = 0.062$  for Spearman's test and  $p = 0.075$  for tau-Kendall's test). For the autumn period, there is a significant, positive trend for November ( $a = 0.119$ ,  $R^2 = 0.123$ ), whereas for winter an increasing trend for February ( $a = 0.131$ ,  $R^2 = 0.055$ ) is observed, which is not, however, significant ( $p = 0.115$  of Spearman's test,  $p = 0.116$  of tau-Kendall's test).

In many monthly courses, the interesting phenomenon, particularly in February, July, August and October, of a strong wave characterizing the 12-year (ks12y) moving averages is observed (Fig. 4). The top of the wave in February coincides with the second part of the 1980s, while July and October it is observed in first part of the 1990s, and in August, in the mid-1990s and the first years of second part of the 1990s. The similar top of the wave for the whole summer season is observed in the first part of the 1990s (Fig. 2), as with the whole year and warm half-year (Fig. 3). Most likely, for these last cases (Fig. 3), a new wave is current forming, or will form in the close future (around 2020). Such phenomena are an important radiation feature of natural climatic fluctuations over many years.

Similar trends and variations of  $K\downarrow$  annual sums between the two compared circulation periods were reached in Potsdam (Fig. 5 and Fig. 6) and Warsaw (Fig. 6). As in Wrocław, for these stations, a boundary is noted around year 1987, between the first period (1961-1987) with low values of these sums and the later period (1988-2015, or 2016), with relatively high values of these sums. A comparison of trends for Potsdam, Wrocław and Warsaw proves that the strongest positive trend of  $K\downarrow$  annual sums is observed in Warsaw (Fig 6), closely followed by Wrocław (Fig. 3 and Fig. 7), and the weakest in Potsdam (Fig. 5 and Fig. 6).

In the period of 1961-2015, the highest annual sum of  $K\downarrow$  was noted in Wrocław ( $4246.7 \text{ MJ}\cdot\text{m}^{-2}$  in 2015), 2.1% lower in Potsdam ( $4158.6 \text{ MJ}\cdot\text{m}^{-2}$  in 2003), and 5.0% lower than the Wrocław maximum in Warsaw ( $4033.2 \text{ MJ}\cdot\text{m}^{-2}$  in 2012). The lowest minimum annual sums of  $K\downarrow$  were registered in Potsdam ( $3195.2 \text{ MJ}\cdot\text{m}^{-2}$  in 1984), followed by Warsaw ( $3217.2 \text{ MJ}\cdot\text{m}^{-2}$  in 1980, 0.7% larger than in Potsdam), and in Wrocław ( $3257.4 \text{ MJ}\cdot\text{m}^{-2}$  in 1974, 1.9% larger than in Potsdam). The highest annual average sum in the 55-year research period appears in Wrocław ( $3799.9 \text{ MJ}\cdot\text{m}^{-2}$ ), which is 2.8% higher than in Potsdam ( $3694.9 \text{ MJ}\cdot\text{m}^{-2}$ ), and 3.5% higher than that in Warsaw ( $3671.6 \text{ MJ}\cdot\text{m}^{-2}$ ). The coefficient of variability for the annual sums of  $K\downarrow$  averages is 5.6% for Potsdam, and 6.4% for

both Warsaw and Wrocław. The relatively low annual sums of  $K\downarrow$  for Warsaw in comparison to Belsk, Puławy, and other suburban areas in the radius of approximately 100 km from Warsaw, proves that the radiation values registered in Warsaw were reduced due to the influence of a greater amount of cloudiness generated by a very intensive UHI (Urban Heat Island) and local strong atmospheric pollution (Podogrocki 1984; Podogrocki, Słomka 1993; Bogdańska, Podogrocki 2000; Górski, Górski 2000). However, the radiation data from station Warsaw-Bielany is included in the longest actinometrical series in Poland, thus they have a relatively representative character for the central part of Poland, which is the main aim of the current analysis.

The relationship between  $K\downarrow$  and macro-circulation conditions are very complicated and are linked to oceanic influences based on the solar features of the climate in Central Europe, which varies in time. This influence is a natural derivative of source impact of sun activity on the Earth's climate (Soon et al. 1996) and of the important role of the contrast between the land and the ocean, as two different active global surfaces. They form, together with the influence of the Earth's rotary and circumsolar movement and other astronomical and geophysical conditions (particularly volcanic activity), the main features of a heat, moisture and momentum transfer and climatic diversification, on different spatial and temporal scales. The natural implication of these conditions is the oceanic circulation and layout, the thermal features of oceanic streams in the North Atlantic, and the interaction between the ocean and atmosphere in the formation of the main atmospheric mass flow over the European synoptic area (Paszyński, Niedźwiedz 1991; Woś 1999, 2010; Wibig 2000, 2001; Marsz, Styszyńska 2002, 2006; Żmudzka 2007). The transformation of these atmospheric masses over land, in addition to the duration and direction of advection, depends on many different features of land morphology and types of land cover and their physical properties. The variability of cloudiness over Poland depends not only on source areas and the path of atmospheric mass, but also on circulation epochs (Kožuchowski et al. 2000; Żmudzka 2007).

Based on these conclusions from the above cited papers, the current analysis confirms the conclusions of the earlier studies of the authors (Bryś, Bryś 2002; Bryś 2017), in that the teleconnections between the NAO and  $K\downarrow$  in Central Europe have a very complicated and asynchronous character. Taking the example of August, Figure 8 shows some differences of this asynchronous character between the years 1959-1987 and 1988-2016, which are visible both in Wrocław and Potsdam, and demand a wider, more detailed analysis. The relations have a larger, climatological context jointed with long-term variations of circulation

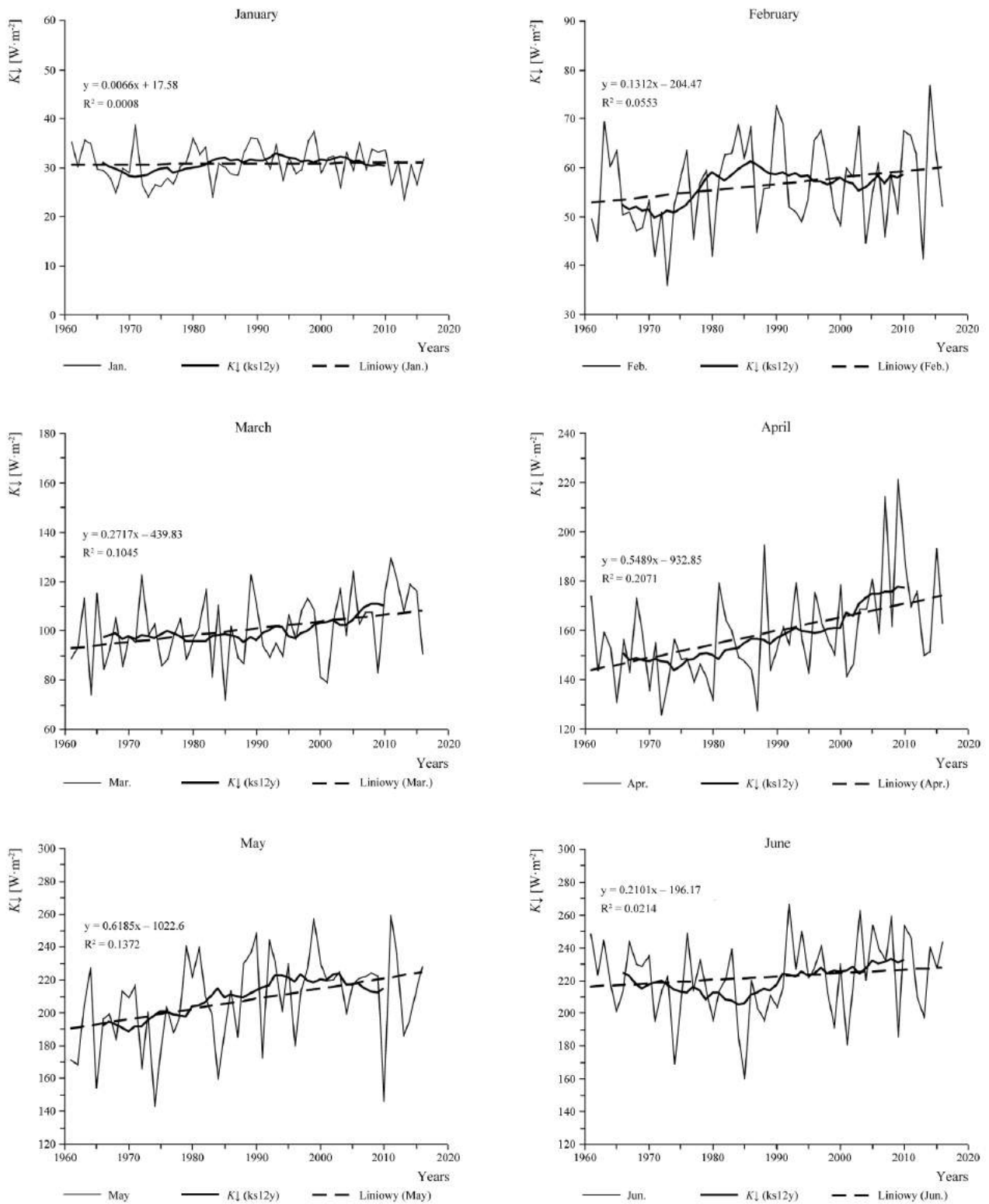


Fig. 4. The courses of average monthly values of global radiation intensity  $K_{\downarrow}$  and their 12-year (ks12y) moving averages in Wrocław-Swojec in the years of 1961-2016 (Liniowy = Linear trend) - Part A

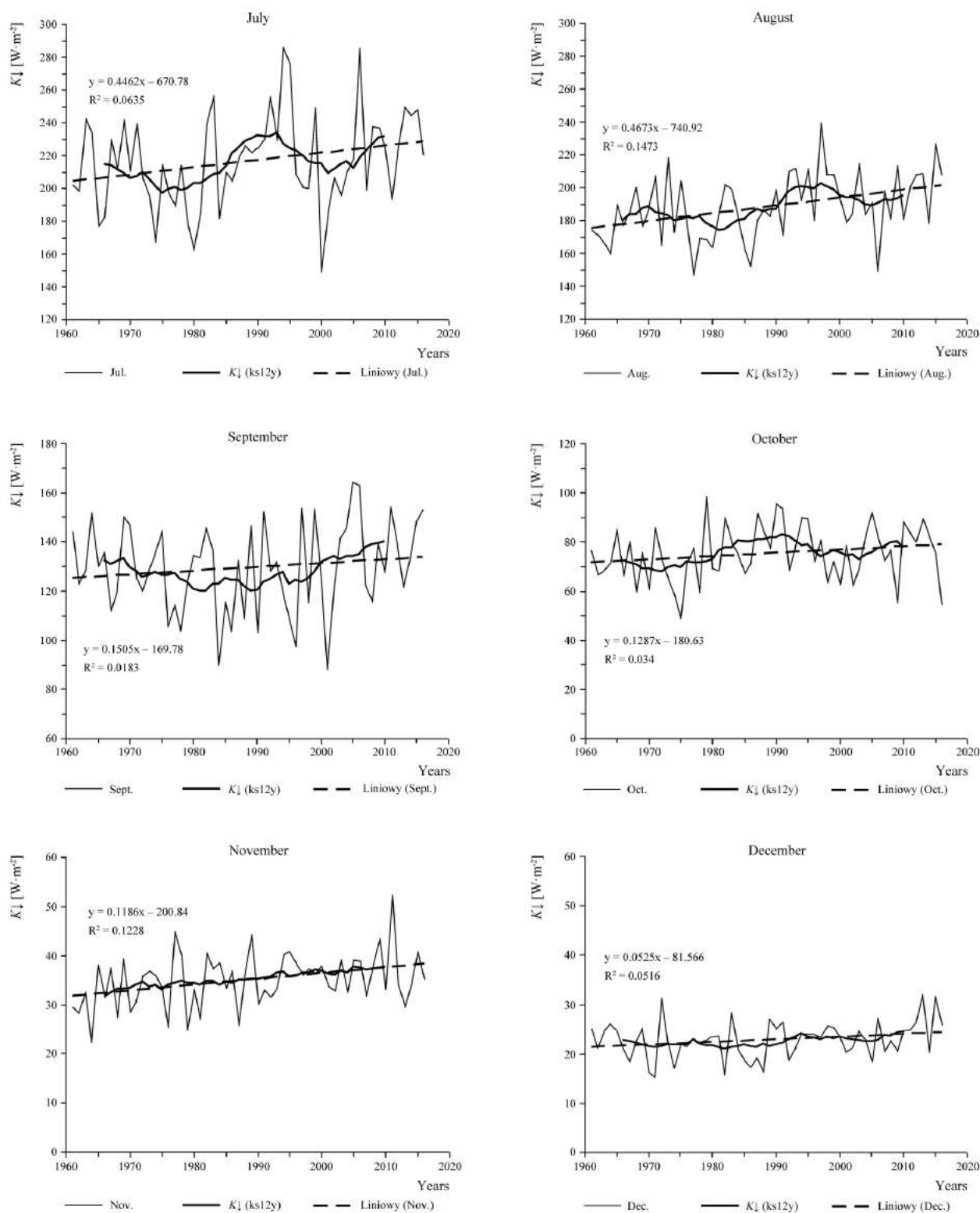


Fig. 4b. The courses of average monthly values of global radiation intensity  $K_{\downarrow}$  and their 12-year (ks12y) moving averages in Wrocław-Swojec in the years of 1961-2016 (Liniowy = Linear trend) – Part B

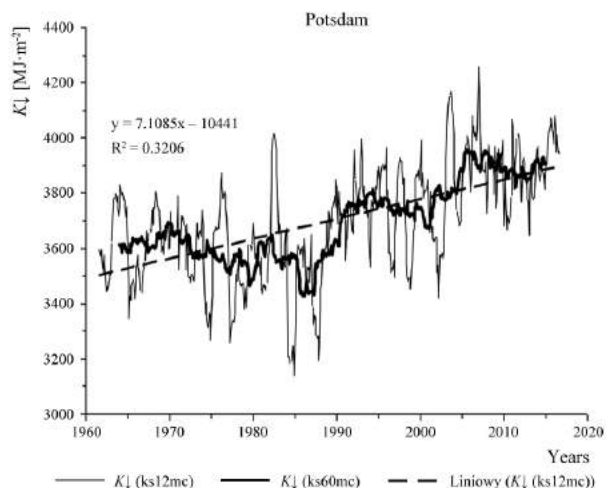


Fig. 5. The runs of 12- and 60-month (mean yearly values) moving sums (ks12m and ks60m) of global radiation  $K_{\downarrow}$  in Potsdam in the years of 1961-2016 (Liniowy = Linear trend)

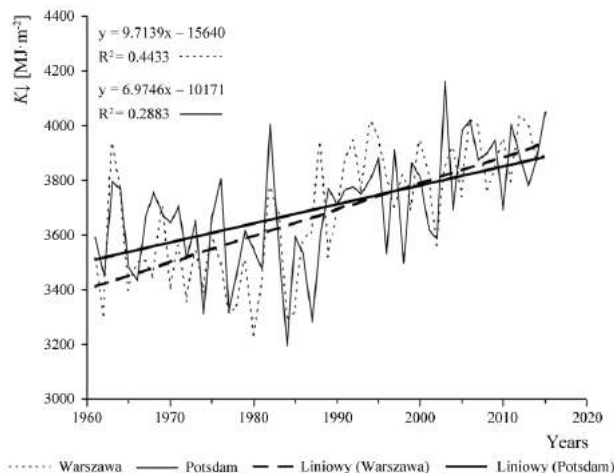


Fig. 6. The comparison of runs of annual (Jan.-Dec.) sums of  $K_{\downarrow}$  and their trends in Potsdam and Warsaw (Warszawa) in the years of 1961-2015 (Liniowy = Linear trend)

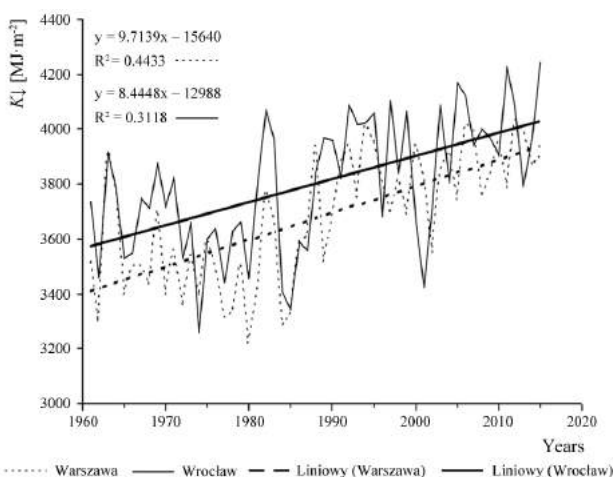


Fig. 7. The comparison of runs of annual (Jan.-Dec.) sums of  $K_{\downarrow}$  and their trends in Wrocław and Warsaw (Warszawa) in the years of 1961-2015 (Liniowy = Linear trend)

patterns in the synoptic broad scale not only over Europe and the North Atlantic, but also over the Middle East, the west part of Siberia and the north peripheries of Africa.

Strong positive phases of the NAO tend to be associated with above-average temperatures in northern Europe, and below-average temperatures across southern Europe and the Middle East. They are also associated with above-average precipitation over northern Europe and Scandinavia in winter, and below-average precipitation over southern and central Europe. Opposite patterns of temperature and precipitation anomalies are typically observed during strong negative phases of the NAO<sup>5</sup>. Such spatial teleconnections of the winter NAO are likely to impact future barometric patterns over the European Synoptic Area (Marsz, Styszyńska 2006; Marsz 2010) and the directions

and features of atmospheric advection in Central Europe during the summer.

A detailed analysis of these teleconnections demands a different study. In addition to the NAO, such analysis needs to also explore the topic of climatological influences of other circulation patterns on the main radiation climatic features in Poland and Central Europe.

#### 4. Summary

The observed positive trends show significant increasing values of the investigated global radiation sums for Lower Silesia, Central Poland and the east part of Germany. The growth of the  $K_{\downarrow}$  sums is linked to the macro-regional circulation changes, particularly with the basic stages of the NAO positive phase and their influence on the weather in Central Europe. The first, juvenile stage of the phase (the 1970s and 1980s), when annual sums of  $K_{\downarrow}$  in Wrocław-Swojec only reached the average level of approximately  $3700 \text{ MJ}\cdot\text{m}^{-2}$  and the warm half-year approximately  $2800 \text{ MJ}\cdot\text{m}^{-2}$ , was cloudy and rainy. This period was distinctly different compared to the advanced stage (the 1990s and later years), with a longer sunshine duration and smaller annual precipitation, with adequate radiation sums amounting to  $3900\text{-}4000 \text{ MJ}\cdot\text{m}^{-2}$  and  $3000\text{-}3100 \text{ MJ}\cdot\text{m}^{-2}$ , respectively. Similar variations were reached in Warsaw and Potsdam. The noted trends and periods of solar change are linked to similar variations in cloudiness and sunshine duration, which are typically observed in Poland (Morawska-Horawska 1985, 2002; Dubicka, Pyka 2001; Podstawczyńska 2003, 2007; Koźmiński, Michalska 2005; Matuszko 2009; Bryś 2015) and Central Europe (Ohrvil et al. 2009; Bryś 2013). The paper confirms the conclusions of previous studies made by the authors (Bryś, Bryś 2002,

<sup>5</sup> <http://www.cpc.ncep.noaa.gov/data/teledoc/nao.shtml>

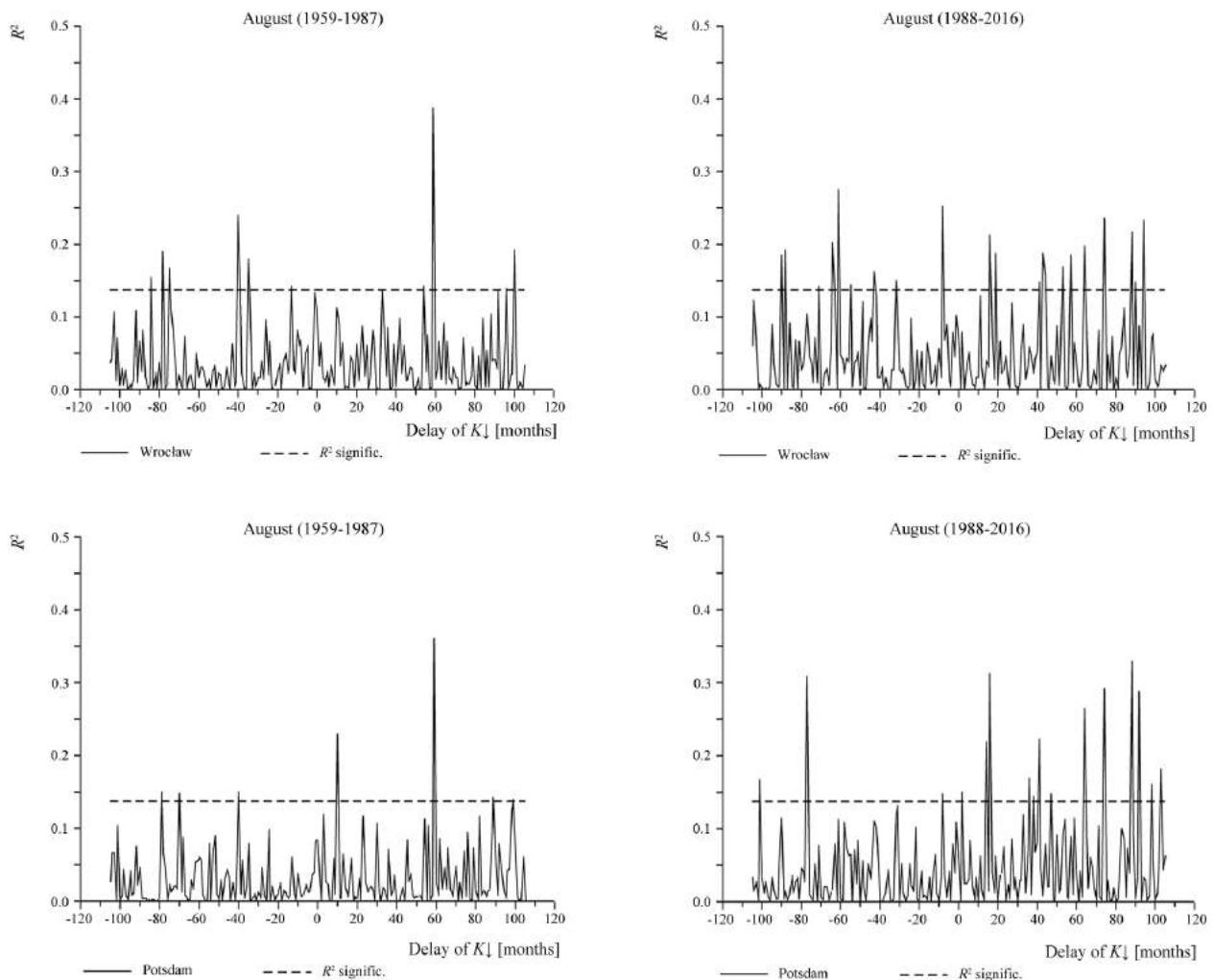


Fig. 8. The comparison of runs of the asynchronous coefficient of determination ( $R^2$ ) for the correlations between monthly indices of the NAO and monthly sums of  $K_{\downarrow}$  in Wrocław and Potsdam in the years 1959-1987 and 1988-2016 for the month of August. Explanation: delay of  $K_{\downarrow}$  from  $-105$  to  $105$  months,  $0$  – the synchronous correlation,  $R^2$  significant. – the lower boundary of a value for the coefficient of determination ( $R^2$ ), which is statistical significant

2003, 2007; Bryś 2013, 2015, 2017), on the main role of naturally observed radiation trends. The derived results point out that radiation trends are strongly connected to natural long-term macro-circulation changes (Marsz, Styszyńska 2002, 2006, 2009; Marsz 2005; Pisek, Brazdil 2006; Ohrvil et al. 2009) in the Northern Hemisphere. In addition to influences of other north hemispheric barometric patterns (Marsz, Styszyńska 2006), they are relatively strongly related to the phases and sub-phases of the North Atlantic Oscillation. These atmospheric changes are connected with long-term changes in oceanic circulation, particularly with wind-driven circulation or the meridional overturning circulation (MOC) and the behaviors and features of oceanic surface currents (Marsz, Styszyńska 2009; Olbers et al. 2012). Teleconnections most often have an asynchronous character and perform quasi-periodically, with several year long waves of radiation changes as an important phenomenon for many years of climatic fluctuations. Further studies should involve a detailed analysis of atmospheric pollution

emissions and their influence on global radiation. Such studies can determine whether the macro-circulation, natural genesis of the radiation changes is more important than the influence of anthropogenic aerosols on climate, as suggested by Ahrens (2008), Wibig (2009) and other researchers that support the main theses of the IPCC Report (2013).

#### Bibliography

- Abakumova G.M., Feigelson E.M., Russak V., Stadnik V.V., 1996, Evaluation of long-term changes in radiation, cloudiness and surface temperature on the territory of the former Soviet Union, *Journal of Climate*, 9 (6), 1319-1327, DOI:10.1175/1520-0442(1996)009<1319:EOLTTCI>2.0.CO;2
- Abakumova G.M., Gorbarenko E.V., 2008, Transparency in Moscow during the last 50 years, its changes on the territory of Russia, (in Russian), Izdatelstvo LKI, Moscow, 193 pp.
- Ahrens C.D., 2008, *Meteorology today: an introduction to weather, climate and the environment*, Cengage Learning, 624 pp.

- Alpert P., Kishcha P., Kaufman Y.J., Schwarzbard R., 2005, Global dimming or local dimming? Effect of urbanization on sunlight availability, *Geophysical Research Letters*, 32 (17), L17802, DOI: 10.1029/2005GL023320
- Bogdańska B., Podogrocki J., 2000, Variation in global solar radiation on Polish territory in the period 1961-1995, (in Polish), *Materiały Badawcze IMGW. Seria: Meteorology*, 30, 43 pp.
- Bryś K., 2006, Radiation potential of Lower Silesia as a source for utilization of solar energy in the future, (in Polish), [in:] *Zintegrowany Program Operacyjny Rozwoju Regionalnego. Biuletyn Innowacyjny CEPRIN, Europejski Fundusz Społeczny*, Wrocław, 19-31
- Bryś T., 2007a, Study of representativeness for the Wrocław-Swojec observatory as an agrimeteorological and climatic station, (in Polish), [in:] *Zintegrowany Monitoring Środowiska Przyrodniczego*, A. Kostrzewski, A. Andrzejewska (eds.), *Biblioteka Monitoringu Środowiska*, Warszawa, 255-267
- Bryś K., 2007b, Variability of sunshine duration in Wrocław-Swojec in the years 1961-2006 on the background of its secular changes, (in Polish), [in:] *Funkcjonowanie i monitoring geosystemów Polski w warunkach narastającej antropopresji*, A. Kostrzewski, A. Andrzejewska (eds.), *Biblioteka Monitoringu Środowiska*, Warszawa, 243-255
- Bryś K., 2013, Dynamics of net radiation balance of grass surface and bare soil, (in Polish), *Monografie Uniwersytetu Przyrodniczego we Wrocławiu*, 162, 288 pp.
- Bryś K., 2015, Resources of solar energy in the valley of the Widawa River, (in Polish), *Inżynieria Ekologiczna*, 44, 53-61, DOI: 10.12912/23920629/60025
- Bryś K., 2017, Variability of solar features of Lower Silesia agroclimate, (in Polish), *Zeszyty Naukowe Uniwersytetu Przyrodniczego we Wrocławiu: Rolnictwo*, 624, 15-31
- Bryś K., Bryś T., 2002, Influence of the NAO changes on a variability of the humidity, radiation, wind dynamics and evaporation in Wrocław-Swojec in the years 1946-2000, (in Polish), [in:] *Oscylacja Północnoatlantycka i jej wpływ na warunki klimatyczne i hydrologiczne Polski*, A.A. Marsz, A. Styszyńska (eds.), *Akademia Morska*, Gdynia, 147-160
- Bryś K., Bryś T., 2003, Fluctuations of global solar radiation in 20<sup>th</sup> century at Wrocław and their relations to Wolf's number and circulation changes, *Acta Universitatis Wratislaviensis. Studia Geograficzne*, 75, 189-202
- Bryś K., Bryś T., 2007, Variability of solar features of the Wrocław climate in the years 1875-2004, (in Polish), *Pamiętnik Puławski*, 144, 13-34
- Dubicka M., 1994, Influence of atmospheric circulation on the climate conditions shaping (on Wrocław example), (in Polish), *Acta Universitatis Wratislaviensis. Studia Geograficzne*, 60, 296 pp.
- Dubicka M., 1998, Ninety-five-year series of the sunshine duration measurements on Mount Śnieżka, (in Polish), [in:] *Geologiczne Problemy Karkonoszy*, Wydawnictwo Acarus, Poznań, 133-144
- Dubicka M., Karal J., 1994, Sunshine duration on Mount Szrenica and its relation to atmospheric circulation, (in Polish), *Acta Universitatis Wratislaviensis. Prace Instytutu Geograficznego. Seria C: Meteorologia i Klimatologia*, 1, 9-43
- Dubicka M., Karal J., Ropuszyński P., 1995, Sunshine duration in Wrocław in the years 1981-1992 on the background of the secular measurement series, (in Polish), *Acta Universitatis Wratislaviensis. Prace Instytutu Geograficznego. Seria C: Meteorologia i Klimatologia*, 2, 5-21
- Dubicka M., Limanówka D., 1994, Variability of cloudiness and sunshine duration in the Sudeten and Carpathian Mts. and their foothills, (in Polish), *Acta Universitatis Wratislaviensis. Prace Instytutu Geograficznego. Seria C: Meteorologia i Klimatologia*, 1, 45-60
- Dubicka M., Migala K., 1997, Variation of sunshine duration in selected mountains regions of Central Europe, (in Polish), *Acta Universitatis Wratislaviensis. Prace Instytutu Geograficznego. Seria C: Meteorologia i Klimatologia*, 4, 31-41
- Dubicka M., Pyka J.L., 2001, Climate of Wrocław in 20<sup>th</sup> century, (in Polish), *Prace i Studia Geograficzne*, 29, 101-112
- Górski T., Górka K., 2000, Sunshine duration in Puławy in span of the years 1923-1992, (in Polish), *Acta Universitatis Nicolai Copernici. Geografia. Nauki Matematyczno-Przyrodnicze*, 106, 141-156
- Hurrell J.W., 1995, Decadal trends in the North Atlantic Oscillation: regional temperatures and precipitation, *Science*, 269 (5224), 676-679, DOI: 10.1126/science.269.5224.676
- IPCC, 2013, *Climate change 2013: the physical science basis, Contribution of Working Group I to the Fifth Assessment Report of the Intergovernmental Panel on Climate Change*, IPCC, Cambridge University Press, Cambridge, United Kingdom and New York, NY, USA, 1535 pp.
- Jaworowski Z., 2003, Solar cycles, not CO<sub>2</sub>, determine climate, *21st Century Science and Technology*, 52-65, available at [https://21sci-tech.com/Articles%202004/Winter2003-4/global\\_warming.pdf](https://21sci-tech.com/Articles%202004/Winter2003-4/global_warming.pdf) (data access 31.01.2019)
- Jaworowski Z., 2007, CO<sub>2</sub>: The greatest scientific scandal of our time, *EIR Science*, 38-53, available at <http://folk.uio.no/tomvs/esef/Jaworowski%20CO2%20EIR%202007.pdf> (data access 31.01.2019)
- Kleniewska M., Chojnicki B.H., Acosta M., 2016, Long-term total solar radiation variability at the Polish Baltic coast in Kołobrzeg with in the period 1964-2013, *Meteorology, Hydrology and Water Management*, 4 (2), 35-40, DOI: 10.26491/mhwm/64594
- Kondratyev K.Y., Galindo I., 1997, *Volcanic activity and climate*. A Deepak Publishing, Hampton, VA, USA, 382 pp.

- Koźmiński C., Michalska B., 2005, Sunshine duration in Poland, (in Polish), Akademia Rolnicza w Szczecinie, Uniwersytet Szczeciński, Szczecin, 110 pp.
- Kożuchowski K., Degirmendzić J., Fortuniak, K., Wibig J., 2000, Trends to changes in seasonal aspects of the climate of Poland, *Geographia Polonica*, 73 (2), 7-24
- Kuczmarzka L., Kuczmarzki M., 1998, Structure of sunshine duration in Poland, (in Polish), *Przegląd Geograficzny*, 1/2, 101-110
- Kuczmarzki M., 1990, Sunshine duration of Poland and its usefulness for heliotherapy, (in Polish), *Dokumentacja Geograficzna*, 4, 70 pp.
- Marsz A.A., 2005, About oceanic conditionings of circulation and thermal nature of wintertime in Poland and the middle Europe, (in Polish), Akademia Morska, Gdynia, 63 pp.
- Marsz A.A., 2010, Role interzonal meridional circulation over the east of the North Atlantic in a shaping of some climate features of the Atlantic Arctic, (in Polish), *Problemy Klimatologii Polarnej*, 20, 7-30
- Marsz A., Styszyńska A., 2002, North Atlantic Oscillation and its influence on climatic and hydrological conditions in Poland, (in Polish) Akademia Morska, Gdynia, 222 pp.
- Marsz A., Styszyńska A., 2006, About „Arctic” and „Atlantic” mechanisms which control variability of the air temperature on Europe territory and the north-west Asia, (in Polish), *Problemy Klimatologii Polarnej*, 16, 47-89
- Marsz A.A., Styszyńska A., 2009, Oceanic control of the warming processes in the Arctic – a different point of view for the reasons of changes in the Arctic climate, *Problemy Klimatologii Polarnej*, 19, 7-31
- Matuszko D., 2009, Influence of cloudiness on sunshine duration and global solar radiation on example of the Cracow measurement series, (in Polish), Wydawnictwo Uniwersytetu Jagiellońskiego, Kraków, 232 pp.
- Matuszko D., 2012, Influence of the extent and genera of cloud cover on solar radiation intensity, *International Journal of Climatology*, 32 (15), 2403-2414, DOI: 10.1002/joc.2432
- Matuszko D., 2014, Long-term variability in solar radiation in Krakow based on measurements of sunshine duration, *International Journal of Climatology*, 34 (1), 228-234, DOI:10.1002/joc.3681
- Marciniak K., Wójcik G., 1991, The variation of sunshine duration in the middle part of northern Poland during the period 1946-1989, *Zeszyty Problemowe Postępów Nauk Rolniczych*, 396, 109-115
- Morawska-Horawska M., 1985, Cloudiness and sunshine in Cracow 1861-1980 and its contemporary tendencies, *International Journal of Climatology*, 5 (6), 633-642, DOI: 10.1002/joc.3370050605
- Morawska-Horawska M., 2002, Tendencies of cloudiness and sunshine duration in Cracow 1861-1990, (in Polish), [in:] *Działalność naukowa prof. Władysława Gorczyńskiego i jej kontynuacja*, G. Wójcik, K. Marciniak (eds.), Wydawnictwo Naukowe Uniwersytetu Mikołaja Kopernika, Toruń, 341-351
- Norris J.R., Wild M., 2007, Trends in aerosol radiative effects over Europe inferred from observed cloud cover, solar “dimming,” and solar “brightening”, *Journal of Geophysical Research: Atmospheres*, 112 (D8), DOI: 10.1029/2006JD007794
- Ohvril H., Teral H., Lennart N., Kannel M., Uustare M., Tee M., Russak V., Okulov O., Jõeveer A., Kallis A., Ohvril T., Terez E., Terez G., Gushchin G.K., Abakumova G.M., Gorbarenko E.V., Tsvetkov A.V., Laulainen N., 2009, Global dimming and brightening versus atmospheric column transparency, Europe, 1906-2007, *Journal of Geophysical Research: Atmospheres*, 114 (D10), DOI: 10.1029/2008JD010644
- Olbers D., Willebrand J., Eden C., 2012, *Ocean dynamics*, Springer, Berlin, Heidelberg, 708 pp.
- Paszyński J., Niedźwiedz T., 1991, *Climate*, (in Polish), [in:] *Geografia Polski – środowisko przyrodnicze*, L. Starkel (ed.), PWN, Warszawa, 288-343
- Pisek J., Brázdil J., 2006, Responses of large volcanic eruptions in the instrumental and documentary climatic data over Central Europe, *International Journal of Climatology*, 26 (4), 439-459, DOI: 10.1002/joc.1249
- Podogrocki J., 1984, Solar radiation at selected stations of the Polish network 1983 and 1961-1980, *Publications of the Institute of Geophysics Polish Academy of Science. Physics and Atmosphere*, D-20 (178), 45-52
- Podogrocki J., 1989, On solar energy resources in Poland during the vegetation period, *Zeszyty Problemowe Postępów Nauk Rolniczych*, 396, 245-250
- Podogrocki J., 2001, The chart of spatial distribution of global solar radiation intensity in Poland, (in Polish), [in:] *Atlas klimatycznego ryzyka uprawy roślin w Polsce*, C. Koźmiński, B. Michalska (eds.), Uniwersytet Szczeciński, Szczecin, 26 a-c
- Podogrocki J., 2007, Climatic and meteorological conditions to an utilization of the solar radiation energy in Poland, (in Polish), available at [http://solis.pl/index.php/pliki\\_do\\_pobrania/publikacje\\_i\\_artykuly/warunki\\_do\\_wykorzystania\\_energii\\_promieniowania\\_slonecznego\\_w\\_polsce](http://solis.pl/index.php/pliki_do_pobrania/publikacje_i_artykuly/warunki_do_wykorzystania_energii_promieniowania_slonecznego_w_polsce) (31.01.2019)
- Podogrocki J., Słomka J., 1993, Selected results of many year recording of sunshine duration in Warsaw and Belsk, *Publications of the Institute of Geophysics Polish Academy of Science. Physics and Atmosphere*, D-40 (263), 83-???
- Podstawczyńska A., 2003, Variability of sunshine duration in Łódź in 1951-2000. *Acta Universitatis Wratislaviensis. Studia Geograficzne*, 75, 295-304
- Podstawczyńska A., 2007, Solar features of the Lodz's climate, (in Polish), *Acta Universitatis Lodzianensis. Folia Geographica Physica*, 7, 294 pp.

- Ruckstuhl C., Norris J.R., 2009, How do aerosol histories affect solar “dimming” and “brightening” over Europe? IPCC-AR4 models versus observations, *Journal of Geophysical Research: Atmospheres*, 114 (D10), DOI: 10.1029/2008JD011066
- Russak V.K., 1987, On modern changes in atmospheric transparency, *Meteorologija i Hidrologija*, 3, 53-57
- Russak V.K., 1990, Trends of solar radiation, cloudiness and atmospheric transparency during recent decades in Estonia, *Tellus*, 42 (2), 206-210, DOI: 10.1034/j.1600-0889.1990.t01-1-00006.x
- Sanchez-Lorenzo A., Brunetti M., Calbó J., Martin-Vide J., 2007, Recent spatial and temporal variability and trends of sunshine duration over the Iberian Peninsula from a homogenized dataset, *Journal of Geophysical Research: Atmospheres*, 112 (D20), DOI: 10.1029/2007JD008677
- Sanchez-Lorenzo A., Enriquez-Alonso A., Wild M., Trentmann J., Vicente-Serrano S.M., Sanchez-Romero A., Posselt R., Hakuba M.Z., 2017, Trends in downward surface solar radiation from satellites and ground observations over Europe during 1983-2010, *Remote Sensing of Environment*, 189, 108-117, DOI: 10.1016/j.rse.2016.11.018
- Soon W.H., Posmentier E.S., Baliunas S.L., 1996, Inference of solar irradiance variability from terrestrial temperature changes 1880-1993: an astrophysical application of the sun-climate connection, *The Astrophysical Journal*, 472 (2), 891-902
- Stanhill G., 2005, Global dimming: a new aspect of climate change, *Weather*, 60 (1), 11-14, DOI: 10.1256/wea.210.03
- Stanhill G., 2007, A perspective on global warming, dimming, and brightening, *Eos, Transactions. American Geophysical Union*, 88 (5), 58-59, DOI: 10.1029/2007EO050007
- Stanhill G., Cohen S., 2001, Global dimming: a review of the evidence for a widespread and significant reduction in global radiation with discussion of its probable causes and possible agricultural consequences, *Agricultural and Forest Meteorology*, 107 (4), 255-278, DOI: 10.1016/S0168-1923(00)00241-0
- Stanhill G., Cohen S., 2005, Solar radiation changes in the United States during the twentieth century: evidence from sunshine duration measurements, *Journal of Climate*, 18 (10), 1503-1512, DOI: 10.1175/JCLI3354.1
- Streets D.G., Wu Y., Chin M., 2006, Two-decadal aerosol trends as a likely explanation of the global dimming/brightening transition, *Geophysical Research Letters*, 33 (15), DOI: 10.1029/2006GL026471
- Stjern C.W., Kristjánsson J.E., Hansen A.W., 2009, Global dimming and global brightening – an analysis of surface radiation and cloud cover data in northern Europe, *International Journal of Climatology*, 29 (5), 643-653, DOI: 10.1002/joc.1735
- Sun B., Groisman P.Y., 2000, Cloudiness variations over the former Soviet Union, *International Journal of Climatology*, 20 (10), 1097-1111, DOI: 10.1002/1097-0088(200008)20:10<1097::AID-JOC541>3.0.CO;2-5
- Tooming H., 2002, Dependence of global radiation on cloudiness and surface albedo in Tartu, Estonia, *Theoretical and Applied Climatology*, 72 (3-4), 165-172, DOI: 10.1007/s00704-002-0671-y
- Uscka-Kowalkowska J., 2008a, Direct solar radiation and its extinction by the atmosphere in Kołobrzeg in the years 1960-2000, (in Polish), *Acta Agrophysica*, 12 (1), 221-233
- Uscka-Kowalkowska J., 2008b, Direct solar radiation and its extinction by the atmosphere on an example of Puławy and Papowo, (in Polish), *Wydawnictwo Naukowe UMK, Toruń*, 133 pp.
- Uscka-Kowalkowska J., 2009, Comparison of direct solar radiation and its extinction by the atmosphere in Warsaw and Mikołajki, (in Polish), *Acta Agrophysica*, 14 (2), 501-514
- Uscka-Kowalkowska J., 2013, An analysis of the extinction of direct solar radiation on Mt. Kasprowy Wierch, Poland, *Atmospheric Research*, 134, 175-185, DOI: 10.1016/j.atmosres.2013.08.002
- Warren S.G., Eastman R.M., Hahn C.J., 2007, A survey of changes in cloud cover and cloud types over land from surface observations, 1971-96, *Journal of Climate*, 20 (4), 717-738, DOI: 10.1175/JCLI4031.1
- Wibig J., 2000, The North Atlantic Oscillation and its impact of weather and climate, (in Polish), *Przegląd Geofizyczny*, 45 (2) 121-137
- Wibig J., 2001, Influence of atmospheric circulation on spatial distribution of temperature and precipitation anomalies in Europe, (in Polish), *Rozprawy Habilitacyjne Uniwersytetu Łódzkiego*, 208 pp.
- Wibig J., 2003, Cloudiness variability in Łódź between 1931 and 2000, *Acta Universitatis Wratislaviensis. Studia Geograficzne*, 75, 305-316
- Wibig J., 2004, Long-term variability of cloudiness and its relation to precipitation on the example of Łódź, [in:] *Potential climate changes and sustainable water management*, M. Liszewska (ed.), *Monographic E-4 (377)*, 25-32
- Wibig J., 2009, Contemporary climatic changes – presumptions of an influence of the anthropogenic factors, (in Polish), available at [http://www.klimat.geo.uj.edu.pl/strony/studenci/artykuly/Artykuly\\_rozne/JWibig\\_antropo.pdf](http://www.klimat.geo.uj.edu.pl/strony/studenci/artykuly/Artykuly_rozne/JWibig_antropo.pdf) (data access 01.02.2019)
- Wild M., 2009, Global dimming and brightening: a review, *Journal of Geophysical Research: Atmospheres*, 114 (D10), DOI: 10.1029/2008JD011470
- Wild M., Gilgen H., Roesch A., Ohmura A., Long C.N., Dutton E., Forgan B., Kallis A., Russak V., Tsvetkov A., 2005, From dimming to brightening: decadal changes in solar radiation at earth’s surface, *Science*, 308 (5723), 847-850, DOI: 10.1126/science.1103215

- Wild M., Ohmura A., Makowski K., 2007, Impact of global dimming and brightening on global warming, *Geophysical Research Letters*, 34 (4), DOI: 10.1029/2006GL028031
- Wild M., Trüssel B., Ohmura A., Long C.N., König-Langlo G., Dutton E.G., Tsvetkov A., 2009, Global dimming and brightening: an update beyond 2000, *Journal of Geophysical Research: Atmospheres*, 114 (D10), DOI: 10.1029/2008JD011382
- Wilks D., 2005, *Statistical methods in the atmospheric sciences*, Academic Press, 649 pp.
- Woś A., 1999, *Climate of Poland*, (in Polish), Wydawnictwo Naukowe PWN, Warszawa, 302 pp.
- Woś A., 2010, *Climate of Poland in the second half of 20<sup>th</sup> century*, (in Polish), Wydawnictwo Naukowe UAM, Poznań, 489 pp.
- Żmudzka E., 2007, *Variability of cloudiness over Poland and its circulation conditions*, (in Polish), Wydawnictwo Uniwersytetu Warszawskiego, Warszawa, 399 pp.



## Sensitivities of the Tiedtke and Kain-Fritsch Convection Schemes for RegCM4.5 over West Africa

Mojisola Oluwayemisi Adeniyi

University of Ibadan, Department of Physics, Ibadan, Oyo State, Nigeria, e-mail: mojisolaadeniyi@yahoo.com

**Abstract.** Realistic simulation of weather and climate parameters over West Africa is daunting, so the performance of the Tiedtke and Kain-Fritsch convection schemes within version 4.5 of the Regional Climate Model (RegCM4.5) of the International Centre for Theoretical Physics, Trieste is evaluated over West Africa for improved simulation. The two schemes are compared to two traditional mixture schemes (Grell on land and Emanuel on Ocean), outperforming the mixture schemes with reduced magnitude and spatial coverage of dry bias. Both schemes simulate precipitation over West Africa with a low dry bias, however, the Kain-Fritsch convection scheme simulates more realistic precipitation in the West African convective environment. This is associated with the inclusion of a variable cloud radius and the convective available potential energy closure for the Kain-Fritsch in contrast to a fixed cloud radius and moisture convergence of the of the Tiedtke scheme. The simulated outgoing longwave radiation and omega lend support to the spatial variations and amount of simulated precipitation in the different areas by the schemes. The spatial variation of simulated temperature over the target region shows lower bias than precipitation by all the convection schemes. Soil moisture is more accurately simulated (correlation coefficient  $\sim 1$ ) in the savannah (8-10°N) and Sahel (22-28°N) environments by all the convection schemes. Tiedtke performs the most accurate simulations of the pattern and profile of zonal wind which controls climate circulation, with slightly weaker simulations of the Africa easterly jet with core magnitude less than  $10 \text{ m s}^{-1}$ . The accuracy of the KF and Tiedtke in RegCM4.5 in simulating the climate of West Africa is documented for the first time for application in future studies over the region.

**Keywords:** Convective precipitation, West African monsoon, Kain-Fritsch convection scheme, Tiedtke convection scheme, African easterly jet

**Submitted** 17 January 2018, **revised** 17 March 2018, **accepted** 7 February 2019

### 1. Introduction

Rainfall is an important climate parameter and the main source of water for agricultural productivity in West Africa where small-scale farmers dominate the population of farmers. Even when small scale irrigation is used the main source of the irrigation water is rainfall, which increases the water table level during the rainy season such that slight digging near streams and rivers during the dry season yields enough water for small scale irrigation. Accurate prior knowledge of the amount, frequency and intensity of precipitation for a particular rainy season is useful for planning. Understanding of past, present and future climate depends greatly on the use of dynamical General Circulation Models (GCMs), which use a combination of scenarios to represent atmospheric greenhouse gas concentrations and land use for the respective time periods (Adeniyi 2016). The GCMs perform well on continental scales, but their outputs are not realistic on local scales. This calls for the use of either statistical or dynamic Regional Climate Models (RCMs) to transform the output of GCMs on regional scales to a more realistic output closer to observations (Brown et al. 2008; Mendes, Marengo 2010; Jones et al. 2011)

based on their higher resolution and fine scale topography (Gao et al. 2016; Adeniyi, Dilau 2018). The ability of such RCMs should be tested for historical simulation, with reanalysis boundary conditions. The performance of the models depends greatly on the physics of the model and the applied physical parameterizations. Atmospheric processes such as turbulent and convective motions can occur on small scale level, this can be smaller than the model grid size, such that these processes cannot be resolved by the model and are usually parameterized. Examples of the processes are convective precipitation, sensible and latent heat fluxes, water vapour fluxes and momentum fluxes.

The West African climate is greatly influenced by deep convection, which has been reported to be the main phenomenon that maintains the African Easterly Jet (AEJ) and the propagation of the African Easterly Wave (AEW) (Leroux, Hall 2009). Furthermore, a considerable proportion of tropical precipitation is convective (Schumacher, Houze 2003). The importance of convective precipitation has led to the development of various convection schemes used in different RCMs. The sensitivity of most of these schemes has been tested and documented. The convective precipitation scheme of the Kuo, Massachusetts

Institute of Technology-Emanuel is henceforth referred to as Emanuel. The Grell convective precipitation scheme with Arakawa-Schubert (AS) closure is henceforth referred to as Grell 1, while the Grell convective precipitation scheme with Fritsch Chappel closures is referred to as Grell 2. The fourth version of the RCM of the International Centre for Theoretical Physics is henceforth referred to as RegCM4.0. Adeniyi (2014) documented the sensitivity of Emanuel, Grell 1 and Grell 2 schemes in RegCM4.0 for negative and positive El Niño Southern Oscillation phases. It has been documented that Emanuel and Grell2 perform most accurately over ocean and land, respectively (Giorgi et al. 2012; Adeniyi 2014). Gao et al. (2016) compared the performance of both Emanuel and Grell, with one of the models on land and the other on the ocean and the Tiedtke scheme over both the ocean and land in RegCM4.4 over China. Klein et al. (2015) also tested the performance of Betts-Miller-Janjić (BMJ) (Janjić 1994; 2000), Grell-Freitas (GF) (Grell, Freitas 2014) and the Kain-Fritsch (KF) convection trigger (Kain 2004; Ma, Tan 2009) using the WRF model. The KF was found to perform worst compared to Grell Devenyi (GDE) in a simulation of vorticity maxima associated with AEW over West Africa using the WRF model (Noble et al. 2014). Furthermore, Satyaban et al. (2014) tested the sensitivity of the KF, BMJ and GDE schemes using the WRF model over South Africa. Their findings show positive rainfall bias in simulated South African precipitation, with the largest bias in the KF scheme.

Yavinchan et al. (2006) used the KF convection scheme in Numerical Weather Prediction (NWP) models to improve the forecast of convective precipitation over Thailand. The sensitivity of the mass-flux framework of Grell and Dévényi (2002) for convection parameterization with different closures to tracer transport was tested by Arteta et al. (2009), using a coupled model for aerosol tracer transport and a Brazilian regional atmospheric model.

The default schemes in RegCM4 have different trigger mechanism, closure entrainment and detrainment compared to the KF and Tiedtke schemes, thus they are expected to perform differently. Convection in Grell is triggered when a lifted parcel attains moist convection. Convection activation in KF depends on broad scale vertical velocity, while Tiedtke triggers convection near the surface when the parcel temperature is 0.5 K higher than ambient temperature. Tiedtke employs a moisture convergence-based closure while the closure in KF is based on convective available potential energy (CAPE). The default schemes in RegCM4.5 have some deficiencies when simulating the climate over Africa (Abiodun et al. 2012; Nikulin et al. 2012), particularly relating to the diurnal precipita-

tion variation. Another deficiency in the default scheme as documented by Im et al. (2014), is the inability of default scheme to capture the intensity of an isolated maximum precipitation over the southwestern coast of Guinea. The newer schemes are expected to have potentials for improving the performance of RegCM4.5 based on their strong documented performance in other models and areas. For example, the Kain-Fritsch scheme has been reported to simulate a more realistic diurnal precipitation cycle over Africa and Thailand (Yavinchan et al. 2006; Nikulin et al. 2012). Furthermore, moisture convergence-based closure applied to the Tiedtke scheme has been used to improve the simulation of Madden Julian Oscillation (Liu et al. 2005) with respect to the deep convective scheme of Zhang and McFarlane with the CAPE based closure. The sensitivity of the Tiedtke and KF convective precipitation schemes in RegCM4.5 over West Africa is yet to be documented. This is necessary to guide future simulations over the area on the best parameterization for convective precipitation. This study simulates the climate of West Africa using both the Tiedtke and KF convection schemes in RegCM4.5 and evaluates the performance of the convection schemes over this region. The model description, experimental set up and evaluation datasets are presented in Section 2. The results are then analysed and discussed in Section 4, while Section 5 presents the conclusions.

## 2. Model description, simulation datasets and experimental set up

The RegCM4.5 is used to simulate the West African climate by combining the Emanuel and Grell 2 convection schemes with Emanuel used on the ocean and Grell2 on the land). This is performed along with the Tiedtke and KF convection schemes, which are applied over both land and ocean. This is carried out to determine the most accurate schemes over the target area in order to improve future precipitation simulations and downscaling. Six experiments are carried out with the same model parameters varying only the convection schemes and initialization dates.

Simulations are run over West Africa (Fig. 1) with the longitude and latitude centred on 0.0°E and 12.5°N, respectively. The RegCM4.5 model has two cores: hydrostatic and non-hydrostatic. The hydrostatic core is used with 23 pressure levels for the experiments. Pressure levels 1-23 correspond to 25, 75, 125, 175, 225, 275, 325, 375, 425, 475, 525, 575, 625, 675, 725, 775, 825, 870, 910, 945, 970, 995 and 1005 hPa, respectively. Giorgi et al. (2012) documented an accurate performance of the Normal Mercator cartographic projection in the tropics, thus it is used

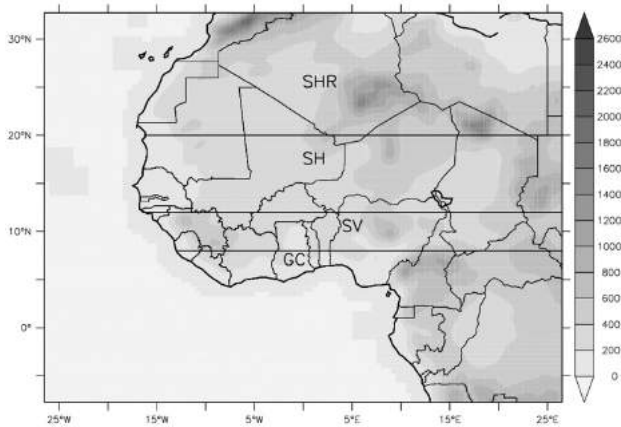


Fig. 1. Map of the simulation domain depicting the key regions over West Africa which are the Guinea Coast represented by GC, the savannah as SV, the Sahel as SH and the Sahara Desert as SHR; the spatial variation of the topography of the simulation domain is filled using inverse grey scale in meters above sea level

to project the simulation datasets to the West African domain on a  $50 \text{ km} \times 50 \text{ km}$  spatial grid. The Global 30 Arc-Second Elevation topography data set is used for these simulations, with a time step of 150 s. Era-Interim 1.5 Reanalysis data sets (Dee et al. 2011) are used as initial and lateral/surface boundary conditions in the six simulations. The Optimum Interpolated (OI) Sea Surface Temperature (SST) weekly SST data, updated every 6 h is used as the oceanic boundary condition for the three simulations. Three of the experiments start from 00 GMT 01 March, 2008 while the remaining three are initialized at 00 GMT 01 January, 2008. All experiments end on 00 GMT 01 November, 2008. The analysis starts from June to allow up to a 3-5 months spin up for the avoidance of possible errors from persisting initial soil moisture properties. Each convective parameterization has two simulations with the two different initialization times. The ensemble mean of the simulations with the different initializations is used for each convective parameterization. The Adeniyi (2017) model configurations with the traditional mixture of Grell (over land) and Emanuel (over ocean) convective parameterizations are used for the simulations, with the exception of the additional simulations with the KF and Tiedtke convective parameterizations. The Tiedtke and KF are used over the whole domain for both land and ocean in order to document their respective performances. The Community Land Model version 4.5 (CLM 4.5) is available in RegCM4.5, and the Land Surface Model (LSM) has been reported for its good performance over West Africa (Diallo 2015) when used with the Emanuel convective precipitation scheme. The response of the Emanuel scheme to surface heating is usually strong, increasing when convection is triggered. The Biosphere Atmosphere Transfer Scheme (BATS) includes only two soil levels and uses the force-restore method making its response to solar heating

very strong with the release of sensible heat to the convective precipitation scheme. It thus underestimates surface albedo and overestimates net radiation (Im et al. 2014). This effect amplifies the convection in Emanuel when used together in a simulation. This corroborates the positive bias in Sahelian precipitation reported by Steiner et al. (2009) with the use of BATS and the Emanuel scheme. On the other hand, CLM includes several layers of soil. This increases the inertia of the soil surface temperature, reduces the response to solar heating and consequently the release of sensible heat to the convective precipitation scheme. As a result, convection forcing is reduced by CLM. Based on this argument and the simulation output, Gao et al. (2016) reported a more realistic climate simulation from the combination of CLM with Emanuel but an unrealistically dry bias when CLM is combined with Grell. Therefore, BATS LSM is used in the three experiments, since both Grell and CLM usually simulate dry bias, and thus a combination of both schemes will lead to an unrealistically dry bias in precipitation simulations. Emanuel usually simulates wet bias over land (Sylla et al. 2011), yet simulations over ocean tend to be more realistic (Giorgi et al. 2012). The radiation scheme used in RegCM4.5 is similar to the scheme used in the National Center for Atmospheric Research (NCAR), Community Climate System Model version 3 (CCM3). More information on the RegCM4.5 model dynamics and physics are described in Giorgi et al. (2012); Elguindi et al. (2014) and Giorgi et al. (2016).

### 3. Data and methods

#### 3.1. Validation datasets

Precipitation simulation is evaluated by comparing the simulations with two different observational datasets: 1) the monthly rainguage based gridded Climate Research Unit (CRU), time series (TS), version 3.22 data on a  $0.5 \times 0.5$  degree grid (Mitchell, Jones 2005) and 2) the Global Precipitation Climatology Project (GPCP) daily precipitation version 1DD V1.1 (mm/day) on a 1 degree grid (Huffman et al. 2001; Yin et al. 2004; Bolvin et al. 2009).

Temperature simulations are compared to two different observational datasets the CRU TS version 3.22 and UDELv4.01. Outgoing longwave radiation (OLR) simulations are compared to the interpolated National Oceanic and Atmospheric Administration (NOAA) OLR satellite retrieved data (Liebmann, Smith 1996). The OLR data is a 1 degree by 1 degree daily mean OLR flux at the top of the atmosphere. It is being derived using multispectral regression models (Ellingson et al. 1989) from high resolution infrared radiation sounder radiance observations on board NOAA television infrared observation

satellite (TIROS-N) series and meteorological operational satellite (MetOp) (Ellingson et al. 1989). Soil moisture simulations are validated using Era-Interim reanalysis data. Omega, zonal and meridional wind from Era-Interim reanalysis are also used as surrogate observed data to validate the simulated zonal ( $u$ ) wind, meridional ( $v$ ) wind, omega vertical velocity and relative vorticity. The reanalysis data are on 30 vertical levels from the surface to 50 hPa.

### 3.2. The Kain-Fritsch and Tiedtke schemes

The KF and Tiedtke schemes share common working principles. They are mass flux parameterizations (Tiedtke 1989; Kain, Fritsch 1993), based on the Lagrangian parcel method (Simpson, Wiggert 1969; Kreitzberg, Perkey 1976), and vertical momentum dynamics (Donner 1993) for the determination of instability and the properties of resulting convective clouds. Both schemes distinguish penetrative and shallow convection. However, they differ in their trigger mechanism, closure entrainment and detrainment (Kain, Fritsch 1990). The Tiedtke scheme compares the temperature of the parcel very close to the surface at ambient temperature, and triggers convection if the parcel is 0.5 K warmer than its environment. Convection triggering in the KF scheme is controlled by large scale velocity in the vertical direction. Mid-level convection above the planetary boundary layer (PBL) is also considered

in the Tiedtke scheme. However, only convection is considered above the PBL in the KF scheme.

The closure assumption in the Tiedtke scheme is based on moisture convergence, while for the KF scheme, it is based on the CAPE for an entraining parcel (Kain, Fritsch 1990; Bechtold et al. 2001). In addition, Tiedtke depends on turbulent mixing and organized inflow, while the KF scheme depends only on turbulent mixing.

The closure in KF is based on undiluted ascent, such that more CAPE is available for elimination.

It provides relatively realistic rainfall rates for a broad range of convective environments leading to a relatively better prediction of convective intensity (Kain et al. 2003) than other convective precipitation schemes. Another difference between the two schemes is that the cloud radius is variable in KF while it is fixed in Tiedtke. As a result, convective precipitation is more realistic in KF entraining/detraining plume model, as described in detail in Kain and Fritsch (1990).

## 4. Results and discussion

### 4.1. Precipitation

Seasonal (JJAS) observed and simulated precipitation [ $\text{mm}\cdot\text{day}^{-1}$ ] are shown in Figure 2. The two observational datasets for precipitation can only be compared over land (Fig. 2b), as CRU (Fig. 2a) has no record over the ocean.

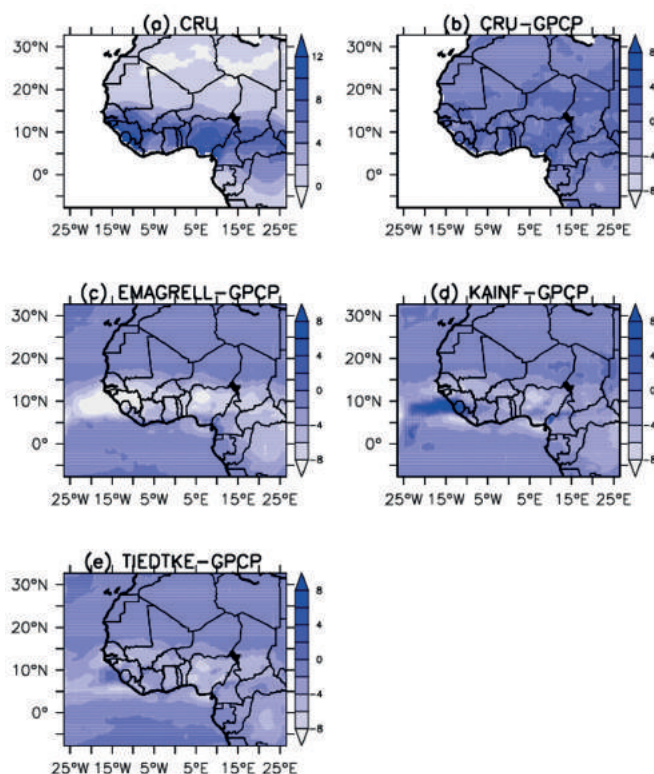


Fig. 2. Mean seasonal June-July-August-September precipitation [ $\text{mm}\cdot\text{day}^{-1}$ ] in 2008 for the (a) GPCP observations, (b) CRU observations minus GPCP observations, (c) Emanuel-Grell scheme simulations minus GPCP observations, (d) Kain-Fritsch scheme simulations minus GPCP observations and (e) Tiedtke scheme simulations minus GPCP observations

The general high values for coastal areas that decrease with distance towards the north are depicted in the two datasets. Furthermore, the two observational datasets agree on the precipitation maxima for the southwestern area of the simulation domain (Guinea highlands, Sierra Leone Mountains, Jos plateau in Nigeria, Cameroon Mountain and the coast of Nigeria). The region with the maximum west-east belt of precipitation is depicted as the inter-tropical convergence zone which undulates between 7 and 12°N latitudes in the observational data (Fig. 2a). Emanuel-Grell simulates the mean daily precipitation rate for the GPCP observation with a dry bias on land at the southern part of the simulation domain (above 5°N), where a substantial mean precipitation rate is observed. This corroborates the reported performance of Grell (Sylla et al. 2011; Adeniyi 2014). Note that the bias is lower below 5°N. The KF scheme (Fig. 2d) captures high observed precipitation for the Coastal Guinea, Sierra Leone, Liberia, and over the ocean, but with wet a bias between 5 and 10°N. It simulates little dry bias over the land and ocean in the remaining areas of the simulation domain. However, the structural pattern of precipitation is comparable with the observations; low (high) precipitation rate is simulated where low (high) precipitation rate is observed. The precipitation rate is better simulated below 10°N within the region of substantial precipitation observations (0°N-15°N, Fig. 2a). Tiedtke (Fig. 2e) simulates little dry bias over the whole area

of the simulation domain. However, it replicates the structural pattern of the observed precipitation distribution from the north to the south. Bias is lower for regions below 8°N and above 17°N on land using Tiedtke. Kothe et al. (2014) also reported dry bias in simulated total precipitation based on the Tiedtke scheme used in WRF over West Africa, specifically between -10°N and 10°N. The KF scheme simulates precipitation relatively accurately with lower dry bias than Tiedtke particularly for the south-eastern part of the simulation domain (Fig. 2). This is in line with the work of Arteta et al. (2009) and Klein et al. (2015), where KF exceeds the performance of other convection schemes used in their investigation. Yavinchan et al. (2006) used KF to improve the simulation of convective precipitation over Thailand. Dierer and Schubiger (unpublished) also reveal a better performance of the KF scheme compared to Tiedtke. The KF and Tiedtke simulate precipitation with a lower bias compared to Emanuel-Grell, and in particular, KF is relatively more accurate than the other schemes in term of lower bias.

#### 4.2. Temperature

The Figure 3 compares the observed and simulated mean JJAS near surface air temperature over West Africa. The CRU and UDEL observational data show a similar pattern of temperature distribution over the simulation domain,

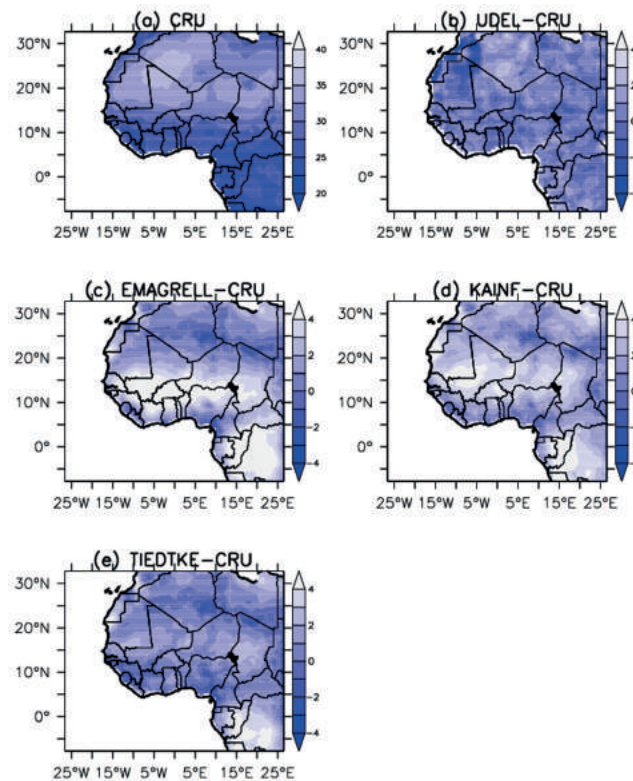


Fig. 3. Mean JJAS near surface air temperature [°C] in 2008 for the (a) CRU observations, (b) observed UDEL minus CRU observations, (c) Emanuel-Grell scheme simulations minus CRU observations, (d) Kain-Fritsch scheme simulations minus CRU observations and (e) Tiedtke scheme simulations minus CRU observations

with the exception of the extended areas of high temperature in UDEL over the northwestern part of the domain, more specifically, over southwestern (SW) Algeria (Figs. 3a and b). For all cases, a warm bias is simulated at the southern part of the simulation domain with Emanuel-Grell attaining the highest bias. All simulations capture the observed region of high temperature, the Sahara Thermal Low (STL) in SW Algeria, at approximately 25°N, with varying spatial coverage and magnitude (Fig. 3c-e). All simulations also capture the general spatial pattern of temperature, with higher temperatures at the north that decrease towards the south. The cold temperature observed at the north western tip of the land area (Morocco) is seen in all cases. In addition, a warm bias between latitudes 10 and 15°N, and also below 0°N (Figs. 3c-e), can be observed in the simulations. In general, temperature is better captured by all the convection schemes compared to precipitation. This is the norm based on the complex processes of convective precipitation.

#### 4.3. Outgoing Longwave Radiation (OLR)

The NOAA and simulated OLR are shown in Figure 4. The simulations are compared with the interpolated NOAA satellite retrieved OLR. The observed OLR pattern is such that OLR below  $240 \text{ W}\cdot\text{m}^{-2}$  lies below 12.5°N on land, while those values greater than  $240 \text{ W}\cdot\text{m}^{-2}$  are located above 12.5°N (Fig. 4a). Areas with a low OLR indicate high cloud coverage and convective activity, which should eventually lead to high precipitation. On the ocean, the region of  $\text{OLR} < 240 \text{ W}\cdot\text{m}^{-2}$  is shifted southwards (Fig 4a). The north generally has higher OLR values, which is as expected, since little or no precipitation is observed or simulated in the north (Figs. 2 and 4). Emanuel-Grell shows higher OLR values at areas with  $< 240 \text{ W}\cdot\text{m}^{-2}$  in the observations (Fig. 4b). This is revealed by positive a bias in simulated OLR between 5 and 15°N, indicating a lower convective activity, which corroborates the dry bias in simulated precipitation by the mixed convection scheme (Figs. 2c and 4b). The KF scheme outputs OLR  $< 240 \text{ W}\cdot\text{m}^{-2}$  almost at the same locations as the NOAA OLR retrievals. This is the reason for low bias in simulated OLR between 5 and 10°N (Fig. 4c). It is in line with the low bias in simulated precipitation by KF (Fig. 2d). Tiedtke slightly overestimates convective activity (medium negative OLR bias) over the SW and part of the south-eastern area of the simulation domain. The increase in convective activity in these areas is not seen in the precipitation bias (Fig. 2e). The region of slight positive bias that should be consistent with the negative OLR bias is shifted to the ocean for precipitation (Figs. 2e, 4c).

#### 4.4. Soil moisture

The correlation coefficient between simulated mean daily accumulated soil moisture at level 2 and Era-Interim soil moisture at level 2 is displayed in Figure 5. Soil moisture is well captured over the larger part of the simulation domain. However, Emanuel-Grell fails to capture the soil moisture pattern at the Sahel. Although it simulates soil moisture well for the northern areas beyond 22°N and at the savannah (8-10°N). The KF scheme captures soil moisture best at the Sahel, with a correlation value of  $\sim 1.0$  for some areas. The Tiedtke scheme performs second to the KF scheme over the Sahel. The performance of Tiedtke in soil moisture simulation is best in Central Africa, followed by KF. The simulated pattern for the savannah area (8-10°N) and the Sahel (22-28°N) is comparable with observations in all the simulations. All model simulations show a reduced wetness (not shown) north from 15-33°N relative to the south.

#### 4.5. African Easterly Jet and Tropical Easterly Jet

The AEJ and the Tropical Easterly Jet (TEJ) in Era-Interim and their simulations are shown from the vertical profile of zonal wind in Figure 6. All simulations show a negative jet around 200 hPa and 600 hPa, which can conveniently represent the TEJ and AEJ, respectively. The TEJ is observed within the documented pressure level and latitudinal locations of 100-200 hPa and 5° to 15°N, respectively (Chen, Loon 1987). However, the surrogate observed data (Era-Interim) shows the TEJ centred at 200 hPa and within  $-2$  to 25°N. This jet has a major influence on weather system development over West Africa and should be simulated correctly for applicability in predictions (Chen, Loon 1987). The vertical and latitudinal patterns of surrogate observed zonal wind is better captured by Tiedtke. Tiedtke simulates TEJ with a centre of  $< -10 \text{ m}\cdot\text{s}^{-1}$  at a pressure level close to that of Era-Interim. The remaining two runs observe the centres above 200 hPa, and with a weaker magnitude than Tiedtke. The influence of AEJ on weather systems over West Africa is reported to be the strongest of all the phenomena that affect the pattern of rainfall in the monsoon region (Cook 1999; Diedhiou et al. 1999). It is important that the AEJ be well simulated by RCMs, as it is required for climate studies, predictions and downscaling. The AEJ in Tiedtke is not strong ( $> -10$ ) though at a latitudinal location (11°N) relatively close to that of Era-Interim (14°N). Emanuel-Grell has the most intensified jet core with the highest low-level baroclinicity ( $< -10 \text{ m}\cdot\text{s}^{-1}$ ) centred at 600 hPa, yet the latitudinal location is centred on 7.5°N. The AEJ in KF is centred

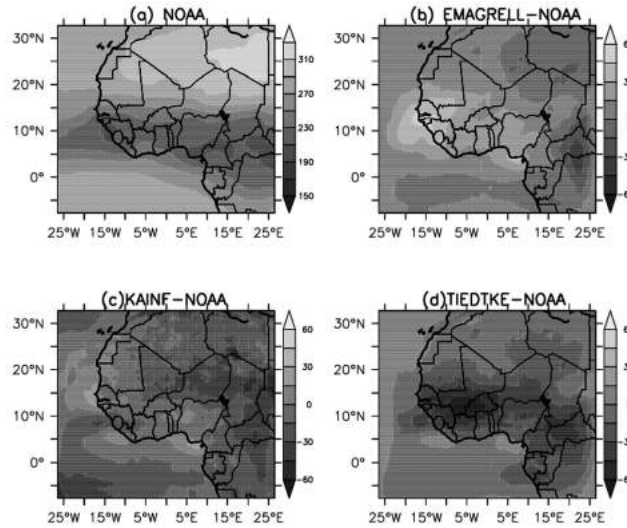


Fig. 4. Mean JJAS outgoing longwave radiation [ $\text{W}\cdot\text{m}^{-2}$ ] in 2008 for the (a) NOAA retrievals, (b) Emanuel-Grell scheme simulations minus NOAA retrievals, (c) Kain-Fritsch scheme simulations minus NOAA retrievals and (d) Tiedtke scheme simulations minus NOAA retrievals

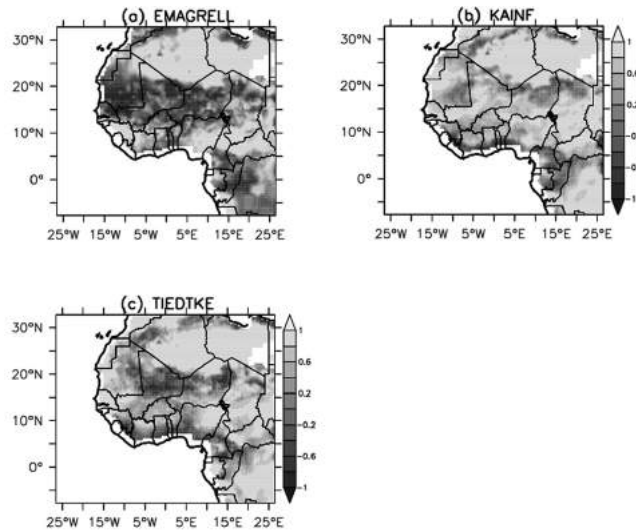


Fig. 5. Correlation coefficient between the Era-Interim reanalysis mean JJAS soil moisture and simulations in 2008 for the (a) Emanuel-Grell scheme, (b) Kain-Fritsch scheme and (c) Tiedtke scheme

at  $9^{\circ}\text{N}$ . All the simulations depict the presence of the AEJ and TEJ, but with weaker wind magnitudes and/or at different latitudinal locations. The Tiedtke simulation pattern of cross-sectional zonal wind is closest to the observations, but with a weaker AEJ.

#### 4.6. Omega vertical velocity

Omega vertical velocity simulation is compared to surrogate observed omega in Figure 7. The Era-Interim reanalysis shows a pattern of latitudinal variations in omega (Fig. 7a). This is fairly depicted in the three model runs, however, the vertical extent of the ascent (negative omega) or descent (positive omega) differs from the surrogate observed omega. The scheme with the closest simulations to the observations is Tiedtke, followed by KF, with the least closest

being Emanuel-Grell. The ascent in KF does not have enough latitudinal extension compared to Era-Interim. The simulated vertical extent of ascent in Emanuel-Grell is comparable with the Era-Interim, but with a low magnitude in the latitudinal extent. The ascent mostly leads to convection in the presence of sufficient humidity and consequent precipitation. This reveals the reason for the reduced amount of precipitation simulated by Emanuel-Grell with respect to other convective precipitation schemes (Fig. 2c).

## 5. Conclusion

In an attempt to lessen the difficulty involved in the realistic simulation of West African climate, the simulation performance of the KF and Tiedtke convection schemes in RegCM4.5 during the monsoon period over West Africa

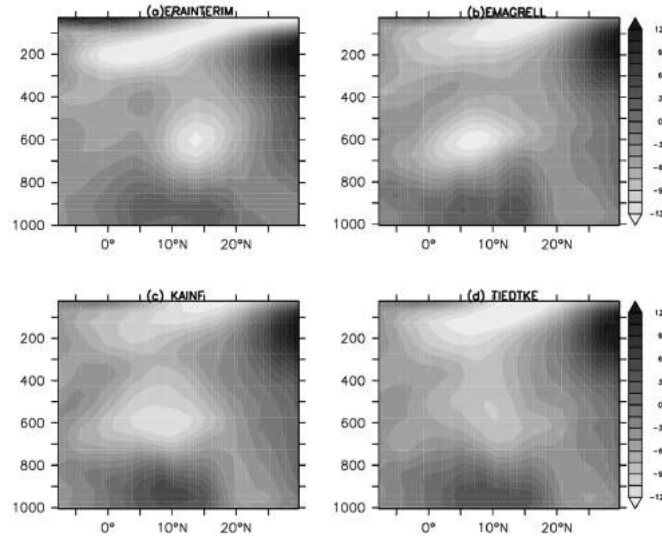


Fig. 6. The vertical profile of the zonal mean JJAS u wind [ $\text{m}\cdot\text{s}^{-1}$ ] in 2008 for the (a) Era-Interim reanalysis, (b) Emanuel-Grell scheme simulations, (c) Kain-Fritsch scheme simulations, and (d) Tiedtke scheme simulations; the zonal mean is taken between  $15^{\circ}\text{W}$  and  $15^{\circ}\text{E}$

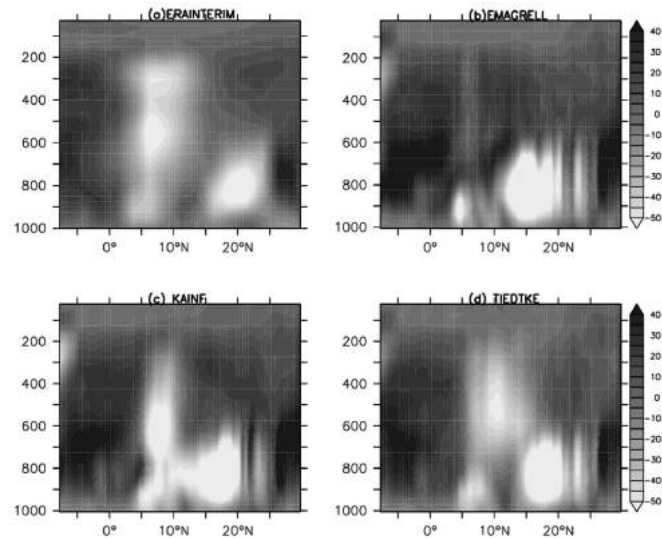


Fig. 7. The vertical profile of the zonal mean JJAS omega vertical velocity [ $\cdot 10^3 \text{ Pa}\cdot\text{s}^{-1}$ ] in 2008 for the (a) Era-Interim reanalysis, (b) Emanuel-Grell scheme simulations, (c) Kain-Fritsch scheme simulations, and (d) Tiedtke scheme simulations; the zonal mean is taken from  $15^{\circ}\text{W}$  to  $15^{\circ}\text{E}$

is tested. The simulation performance of the existing Emanuel and Grell convection schemes are also compared using Emanuel over the ocean and Grell over the land. This was carried out in order to determine the most accurate convective precipitation scheme for improved climate simulation over West Africa. The results reveal similarities in the sensitivities of both schemes, yet a wetter bias in KF exists over the ocean and the coast of Sierra-Leone and Liberia. Both schemes simulate precipitation over the simulation region with a low bias. The KF however, simulates more realistic precipitation compared to Tiedtke. The Emanuel-Grell simulated precipitation shows a dry bias for the southern area of the simulation domain. Spatial coverage of simulated precipitation in Tiedtke and KF are closer to the observations. Temperature is better simulated than precipitation, as expected, due to the complexity of cloud formation

and convective precipitation processes. The general pattern of spatial variation of temperature exhibits high temperature at the north, decreasing towards the south over West Africa. This is well captured by all the schemes. A cold region at the north western part of the simulation domain (Morocco) is also captured by all the schemes. Furthermore, the highest temperatures, located in the northwest central ( $-7$  to  $3^{\circ}\text{E}$ ;  $18$  to  $27^{\circ}\text{N}$ ) region of STL are well simulated. The simulated outgoing longwave radiation and soil moisture have a spatial coverage and magnitude that supports the precipitation simulation i.e. a low OLR in regions of high of precipitation and vice versa. High correlation coefficients exist between the simulated soil moisture and the reanalysis in most areas of the simulation domain. The AEJ and TEJ are fairly captured by all schemes. Tiedtke simulates the most accurate zonal

wind spatial pattern and profile, but with a weaker AEJ. Omega, which is directly related to descent/ascent and suppression/convection, is fairly captured by the schemes. All schemes demonstrate the latitudinal variations in omega, but with varying latitudinal, vertical extent and strength with respect to the Era- Interim datasets. Tiedtke simulates the closest spatial and vertical profile to the Era-Interim omega, followed by KF. The least accurate omega variation is produced by Emanuel-Grell. The simulations improve generally with the use of KF and Tiedtke. Prior to this study, the performance of KF and Tiedtke in RegCM4.5 in climate simulation over West Africa has not been documented. The results show the location where each schemes are more accurate than the others based on the biases, correlation coefficient and pattern. Future simulations can use the accurate schemes documented in this study for specific areas or regions in other studies. The simulation domain of this study covers only West Africa, so the results can only be applied within West Africa and not beyond. For application in other areas or regions, a similar study should be conducted over such a region. In future simulations, higher horizontal and vertical resolutions could be used for more realistic simulations.

### Acknowledgements

The RegCM4.5 used in this study was made available by the Earth System Physics Group of ICTP. Datasets from the Climate Research Unit of the University of East Anglia, the Global Precipitation Climatology Project, the University of Delaware, Era-Interim, the National Oceanic and the Atmospheric Administration are used for model evaluation.

### Bibliography

- Abiodun B.J., Adeyewa Z.D., Oguntunde P.G, Salami A.T. Ajayi V.O., 2012, Modeling the impacts of reforestation on future climate in West Africa, *Theoretical and Applied Climatology*, 110 (1-2), 77-96, DOI: 10.1007/s00704-012-0614-1
- Adeniyi M.O., 2014, Sensitivity of different convection schemes in RegCM4.0 for simulation of precipitation during the Septembers of 1989 and 1998 over West Africa, *Theoretical and Applied Climatology*, 115 (1-2), 305-322, DOI: 10.1007/s00704-013-0881-5
- Adeniyi M.O., 2016, The consequences of the IPCC AR5 RCPs 4.5 and 8.5 climate change scenarios on precipitation in West Africa, *Climatic Change*, 139 (2), 245-263, DOI: 10.1007/s10584-016-1774-2
- Adeniyi M.O., 2017, Modeling the impact of changes in Atlantic sea surface temperature on the climate of West Africa, *Meteorology and Atmospheric Physics*, 129 (2), 187-210, DOI: 10.1007/s00703-016-0473-x
- Adeniyi M.O., Dilau K.A., 2018, Assessing the link between Atlantic Niño 1 and drought over West Africa using CORDEX regional climate models, *Theoretical and Applied Climatology*, 131 (3), 937-949, DOI: 10.1007/s00704-016-2018-0
- Arteta J., Marécal V., Rivière E.D., 2009, Regional modelling of tracer transport by tropical convection – Part 1: Sensitivity to convection parameterization, *Atmospheric Chemistry and Physics*, 9 (18), 7081-7100, DOI: 10.5194/acp-9-7081-2009
- Bechtold P., Bazile E., Guichard F., Mascart P., Richard E., 2001, A mass-flux convection scheme for regional and global models, *Quarterly Journal of the Royal Meteorological Society*, 127 (573), 869-886, DOI: 10.1002/qj.49712757309
- Bolvin D.T., Adler R.F., Huffman G.J., Nelkin E.J., Poutiainen J.P., 2009, Comparison of GPCP monthly and daily precipitation estimates with high-latitude gauge observations, *Journal of Applied Meteorology and Climatology*, 48 (9), 1843-1857, DOI: 10.1175/2009JAMC2147.1
- Brown C., Greene A., Block P., Giannini A., 2008, Review of downscaling methodologies for Africa climate applications, IRI Technical Report 08-05, International Research Institute for Climate and Society, Columbia University, DOI: 10.7916/D8M04C88
- Caminade C., Terray L., 2010, Twentieth century Sahel rainfall variability as simulated by the ARPEGE AGCM, and future changes, *Climate Dynamics*, 35 (1), 75-94, DOI: 10.1007/s00382-009-0545-4
- Chen T.-C., van Loon H., 1987, Interannual variation of the tropical easterly jet, *Monthly Weather Review*, 115 (8), 1739-1759, DOI: 10.1175/1520-0493(1987)115<1739:IVOTTE>2.0.CO;2
- Cook K.H., 1999, Generation of the African easterly jet and its role in determining West African precipitation, *Journal of Climate*, 12 (5), 1165-1184, DOI: 10.1175/1520-0442(1999)012<1165:GOTAEJ>2.0.CO;2
- Dee D.P., Uppala S.M., Simmons A.J., Berrisford P., Poli P., Kobayashi S., Andrae U., Balsameda M.A., Balsamo G., Bauer P., Bechtold P., Beljaars A.C.M., van de Berg L., Bidlot J., Bormann N., Delsol C., Dragani R., Fuentes M., Geer A.J., Haimberger L., Healy S.B., Hersbach H., Hólm E.V., Isaksen L., Kållberg P., Köhler M., Matricardi M., McNally A.P., Monge-Sanz B.M., Morcrette J.-J., Park B.-K., Peubey C., de Rosnay P., Tavolato C., Thépaut J.-N., Vitart F., 2011, The ERA-Interim reanalysis: configuration and performance of the data assimilation system, *Quarterly Journal of the Royal Meteorological Society*, 137 (656), 553-597, DOI: 10.1002/qj.828
- Diallo I., 2015, Sensitivity of West African Monsoon water cycle to land surface schemes in RegCM4, AGU Fall Meeting, San Francisco, 16 December 2015, Abstract id. A33J-0322

- Diedhiou A., Janicot S., Viltard A., de Felice P., Laurent H., 1999, Easterly wave regimes and associated convection over West Africa and tropical Atlantic: results from NCEP/NCAR and ECMWF reanalyses, *Climate Dynamics*, 15 (11), 795-822, DOI: 10.1007/s003820050316
- Donner L.J., 1993, A Cumulus parameterization including mass fluxes, vertical momentum dynamics, and mesoscale effects, *Journal of Atmospheric Sciences*, 50 (6), 889-906, DOI: 10.1175/1520-0469(1993)050<0889:ACPIMF>2.0.CO;2
- Elguindi N., Bi X., Giorgi F., Nagarajan B., Pal J., Solmon F., Rauscher S., Zakey A., O'Brien T., Nogherotto R., Giuliani G., 2014, Regional Climate Model RegCM Reference Manual, version 4.5, Trieste, Italy, available at <https://gforge.ictp.it/gf/download/docmanfileversion/95/1585/ReferenceMan.pdf> (data access 13.02.2019)
- Ellingson R.G., Yanuk D.J., Lee H.-T., Gruber A., 1989, A technique for estimating outgoing longwave radiation from HIRS radiance observations, *Journal of Atmospheric and Oceanic Technology*, 6, 706-711, DOI: 10.1175/1520-0426(1989)006<0706:ATFEOL>2.0.CO;2
- Gao X., Shi Y., Giorgi F., 2016, Comparison of convective parameterizations in RegCM4 experiments over China with CLM as the land surface model, *Atmospheric and Oceanic Science Letters*, 9 (4), 246-254, DOI: 10.1080/16742834.2016.1172938
- Giorgi F., Coppola E., Solmon F., Mariotti L., Sylla M.B., Bi X., Elguindi N., Diro G.T., Nair V., Giuliani G., Turuncoglu U.U., Cozzini S., Güttler I., O'Brien T.A., Tawfik A.B., Shalaby A., Zakey A.S., Steiner A.L., Stordal F., Sloan L.C., Brankovic C., 2012, RegCM4: model description and preliminary tests over multiple CORDEX domains, *Climate Research*, 52, 7-29, DOI: 10.3354/cr01018
- Giorgi F., Solmon F., Giuliani G., 2016, Regional Climatic Model RegCM User's Guide, version 4.5, Trieste, Italy, available at <https://gforge.ictp.it/gf/download/docmanfileversion/94/1584/UserGuide.pdf> (data access 13.02.2019)
- Grell G.A., Dévényi D., 2002, A generalized approach to parameterizing convection combining ensemble and data assimilation techniques, *Geophysical Research Letters*, 29 (14), DOI: 10.1029/2002GL015311
- Grell G.A., Freitas S.R., 2014, A scale and aerosol aware stochastic convective parameterization for weather and air quality modeling, *Atmospheric Chemistry and Physics*, 14 (10), 5233-5250, DOI: 10.5194/acp-14-5233-2014
- Huffman G.J., Adler R.F., Morrissey M., Bolvin D., Curtis S., Joyce R., McGavock B., Susskind J., 2001, Global precipitation at one-degree daily resolution from multi-satellite observations, *Journal of Hydrometeorology*, 2 (1), 36-50, DOI: 10.1175/1525-7541(2001)002<0036:GPAODD>2.0.CO;2
- Im E.-S., Gianotti R.L., Eltahir E.A.B., 2014, Improving the simulation of the West African Monsoon using the MIT regional climate model, *Journal of Climate*, 27, 2209-2229, DOI: 10.1175/JCLI-D-13-00188.1
- Janjić Z.I., 1994, The step-mountain eta coordinate model: further developments of the convection, viscous sublayer, and turbulence closure schemes, *Monthly Weather Review*, 122 (5), 927-945, DOI: 10.1175/1520-0493(1994)122<0927:TSM ECM>2.0.CO;2
- Janjić Z.I., 2000, Comments on "Development and evaluation of a convection scheme for use in climate models", *Journal of the Atmospheric Sciences*, 57 (21), 3686-3686, DOI: 10.1175/1520-0469(2000)057<3686:CODAEO>2.0.CO;2
- Jones C., Giorgi F., Asrar G., 2011, The Coordinated Regional Downscaling Experiment: CORDEX. An international downscaling link to CMIP5, *CLIVAR Exchanges*, 56 (16), 34-41, <http://www.clivar.org/sites/default/files/documents/Exchanges56.pdf>
- Kain J.S., 2004, The Kain-Fritsch convective parameterization: an update, *Journal of Applied Meteorology*, 43 (1), 170-181, DOI: 10.1175/1520-0450(2004)043<0170:TKCPAU>2.0.CO;2
- Kain J.S., Baldwin M.E., Weiss S.J., 2003, Parameterization updraft mass flux as a predictor of convective intensity, *Weather Forecasting*, 18 (1), 106-116, DOI: 10.1175/1520-0434(2003)018<0106:PUMFAA>2.0.CO;2
- Kain J.S., Fritsch J.M., 1990, A one-dimensional entraining/detraining plume model and its application in convective parameterization, *Journal of the Atmospheric Sciences*, 47 (23), 2784-2802, DOI: 10.1175/1520-0469(1990)047<2784:AOD EPM>2.0.CO;2
- Kain J.S., Fritsch J.M., 1993, Convective parameterization for mesoscale models: The Kain-Fritsch scheme, [in:] *The representation of cumulus convection in numerical models*, K.A. Emanuel, D.J. Raymond (eds.), American Meteorological Society, 165-170, DOI: 10.1007/978-1-935704-13-3\_16
- Klein C., Heinzeller D., Bliefernicht J., Kunstmann H., 2015, Variability of West African monsoon patterns generated by a WRF multi-physics ensemble, *Climate Dynamics*, 45 (9-10), 2733-2755, DOI: 10.1007/s00382-015-2505-5
- Kohe S., Lüthi D., Ahrens B., 2014, Analysis of the West African Monsoon system in the regional climate model COSMO-CLM, *International Journal of Climatology*, 34 (2), 481-493, DOI: 10.1002/joc.3702
- Kreitzberg C.W., Perkey D.J., 1976, Release of potential instability: Part I, A sequential plume model within a hydrostatic primitive equation model, *Journal of the Atmospheric Sciences*, 33 (3), 456-475, DOI: 10.1175/1520-0469(1976)033<0456:ROPIPI>2.0.CO;2
- Leroux S., Hall N.M.J., 2009, On the relationship between African easterly waves and the African easterly jet, *Journal of the Atmospheric Sciences*, 66 (8), 2303-2316, DOI: 10.1175/2009JAS2988.1

- Liebmann B., Smith, C.A., 1996, Description of a complete (interpolated) Outgoing Longwave Radiation Dataset, *Bulletin of the American Meteorological Society*, 77 (6), 1275-1277, <https://www.jstor.org/stable/26233278>
- Liu P., Wang B., Sperber K.R., Li T., Meehl G.A., 2005, MJO in the NCAR CAM2 with the Tiedtke convective scheme, *Journal of Climate*, 18 (15), 3007-3020, DOI: 10.1175/JCLI3458.1
- Ma L.-M., Tan Z.-M., 2009, Improving the behaviour of the cumulus parameterization for tropical cyclone prediction: Convection trigger, *Atmospheric Research*, 92 (2), 190-211, DOI: 10.1016/j.atmosres.2008.09.022
- Mendes D., Marengo J.A., 2010, Temporal downscaling: a comparison between artificial neural network and autocorrelation techniques over the Amazon Basin in present and future climate change scenarios, *Theoretical and Applied Climatology*, 100 (3-4), 413-421, DOI: 10.1007/s00704-009-0193-y
- Mitchell T.D., Jones P.D., 2005, An improved method of constructing a database of monthly climate observations and associated high-resolution grids, *International Journal of Climatology*, 25 (6), 693-712, DOI: 10.1002/joc.1181
- Nikulin G., Jones C., Giorgi F., Asrar G., Büchner M., Cerezoto Mota R., Christensen O.B., Déqué M., Fernandez J., Hänsler A., Meijgaard E.V., Samuelsson P., Sylla M.B., Sushama L., 2012, Precipitation climatology in an ensemble of CORDEX-Africa regional climate simulations, *Journal of Climate*, 25 (18), 6057-6078, DOI: 10.1175/JCLI-D-11-00375.1
- Noble E., Druyan L.M., Fulakeza M., 2014, The sensitivity of WRF daily summer time simulations over West Africa to alternative parameterizations, Part I: African Wave Circulation, *Monthly Weather Review*, 142 (4), 1588-1608, DOI: 10.1175/MWR-D-13-00194.1
- Satyaban B., Ratnam J.V., Ratnam S.K., Behera C.J., de Rautenbach W., Ndarana T., Takahashi K., Yamagata T., 2014, Performance assessment of three convective parameterization schemes in WRF for downscaling summer rainfall over South Africa, *Climate Dynamics*, 42 (11-12), 2931-2953, DOI: 10.1007/s00382-013-1918-2
- Schumacher C., Houze Jr. R.A., 2003, Stratiform rain in the tropics as seen by the TRMM precipitation radar, *Journal of Climate*, 16 (11), 1739-1756, DOI: 10.1175/1520-0442(2003)016<1739:SRITTA>2.0.CO;2
- Simpson J., Wiggert V., 1969, Models of precipitating cumulus towers, *Monthly Weather Review*, 97 (7), 471-489, DOI: 10.1175/1520-0493(1969)097<0471:MOPCT>2.3.CO;2
- Steiner A.L., Pal J.S., Rauscher S.A., Bell J.L., Diffenbaugh N.S., Boone A., Sloan L.C., Giorgi F., 2009, Land surface coupling in regional climate simulations of the West African monsoon, *Climate Dynamics*, 33 (6), 869-892, DOI: 10.1007/s00382-009-0543-6
- Sylla M.B., Giorgi F., Ruti P.M., Calmanti S., Dell'Aquila A., 2011, The impact of deep convection on the West African summer monsoon climate: a regional climate model sensitivity study, *Quarterly Journal of the Royal Meteorological Society*, 137 (659), 1417-1430, DOI: 10.1002/qj.853
- Tiedtke M., 1989, A comprehensive mass flux scheme for cumulus parameterization in large-scale models, *Monthly Weather Review*, 117 (8), 1779-1800, DOI: 10.1175/1520-0493(1989)117<1779:ACMFSF>2.0.CO;2
- Yavinchan S., Exell R.H.B., Sukawat D., 2006, Precipitation forecasts by the new Kain-Fritsch convection scheme during the extreme precipitation event in Southern Thailand, [in:] *The 2<sup>nd</sup> Joint International Conference on "Sustainable Energy and Environment"*, 21-23 November 2006, Bangkok, Thailand, available at <http://www.jgsee.kmutt.ac.th/see1/cd/file/D-006.pdf> (data access 13.02.2019)
- Yin X., Gruber A., Arkin P., 2004, Comparison of the GPCP and CMAP merged gauge-satellite monthly precipitation products for the period 1979-2001, *Journal of Hydrometeorology*, 5 (6), 1207-1222, DOI: 10.1175/JHM-392.1



## Water vapor induced airborne rotational features

Roman Marks

*University of Szczecin, Faculty of Geosciences, Physical Oceanography Unit, Mickiewicza 16, 70-383 Szczecin, Poland, e-mail: roman.marks@usz.edu.pl*

**Abstract.** In order to study the rotational features induced by evaporating water several laboratory experiments were conducted with airborne rotary detection discs made of absorbent cotton wool and ultralight polyurethane foam discs. Measurements indicated that water vapor develops and transits into the air an upwardly directed counterclockwise rotary motion in the Northern Hemisphere, and a clockwise motion in the Southern Hemisphere. Additionally, measurements of the thermal structure of the air/water interface indicated that evaporating water may gather rotational momentum in the warmer subsurface layer. The conducted observations suggest that the process of water evaporation may be based on the grouping of some coherently spiraling molecules in the liquid phase. The interacting molecules combine their partial rotational momentums, thus allowing the top molecule to transit via the surface tension microlayer and become airborne. At the moment of evaporation, the gathered rotational energy is taken over by the free bi-hydrogen rotor-arm of the evaporating molecule that starts to revolve. Next, the water vapor-induced rotational share of the kinetic energy is likely to be redistributed among other gaseous molecules and transferred into heat (during condensation) that further energizes the airborne convective loops. In order to confirm the rotary effects induced by water vapor, several field experiments were conducted with airborne rotary detection ribbons in the Northern Hemisphere. The observations confirmed that a more enhanced counterclockwise spiraling motion of air is found with air currents under atmospheric lows of a higher relative humidity, while weaker and clockwise directed rotary dominates under atmospheric highs.

**Keywords:** rotational configuration of water molecule, airborne eddies, rotational features of greenhouse gasses

**Submitted** 24 May 2018, **revised** 6 December 2018, **accepted** 22 February 2019

### 1. Introduction

Considering that approximately 80% of solar energy is intercepted by the oceanic water up to 100 m depth, and that approximately 90% of the Earth's surface in the tropics is covered by oceans, the tropical oceanic belt accumulates most of the solar energy intercepted by the Earth. The accumulated energy is then redistributed by surface oceanic currents that transport heat mainly along the east coasts of the Earth's continents (Yu 2007), where evaporation is enhanced. This is particularly true during wintertime, from December to February in the Northern Hemisphere (NH) and from June to August in the Southern Hemisphere (SH). Moreover, the wintertime evaporation is subject to polar-ward transport, thus it contributes to the global warming of the polar regions and is especially pronounced in the Arctic, where the northward transport of oceanic currents is most extended.

When describing the efficiency of water evaporation at the global scale, the contribution of the Earth's rotary motion must be mentioned, as the lower weight of all objects at the Equator (c. 0.5%) compared to the Poles (Persson 1998). Therefore, evaporating molecules are "pulled-

outwards" from the rotating planet, particularly within the tropics. This enhances the rate of evaporation in the tropics, especially within the Intertropical Convergence Zone, located in the NH. Thus, the rotating Earth also imparts airborne eddies that are enhanced within the Hadley and Mid-latitude cells in the NH (Garbalewski, Marks 1987).

As c. 505,000 km<sup>3</sup> of water vaporizes annually from the Earth (Woś 2000), with the dominating share of evaporation (accounted for 86%) originating from the ocean, (e.g. Deese 2008), the contribution of water vapor to airborne rotary over the oceans enforces the overall circulatory motion that forms gyrating convective cells within the main tropospheric lows. Thus, water vapor induced upward motion is here presented as an important factor that contributes to convections, impacting on pressure gradients and related wind fields, as well as humidity and precipitation fields over water compartments, and less so over snow/ice and land/vegetation surfaces.

Considering that water vapor is the main renewable and vertically movable compound of air, the upward flux of moisture controls the vertical distribution of energy, which is mainly rotational, and is subtracted from the evap-

orating surfaces. This enforces the overall eddy motion of air, which is particularly enhanced under a high relative humidity and is increases with elevation. The enhanced rotary motion was also found under gusty events (Marks 1985), who correlated the rates of wind speed increments with related phase changes in wind direction.

Under an up-draft, the ambient air temperature decreases, and water vapor tends to condense on aerosols, ice crystals and droplets, particularly if these contain ions (Marks 2014). The condensed water ceases the rotary motion and forms droplets that precipitate. At that stage, the upward directed motion is replaced by the downward motion of air that begins to rotate in the opposite direction.

In the liquid phase, the displacement of a single water molecule may be based on both rotational and oscillatory motions that result in spiraling advancement performed among other molecules in fresh water, or among spherical ionic hydrates in saline waters. During such motions, a set of interactions and related dissipation of rotational-oscillatory energy, as well as the gaining of rotational energy from thermal or solar radiation, may simultaneously take place.

A single airborne water molecule may be described as a dipole object with dominating mass positioned in an oxygen nucleus (Miessler, Tarr 2003), and a much lighter hydrogen arm that may develop strong and an upwardly directed rotary movement. Such a unique configuration of a water molecule with a distinct bi-hydrogen rotor-arm is presented in Figure 1.

Assuming that the rotary motion of the H-O-H molecule is induced by a bi-hydrogen-rotor containing only 11% of the molecule mass, the bi-hydrogen arm is presented as the most distinct rotational feature that is unique among other airborne molecules. The perfect rotational configuration of the water molecule is likely induced by the H-H rotor, which may immediately initiate and then sustain the rotational motion around the oxygen atom that bears 89% of mass. Considering that the overwhelming mass

in the molecule is located in extremely small, centrally positioned nuclei of ( $D/d = 105$ ), gathering approximately 99.9% of mass (Sobkowski 1981), such an object with an angle of  $104.45^\circ$  between three centers of mass (Finney 2001) may immediately tend to initiate rotary motion, particularly when a molecule is forced into displacement or acceleration.

## 2. Experimental methods

This section presents the methodological approach used to detect the rotational features of evaporating water molecules. The features were firstly sensed in laboratory conditions by means of airborne rotary detection discs suspended over evaporating water surfaces and are presented in Section 2.1. Next, the experimental method used to trace airborne turbulence effects during field observations is presented in Section 2.2.

### 2.1. Laboratory experiments

The first set of experiments was conducted using airborne rotary detection discs (ARDD), made of an absorbent cotton wool of 60 mm diameter, 2-3 mm thickness and a weight of 0.2-0.26 g. Discs were suspended c. 2-6 cm above a clean tap water surface, allowing continuous absorption of just the evaporating water molecules and the inception of upwardly directed rotational features. Discs were suspended over water by a 2-3 m long polyamide thread and placed in the center of a water vessel covered by a hood with an open slot. Such a setup allowed for the observing of the rotational features steadily integrated to discs that absorbed the upwardly directed water vapor and started to rotate.

A second set of experiments was conducted using ultra-light polyurethane foam discs of 36 mm diameter, 1 mm thickness and a 0.05-0.07 g weight. Discs were suspended

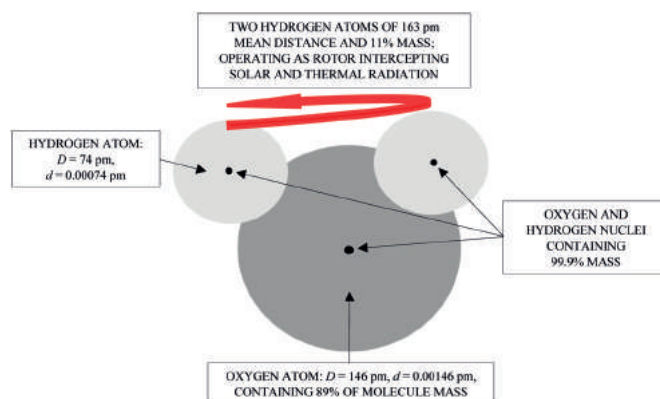


Fig. 1. A perfect rotational configuration of a water molecule posing a light bi-hydrogen rotor-arm revolving around a centrally positioned and heavy oxygen nucleus, along with marked diameters of the oxygen and hydrogen atoms ( $D$ ) and their nuclei ( $d$ ) (Finney 2001; Silberberg 2006)

on c. 10 cm long polyamide thread attached to a light Styrofoam float of 3-4 mm diameter, placed in the center of a petri dish with a centrally positioned slot. After filling the petri dish with a small volume of distilled water, the float and the thread were free to rotate, since the disc and the float were suspended by means of water surface tension (Fig. 2).

The ultralight discs were more sensitive to the detection of upwardly directed rotary motion of water vapor due to an approximately 4 times lower weight compared to cotton discs. During the experiments, the disc rotary was observed or recorded by a camera. Special attention was given to limit the turbulent motion in the room prior to each observation, thus experiments started after the airborne rotary indicated by the exposed disc ceased. The most visible effects were observed under a relatively low air humidity ( $RH$ ) of 30-60% and water temperatures c. 5-20°C higher than the air temperature in the laboratory room. Typically, tap water evaporated from a clean glass or plastic container placed below the suspended disc. In the preceding phase of the experiments, both water/air and disc motions ceased. During the experiments, air temperature ( $Ta$ ) and air relative humidity ( $RH$ ) were measured using thermocouples, while water surface temperature ( $Tw$ ) and temperature radiated by the discs ( $Td$ ) were measured with a pyrometer. Typically, all thermal parameters were traced before and just after exposition. The majority of observations were conducted within the latitudes of 53°40'N-54°30'N, while one experiment was conducted in the SH on the plane flying from Bali (Indonesia) to Kuala Lumpur (Malaysia) within the latitudes of 5°S to 6°S.

To detect the direction of the water molecules rotary motion in the SH, a simplified setup was used. During this experiment, a cotton disc was positioned at the center of a c. 30 cm<sup>3</sup> glass vessel over semi-still water covered by a hood under an air temperature of c. 20-22°C.

## 2.2. Field experiments

Field observations were completed in several locations, with the majority situated within the coastal zone of the Pomeranian Bay (southern Baltic Sea) from 2015 to 2018. In order to trace the direction of the rotary motion that composed the airborne eddies, a set of ribbons exposed in a vertical profile, visualizing the “undulation” of air currents, was used. Ribbons with a width of 1 cm and a length of c. 2.5 m were kept in the air on a 20 cm long polyamide thread fastened to a mast or pole and exposed in a vertical profile at 2, 4, and 6 m (Fig. 3A) or at 2, 2.5 and 3 m above the ground (Fig. 3B). The ribbons allowed for the obser-

vation of the dominating direction of the rotary motion composing the airborne eddies and related sequence changes in wind direction, as well as for the counting of the number of turns performed by each ribbon during the exposition.

In addition, air temperature, air humidity and atmospheric pressure were recorded by a routine meteorology station operated by the Marine Station of the University of Szczecin, located in Międzyzdroje at the Pomeranian Bay (southern Baltic Sea coast). Special attention was given to observing the rotational behavior of the ribbons under gusty winds.

Over 60 observations were completed from 2015 to 2018. However, the obtained results are rather qualitative since they were collected in two locations on the beach using a mast with a height of 6.5 m (Fig. 3A), or on the top of a dune using a wooden pole reaching only 3.5 m elevation (Fig. 3B). In addition, each experiment was conducted under different atmospheric settings that configured turbulent motion in air, reflecting changes in spatial and temporal baric conditions, as well as fluctuations in air relative humidity.

## 3. Results

This section presents both the results obtained during laboratory investigations conducted under different thermal conditions (Section 3.1), and those obtained during field observations performed in the coastal zone within the southern Baltic Sea (Section 3.2).

### 3.1. Laboratory experiments

The first set of experiments was conducted using cotton discs under conditions of similar water and air temperature ( $Tw/Ta/Td$  of 19.0/19.6/19.6°C) and a  $RH$  of 40%. The observations revealed that a disc placed above evaporating water collected vapor and slowly developed a rotational motion depicted by a 1/4; 2/4; 3/4 and full disc turn, completed in 5, 9, 12 and 28 minutes of exposition, respectively. The motion of the disc indicated a very slow, but visibly counter-clockwise (CCW) direction of the rotary motion that was observed from above the disc.

After exposition, the set of thermal parameters  $Tw/Ta/Td$  was 18.5/19.6/17.5°C, indicating that the temperature of the water surface decreased by c. 0.5°C, while the temperature of the exposed disc decreased by 2.1°C, indicating that the disc absorbed a significant portion of water vapor, which in turn started to evaporate from the disc. The obtained results confirmed that the water molecules under transition from a liquid to a gaseous phase develop a dominating CCW rotary motion in the NH.

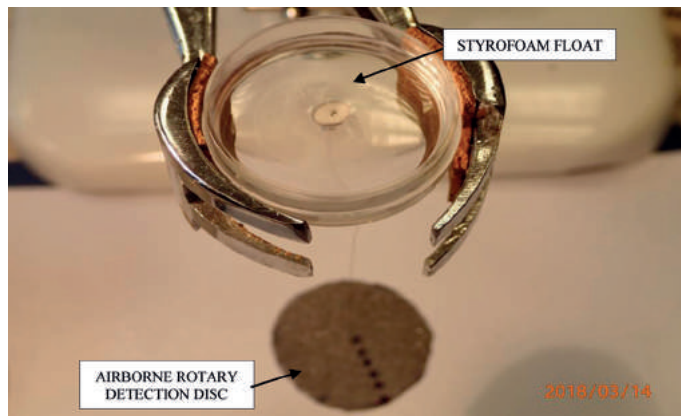


Fig. 2. Experimental setup used to sense the rotational features of water vapor with the exposition of an ultralight airborne rotary detection disc, kept in place by a Styrofoam float placed in a petri dish with central slot



Fig. 3. Sets of ribbons indicating spiraling motion in air under atmospheric low (A) and high (B) pressure patterns at 2, 4, 6 m (A) and at 2, 2.5, 3 m above the ground (B)

An additional experiment was conducted at the initial conditions of water temperature  $T_w = 30^\circ\text{C}$ , and  $(T_a) = (T_d)$  at  $19.8^\circ\text{C}$ . During the observation, the disc developed a faster rotational motion compared to the experiment under  $T_w \approx T_a$  ( $19.0$ - $19.6^\circ\text{C}$ ), and performed 1, 2, 3 and 4 full turns in a CCW direction in 5, 10, 14 and 19 minutes, respectively. After 20 minutes of exposition, the set of  $(T_w)/(T_a)/(T_d)$  parameters were observed as  $28.0/19.9/19.0^\circ\text{C}$ , and the surface temperatures of ARDD decreased by  $0.8^\circ\text{C}$ , indicating that the cotton material was saturated by water vapor, which started to re-evaporate.

Next, a set of experiments with  $(T_w - T_a) > 20^\circ\text{C}$  were conducted after previously boiling and then cooling water to  $60$ - $40^\circ\text{C}$ . During experiments, a vessel with steaming water was placed below a disc, which started to rotate almost instantly. This observation indicated that the disc developed a more vigorous rotational motion, although after 2-3 CCW turns, completed during 2-3 minutes, the rotary movement typically attenuated. This showed that the rotary movement of the disc introduced in the first phase (when the water vapor was collected into the disc

pores) was subsequently reduced due to condensation and re-evaporation. Thus, the results also indicated that the process of condensation may be based on a sudden reduction of rotary motion.

Observations in the SH indicated that evaporating water molecules develop a clockwise (CW) directed rotary motion, the opposite direction to that detected in the NH.

Experiments with ultralight polyurethane discs confirmed the above reported direction of water vapor induced rotational features; however, the rotary motion was significantly faster. For example, a disc exposed 6 cm over the water at a room temperature of  $25^\circ\text{C}$  performed 1-2 turns during the first 20 seconds of exposition, and the number of turns recorded in the first phase of the experiments typically increased with the temperature of water.

### 3.2. Field experiments

Three ribbons exposed in a vertical profile allowed for the observation of the direction of rotary motion and for the qualification of a scale of eddies. In general, the read-

ings conducted under low pressure conditions indicated that CCW spiraling eddies dominate (see Fig. 3A). Typically, the number of circuits performed by the ribbons during 1-minute intervals at a 3 m elevation exceeded 10 under atmospheric lows of high wind speed conditions and dropped to 0-2 under the atmospheric highs of low wind speed. In general, the recorded number of turns also tended to increase with elevation, as indicated by the blue ribbon exposed at 6 m above ground (see Fig. 3A). In addition, during gusty events, the frequency of rotaries significantly increased. In general, with increasing wind speed and a rise in air humidity, the number of airborne eddies increased. However, the airborne rotational activity was also found to depend on a static stability (difference in temperature between water and air) that typically overshadowed the impact of air humidity under  $T_w < T_a$ .

In contrast, under high pressure conditions, the dominance of clockwise directed airborne eddies was observed in Międzyzdroje (southern Baltic Sea coast). In addition, the comparison of ribbon turns observed under moderate wind speed conditions indicated roughly 3-5 times more CCW turns of ribbons during 5-minute intervals conducted under the low-pressure conditions with an air humidity of 95-98% compared to CW turns performed under high pressure systems with an air humidity of 50-55%. However, under the transition from low to high baric conditions, both directed rotaries were observed, with a dominance of CCW eddies at lower elevations.

#### 4. Discussion

In this section, the rotational principles that configure the process of water evaporation, and the concept of bi-hydrogen bounds that allow the grouping of the water molecules, are presented (Section 4.1). The related airborne interactions that impact the turbulent eddies in the troposphere are elucidated in Section 4.2. The subsequent process of water vapor condensation is presented as a result of rotational energy dissipation in Section 4.3. In addition, the rotational configuration of greenhouse gases is presented in Section 4.4.

##### 4.1. Rotational principles of evaporation

Considering that water molecules transit an upwardly directed rotary movement, it is inferred that the process of water evaporation operates on rotational principles that are assembled in a warmer sub-surface microlayer that is placed just below the air-water interface layer (Fig. 4).

Furthermore, considering that evaporating water transits a very high and precise rate of energy, it is assumed

that the process of evaporation may be based on the rotational momentum. Thus, the combined partial momentums collected by the polymeric chain of  $(^H-O^H)_n$  allow the transition of water molecules via a typically colder surface tension layer and evaporate i.e. one molecule become airborne (Fig. 4).

Considering that water molecules in the subsurface and in the immediate surface tension layer may have a fairly random character (Holman, Stone 2001), and that the surface tension layer is typically colder than the layer below, it is inferred that the process of lining-up and spiraling water molecules originates in the warmer subsurface layer (Fig. 4). In this way, the rate of rotational energy gathered by the grouped  $(^H-O^H)_n$  polymers may randomly exceed the energy of the hydrogen bounds (Silberberg 2006). Thus, the evaporating molecules undergo wrenching with a substantial (rotational) share of energy. This energy is subtracted from the immediate water surface microlayer. Therefore, the rotational hydrogen bounds termed here may operate based on hydrogens-to-oxygen-to-hydrogens rotational bounds or rotational fastening, i.e. the arms of interacting molecules may be positioned perpendicularly to each other (Fig. 5).

In this way, the grouping of water molecules may be based on the rotational interactions among bi-hydrogen rotors, inducing bi-hydrogen bounds combining the energy of contributing molecules. This allows for the top water molecule to evaporate with the share of rotational energy that is taken over. However, the anticipated rotational principles of bi-hydrogen bounds and related interactions among water molecules need to be confirmed with future experiments.

Furthermore, it is inferred that all processes of evaporation that transit a substantial rate of latent heat may operate on the same rotational principles that allow the liquid to gaseous phase change for water molecules.

##### 4.2. Water vapor induced rotational interactions

The molecular weight of  $H_2O$  is 18 u, and a single water molecule is 1.55 lighter compared to 28 u for  $N_2$  and 1.77 lighter compared to 32 u for  $O_2$ . Thus, water vapor may play an enforcing role in airborne motion (Holman, Stone 2001). For example, the oscillatory motion of water molecules in the air, as estimated by the root mean square speed ( $rmss$ ) according to equation (1) (Lerner, Trigg 1991), ranges from 2,215 km/h to 2,322 km/h at air temperatures of 0°C and 27°C, respectively (Table 1). The values of  $rmss$  were calculated as follows:

$$rmss = (3kT/M)^{1/2} \quad (1)$$

Table 1. Estimated values of oscillatory motion (*r<sub>mss</sub>*) under temperature of 0°C and 27°C for some gases in troposphere

Gas	Atomic Mass <i>M</i> in u	<i>r<sub>mss</sub></i> in km/h under temperature of	
		0°C	27°C
N <sub>2</sub>	28	1,776	1,861
O <sub>2</sub>	32	1,661	1,741
H <sub>2</sub> O	18	2,215	2,322
CO <sub>2</sub>	44	1,409	1,485
CH <sub>4</sub>	16	2,349	2,462

where:  $k = 1.38064852(79) \times 10^{-23}$  is a Boltzmann constant (J/K),  $T$  is absolute temperature (K), and  $M$  is the atomic mass of gaseous molecule (u).

The calculated values of *r<sub>mss</sub>* due to H<sub>2</sub>O are significantly higher compared with that estimated for N<sub>2</sub> and O<sub>2</sub> (1,776 km/h, 1,861 km/h for N<sub>2</sub> and 1,660 km/h, 1,741 km/h for O<sub>2</sub>, at air temperatures of 0°C and 27°C, respectively). The comparison of these values indicates that water molecules that are both lighter and c. 500 km/h faster may enforce the motion of other airborne molecules, i.e. N<sub>2</sub> and O<sub>2</sub>, which are slower. This indicates that the motion of air is driven by faster spiraling and oscillating molecules of water vapor.

In addition, the airborne water intercepts thermal radiation that is directed upward from typically warmer water or land surfaces (Fig. 6). Thus, the net motion of air is further enhanced by water molecules, which interacts with nitrogen and oxygen diatomic molecules that are more abundant in the air. For example, the maximum concentration of water vapor molecules in the air above the water surface under an air temperature of 10°C indicates that a single water vapor molecule interacts with 67 dinitrogen and 16 dioxygen molecules. However, at a temperature of 30°C, a single H<sub>2</sub>O interacts with 9 N<sub>2</sub> and 5 O<sub>2</sub> molecules. Thus, by increasing the air temperature, the air parcels develop a more enhanced rotary motion that is further energized by the continuous flux of rotating H<sub>2</sub>O molecules and the related inception of thermal radiation.

Considering that the flux of water vapor is the main factor enforcing the upward motion in the air, its integrated flux generates baric gradients and a related compensative transport of air towards the centers of atmospheric lows. However, since gaseous molecules are in free motion, the airborne transport of air parcels is modified by the Coriolis force (Persson 1998), as well as continental/land barriers and surface roughness, along with

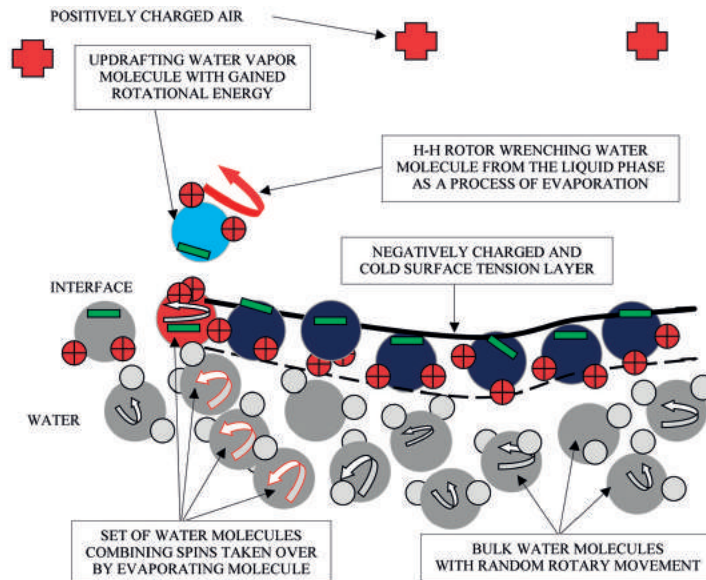


Fig. 4. Simplified cross-section of the air-water interface introducing the process of evaporation as a result of the rotational grouping of water molecules in the liquid phase, allowing for the transition of a top molecule via the surface tension layer with a precise portion of rotational energy (latent heat)

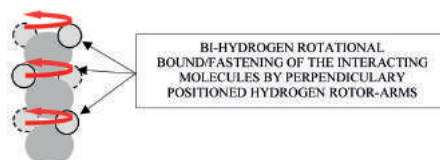


Fig. 5. General scheme of perpendicular bi-hydrogen-to-oxygen-to-bi-hydrogen (<sup>H</sup>O<sup>H</sup>)<sub>3</sub> rotational bound, allowing the grouping of successive water molecules that combine their partial rotational spins in the liquid phase

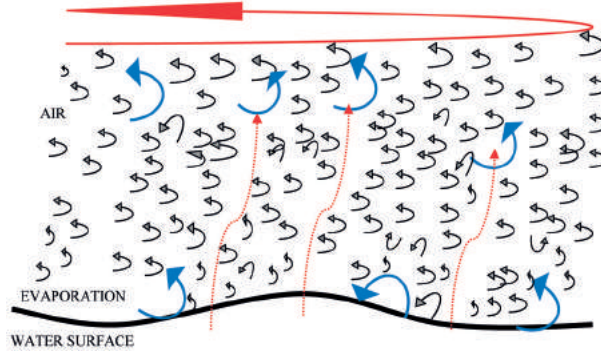


Fig. 6. Illustration of the counter-clockwise, convective rotational-translational motion of water vapor in the NH (marked by blue arrows), enforcing motions of  $N_2$  and  $O_2$  (marked by small black arrows) that may result in a whirling parcel of air (marked by large red arrow). In addition, a contribution of thermal radiation intercepted by water vapor is indicated by broken red arrows

thermal stability of air/water, air/land, air/snow/ice or air/vegetation interfaces. The superimposition of these factors shapes a spatial and temporal motion of air parcels from molecular-microscopic to macroscopic scales within the whole column of troposphere, as shown in Figure 6.

Both, the upward motion and the “memorized” Coriolis momentum of the Earth rotary movement (at a given place of evaporation) forces the water vapor molecules, as well as all air parcels, to whirl in the CCW or CW direction in the respective NH or SH, as depicted in Figure 6. This enforcement is continued until the water molecules condense and release the rotational share of latent heat. From this stage onwards, the previously uplifted air molecules descent and slowly develop a clockwise rotary motion in the NH, and counterclockwise in the SH.

The  $r_{mss}$  values listed in Table 1 may be used to calculate the rate of energy due to oscillatory motion  $E_o$ , which can be estimated using equation (2):

$$E_o = M(r_{mss})^2/2 \quad (2)$$

A comparison of  $E_o$  with “latent heat of water vaporization ( $lh_{wv}$ ) that range from 2,250 J/g to 2,259 J/g under the water temperature of 0°C and 100°C respectively, indicates the overwhelming domination of the rotational share of energy due to  $lh_{wv}$  that significantly exceeds the energy due to oscillatory  $E_o$ , under all ranges of tropospheric temperatures.

### 4.3. Water vapor impact on airborne eddies

The outlined research allows to perceiving airborne turbulence as induced by rotating and up-drafting water vapor molecules. Thus, steadily renewed fluxes of water vapor generate the upward motion of air that originates at the molecular scale and is proceeded up to a thousand km eddies, forming cyclones and hurricanes. In addition, water vapor intercepts heat that is radiated by typically

warmer surfaces. However, at all stages of airborne turbulence development, a share of rotational energy is simultaneously dissipated among other molecules, until the condensation of water occurs. This ceases the upward motion in the troposphere, and from this stage onwards, the energy dissipation goes downward, is proceeded from large to smaller eddies, and finally to the molecular interactions and heat (Kraus 1972).

The above presented research may be of significance for the more precise modeling of water vapor related tropospheric processes, which are rotational (non-linear) in nature. Note that water vapor fluxes also depend on humidity gradients at the water/air interface, i.e. the lower values of humidity enhance the evaporation. On the other hand, the rate of evaporation also increases with rising water temperatures and wind speed e.g. (DeCosmo et al. 1996; Smith et al. 1996). In this way, air continuously exchanges and equilibrates water vapor partial pressures and relative humidity acts as an interactive factor controlling both upward and downward directed water vapor fluxes (Kraus 1972; Yu 2007; Kolendowicz et al. 2016; Szejewski et al. 2017).

### 4.4. Rotational configuration of greenhouse gasses

All greenhouse gases also pose a distinct rotational shape. For example,  $CO_2$ ,  $CH_4$  and trace gases such as:  $O_3$ ,  $NO_2$ ,  $N_2O$ , and  $SO_2$ . Thus, they may effectively absorb heat (IPCC 2014). Among them,  $CH_4$  (the second important greenhouse gas, considering its present impact on warming the troposphere) is particularly regarded as the most efficiently absorbing constituent. Since  $CH_4$  poses active rotors composed of four hydrogens, the molecule absorbs heat even more efficiently than water. In addition, the limited methane weight of 16u offers enhanced vertical penetrability in the troposphere (Table 1).

Moreover, the comparison of water vapor atomic mass and  $r_{mss}$  with other tropospheric gases (Table 1) indicates

that among greenhouse gasses, significantly heavier CO<sub>2</sub> may tend to compose the lower troposphere, while substantially lighter CH<sub>4</sub> and H<sub>2</sub>O may be responsible for the updraft and radiative forcing in the whole troposphere. On the other hand, warmer troposphere enhances evaporation of water that further contributes to the interception of heat, and enhances the net effect of radiative warming. Therefore, CO<sub>2</sub> and CH<sub>4</sub> mainly mediated the trapping of heat and should be regarded as the primary cause of warming, as pointed by Storch and Bray (2017). On the other hand, enhanced evaporation of water has a more indirect, but dominating contribution. In general, the rotational absorption of heat by gaseous compounds in the troposphere contributes to the overall energy budget of the Earth.

In general, the rotational features induced by water vapor and greenhouse gases call for more expanded and interdisciplinary research. In particular, the unique rotational configuration of hydrogen rotors seems to be responsible for the gain and distribution of rotational "latent" heat by water vapor and greenhouse molecules in the whole column of troposphere. However, the most profound question refers to the rotational nature of solar and thermal radiation, and the overall importance of rotary motion in biological molecules as well as in the whole Universe.

## 5. Conclusions

Laboratory and field experiments allowed for the following conclusions:

- The process of water evaporation may be based on the unique ability to combine partial spins of a few water molecules after gaining a sufficient energy that allow the top molecule to transit via the surface tension microlayer.
- The evaporating water molecules develop counterclockwise rotational kinetics in the Northern Hemisphere, while the clockwise rotary motion in the Southern Hemisphere needs to be confirmed.
- At the moment of evaporation, the water molecules gain a very high share of rotational energy, denoted as "latent heat of evaporation", which is transited by the rotating bi-hydrogen arm into the air.
- The rate of "latent heat" carried with water vapor may be shared with other molecules in air and is simultaneously renewed by the interception of thermal radiation.
- During the process of condensation, the rotational energy due to water molecules is released in the form of radiation that corresponds to the "latent heat of condensation".
- An increase in air humidity enhances the number of spiraling eddies configuring airflows.
- Further interdisciplinary experiments tracing the unique ability of water molecules to assembly, sustain and transit rotary, especially in biological molecules, are needed.
- The outlined results may be used to enhance the production of electricity from wind farms especially that operating over the high water evaporative areas as maritime and coastal locations.

## Acknowledgement

Ms. Anna Marczak is acknowledged for conducting experiment over the Southern Hemisphere.

## Bibliography

- DeCosmo J., Katsaros K.B, Smith S.D, Anderson R.J., Oost W.A., Bumke K., Chadwick H., 1996, Air-sea exchange of water vapor and sensible heat: The Humidity Exchange Over the Sea (HEXOS) results, *Journal of Geophysical Research*, 101 (C5), 12001-12016, DOI: 10.1029/95JC03796
- Deese W.C., 2008, UXL Encyclopedia of Science, available at <https://www.encyclopedia.com>
- Finney J.L., 2001, The water molecule and its interactions: the interaction between theory, modelling, and experiment, *Journal of Molecular Liquids*, 90 (1-3), 303-312, DOI: 10.1016/S0167-7322(01)00134-9
- Garbalewski C., Marks R., 1987, Latitudinal characteristics of aerosol distribution in the near surface air over the Atlantic. *Acta Geophysica Polonica*, 35 (1), 77-86
- Holman J., Stone P., 2001, *Chemistry*, Nelson Thornes, 314 pp.
- IPCC, 2014, *Climate change 2014: Synthesis Report, Contribution of Working Groups I, II and III to the Fifth Assessment Report of the Intergovernmental Panel on Climate Change*, The Core Writing Team, R.K. Pachauri, L.A. Meyer (eds.), IPCC, Geneva, Switzerland, 151 pp.
- Kolendowicz L., Taszarek M., Czernecki B., 2016, Convective and non-convective wind gusts in Poland, 2001-2015, *Meteorology Hydrology and Water Management*, 4 (2), 15-21, DOI: 10.26491/mhwm/63636
- Kraus E.B., 1972, *Atmosphere-ocean interaction*, Oxford University Press (Clarendon), 275 pp.
- Lerner R.G., Trigg G.L., 1991, *Encyclopedia of Physics*, 2<sup>nd</sup> edition, VHC publishers, 1408 pp.
- Marks R., 1985, Attempt of regarding the effect of wind gustiness of the sea dynamic roughness as a factor of mass exchange through air-sea interface, *Polish Polar Research*, 6 (4), 459-474

- Marks R., 2014, Bubble rotational features – preliminary investigations, *Journal of Oceanography and Marine Research*, 2 (4), DOI: 10.4172/2332-2632.1000128
- Miessler G.L., Tarr D.A., 2003, *Inorganic chemistry*, 3<sup>rd</sup> edition, Prentice Hall, 720 pp.
- Persson A., 1998, How do we understand the Coriolis Force, *Bulletin of the American Meteorological Society* 79 (7), 1373-1385, DOI: 10.1175/1520-0477(1998)079<1373:HDW UTC>2.0.CO;2
- Pidwirny M., 2011, Evaporation, [in:] *Encyclopedia of Earth*, J. Cutler (ed.), available at <http://editors.eol.org/eoearth/wiki/Evaporation> (data access 05.03.2019)
- Silberberg M.S., 2006, *Chemistry. The molecular nature of matter and change*, 4<sup>th</sup> edition, McGraw-Hill, 1088 pp.
- Smith S.D., Katsaros K.B., Oost W.A., Mestayer P.G., 1996, The impact of the Hexos programme, *Boundary-Layer Meteorology*, 78 (1-2), 121-141, DOI: 10.1007/BF00122489
- Sobkowski J., 1981, *Chemia jądrowa*, PWN, Warszawa, 251 pp.
- Storch H., Bray D., 2017, Models manifestation and attribution of climate change, *Meteorology Hydrology and Water Management*, 5 (1), 47-52, DOI: 10.26491/mhwm/67388
- Szwejkowski Z., Dragańska E., Cymes I., Timofte C.M., Suchecki S., Craciun I., 2017, Rainfall and water conditions in the region of the upper glacial in Europe, *Meteorology Hydrology and Water Management*, 5 (1), 15-28, DOI: 10.26491/mhwm/65538
- Woś A., 2000, *Meteorologia dla geografów*, Wydawnictwo Naukowe PWN, Warszawa, 313 pp.
- Yu L., 2007, Global variations in oceanic evaporation (1958-2005): The role of the changing wind speed, *Journal of Climate*, 20 (21), 5376-5390, DOI: 10.1175/2007JCLI1714.1



## Learning to cope with water variability through participatory monitoring: the case study of the mountainous region, Nepal

Santosh Regmi, Jagat K. Bhusal, Praju Gurung

*Society of Hydrologists and Meteorologists (SOHAM Nepal), New Baneshwor, Kathmandu, Nepal, e-mail: sregmi11@yahoo.com*

Zed Zulkaffi

*Universiti Putra Malaysia, Serdang, Faculty of Engineering, Department of Civil Engineering, 43400 UPM Serdang, Selangor Darul Ehsan, Malaysia*

Timothy Karpouzoglou

*Public Administration and Policy Group, Wageningen University & Research, Hollandseweg 1, 6706 KN Wageningen, Building 201, de Leeuwenborch, Netherlands*

Boris Ochoa Tocachi, Wouter Buytaert

*Department of Civil and Environmental Engineering, Imperial College London, South Kensington Campus, London SW7 2AZ, United Kingdom*

Feng Mao

*University of Birmingham, School of Geography, Earth and Environmental Sciences, Edgbaston, Birmingham B15 2TT, United Kingdom*

**Abstract.** Participatory monitoring allows communities to understand the use and management of local water resources and at the same time develop a sense of ownership of environmental information. The data generated through participatory monitoring of stream flow and rainfall generate evidences to corroborate local people's experiences with changing water resources patterns. In this study we evaluate the potential of participatory monitoring of hydrological variables to improve scarce water supply utilization in agriculture. The case study site is the Mustang district in Nepal, which is located in the Upper Kaligandaki River Basin in the Himalayas with unique and complex geographical and climatic features. This region is characterized by a semi-arid climate with total annual precipitation of less than 300 mm. Water supply, agricultural land, and livestock grazing are the key ecosystem services that underpin livelihood security of the local population, particularly socio-economically vulnerable groups. An analysis of the measured stream flow data indicate that annual flow of water in the stream can meet the current crop irrigation water needs for the agricultural land of the research site. The data provide local farmers a new way of understanding local water needs. Participatory monitoring would contribute to an optimization of the use of ecosystem services to support economic development and livelihood improvement.

**Keywords:** ecosystem services, water, participatory monitoring, irrigation, agriculture, Nepal

**Submitted** 29 August 2018, **revised** 16 December 2018, **accepted** 28 March 2019

### 1. Introduction

#### 1.1. Climate change and mountain water resources

Mountains are unique regions for their scenery, their climates, their ecosystems and the large portfolio of ecosystem services they supply. Mountains provide key resources for human activities well beyond their natural boundaries; and they harbor extremely diverse cultures in both the developing and the industrialized

world (Beniston 2005). Mountain regions provide more than 50% of the global river runoff, referred to as "water towers", sources of fresh water for the adjacent low land while more than one-sixth of the Earth's population relies on glaciers and seasonal snow for their water supply (Viviroli et al. 2007). The impacts of climatic change on hydrology are likely to have significant repercussions not only in the mountains themselves but also in populated lowland regions that depend on mountain water resources

for domestic, agricultural, energy and industrial purposes (Beniston 2003; Eriksson et al. 2009). It is widely believed that an increase in the agricultural water use efficiency is the key to mitigating water shortage and reducing environmental problems (Deng et al. 2015) and data scarcity is still a major bottleneck for improving water resources management (Buytaert et al. 2012). There is growing evidence of increasing frequency of climatic extremes (both precipitation and temperature) especially in mountainous regions (Gautam et al. 2013). Viviroli et al. (2011) concluded that more detailed regional studies and more reliable scenario projections are urgently required for effective management of mountain water resources.

Water based ecosystem services are particularly important to the economies of low-income developing countries (WRI 2003). In the Nepal Himalayas rangelands are considered critical ecosystems that provide multiple services which support local livelihoods (Aryal et al. 2013). Water plays a key role to improve the livelihood through increasing agricultural production by improving the irrigation mechanism of agricultural land. The primary exposure to climatic variability is decrease in snowfall, showing most adverse impacts on livelihoods of study area (Kagbeni Village Development Committee). Except for glacial melt water, snow is the most crucial input factor for cultivation as well as food for animals (Duns 2011).

Here, agriculture is an important production sector inextricably linked to the availability of water and watershed-based natural resources. In the country 65.6% of people are engaged in agriculture (Ministry of Agricultural Development 2013) for their livelihood and economic supplement. About 50% of the cultivable area is irrigated. Although the country is rich in water resources, its utilization and management are very limited. A preliminary assessment reveals that forest and water resources have significant livelihood impact at the household level in Nepal, especially for the poor. The increased availability of irrigation water has helped in agricultural production and productivity, cropping intensity, and increased employment opportunities for the poor households (Pant et al. 2005). Local communities in the mountain areas are already experiencing major changes in climate, which have manifested in terms of reduced water availability, rising temperatures, and a shift in growing seasons – all of which impact agricultural production (Kotru et al. 2014).

Warming trends have been observed in most of the Himalayan region and the Middle Mountains (Shrestha et al. 1999). The precipitation extremes show increasing trends in total and heavy precipitation events in Nepal and there is strong evidence that precipitation intensity will also increase in the future (Baidya et al.

2008). Nepal receives 79.6% of annual precipitation during monsoon season whereas 4.2, 3.5 and 12.7%, during post monsoon, winter and pre monsoon seasons respectively (PANO 2009). The temporal and spatial variability in precipitation induced by causes of climate changes resulted into snow accumulation in the ground and field; and snow melt acceleration due to rises in temperature has underpinned the diminishing of water sources and has resulted into conflicts among the households in the mountain area (Bhusal, Subedi 2014).

Apple farming in Nepal started in the Kali Gandaki Valley before the 1960 but first commercial Apple farming in Nepal started at Marpha, Mustang where horticultural farm was established and introduced new varieties of apples and production methods in 1966. A high market value followed by climatic suitability, labor scarcity, and land availability was found to be responsible for the expansion of apples (Manandhar et al. 2013). Because of this reasons many farmers practice a combination of apple farming and cereal crops. The introduction of new crops having different water and irrigation needs, combined with changing precipitation patterns may challenge the traditional methods of irrigation and water management practiced within the community.

## 1.2. Participatory monitoring for water resources management

"Participatory research" is an approach which argues that research has greater relevance when representatives of the targeted beneficiary group (or groups) actively participate in the research process (Sutherland 1998). Monitoring of resource use by professional scientists is often costly and hard to sustain, especially in developing countries, where financial resources are limited (Danielsen et al. 2005). Successful implementation of community-based monitoring programs requires ongoing partnerships between local communities, individuals, and development and state monitoring institutions including academic or government scientists (Johnson et al. 2014). Local community-based monitoring is particularly relevant in developing countries, as it can provide high quality data to help fill observational voids, support rapid decisions to solve the key threats affecting natural resources, and empower local communities to better manage their resources and refine sustainable strategies to improve local livelihoods (Danielsen et al. 2009; Walker et al. 2016). The concept of participatory approach becomes an increasingly popular approach to undertake science and conduct monitoring, because it provides an excellent way to engage with the public whose participation allows for cost-

-efficient collection of data (Buytaert et al. 2014; Pocock et al. 2014).

Volunteer monitoring programs may have positive effects on developing local capacity in relatively short time frames, significantly increase the political participation, personal networks, and feelings of community connectedness among volunteers (Overdevest et al. 2004). A high degree of community engagement is likely to result in observable changes in policy towards sustainable development and environmental management because policy-makers and local stakeholders were included in the same process (Fraser et al. 2005).

For instance in a rural Andean watershed, the participatory monitoring approach involving youth in research stimulated improved management of both land and water resources, and could be applied in other small rural watersheds in developed or developing countries (García, Brown 2009). Other research on integrated participatory approach of monitoring at the Upper Ruvu Sub-Basin, Tanzania perceived that, local people's help in identifying appropriate sites for installation of instruments, protecting the instruments against any type of vandalism and minimizing the costs for installation and monitoring (Gomani et al. 2010).

Intricate social institutions have emerged in various mountain regions to manage the common water resources for irrigation (Bandyopadhyay, Gyawali 1994). Water resource management is a multi-actor, multi-scale, and dynamic decision making process in a complex socio-ecological system (Elsawah et al. 2015). The community involvement in the citizen science projects is of benefit to policy makers (Hollow et al. 2015).

A major challenge of resource in participatory monitoring systems is their maintenance over the long term, especially if they empowered local community to promote greater local autonomy in resource management but are vulnerable to funding uncertainty and challenged institutional power relationships (Constantino et al. 2012). To overcome the limitations, stakeholder participation in water resources monitoring must be institutionalized, creating organizational cultures that can facilitate processes where goals are negotiated and outcomes are necessarily uncertain. In this light, participatory processes may seem very risky, but there is growing evidence that if well designed, these perceived risks may be well worth taking (Reed 2008).

## 2. Research question

The major research question of this study is: how does a participatory monitoring approach of rainfall

and stream-flow data collection help develop a better understanding and quantification of water resources availability and improve their management at the local scales? In this paper, we aim to provide a hydrological analysis of the availability of water as a key ecosystem service and local distribution mechanisms. An assessment of water availability is the first important step in places where low flows are predominant within the entire range of discharge. To do this we follow a participatory approach, whereby non-scientists are actively involved in the process of generating new knowledge regarding their water resources.

## 3. Methodology

### 3.1. Selection of study area

Based on available literature a case study site at the scale of a Village Development Committee (VDC)'s administrative area was selected; where livelihoods are fundamentally dependent on ecosystem services. A predefined set of criteria was used which included population density, pasture land, livestock, agricultural production, irrigated land and per capita income. Based on those data, the Kagbeni VDC was selected as our research site. A socioeconomic house hold survey of the five villages of Kagbeni VDC was carried out. The socioeconomic survey of five villages of Kagbeni VDC (Kagbeni, Tiri, Pakling, Phalyak and Dhakarjhong) covered 55.2% of the total households. On the basis of all these findings the villages of Dhakarjhong and Phalyak were finally selected as the case study sites where people are mostly depended on ecosystem services and are particularly vulnerable in terms of social, economic and environmental pressure such as out migration, loss of agricultural land and water scarcity. Current management of the available water makes it insufficient for irrigation and drinking in both villages.

### 3.2. Engagement of local population

To ensure that the community people participates in the data collection procedures related to stream flow, precipitation and temperature data, the local users were involved from the initial design stage of the monitoring. The research direction undertaken was developed based on their perception of change to local water resources, such that this perception could eventually be verified scientifically through the data collected. This research would therefore be highly tailored to the interest and concerns of the local community. In most of the underdeveloped countries, rural local communities are mostly illiterate and ignorant of the reasons they are adopting primitive tools

for livelihoods. Participatory monitoring includes understanding of methods and data uses by the local through formal and informal consultation with professionals.

A meeting was organized in the community hall of Phalyak and Dhakarjhong to discuss about the work plan. The meeting included the participation of Mukhiya the traditional leader of the local community, users group, youth club, village members, teachers and local social/political leaders. The meeting was used as a platform to agree on a proposal for the establishment of stream flow monitoring station at the Lumbhuk stream and rainfall measurement in the village. The expected output and benefit of stream-flow and rainfall measurement were described in the meeting that is the possibility to calculate the volume of water flowing in the stream, which could guide further planning and designing on water use management and land use management. The concept of participatory monitoring was adopted for the stream flow and rainfall measurement to ensure the monitoring is sustainable for the long term by developing the sense of ownership within the community. During the meeting the community decided to provide its support to the monitoring activities. They appointed an "observer", someone in charge to read and record the daily water level data from the staff gauge installed at Lumbhuk stream and rainfall volume from the rain-gauge installed at Phalyak village. They took responsibility for protecting the instruments from any kind of harm such as theft, litter accumulation, or extreme climatic events. The meeting also agreed to financial support from the research project for payment to the observer for their contribution up to one year. It is to be believed that after one year local people will be encouraged to collect the data without any salary as they identify the importance of these data for improving their activities and supporting resource and risk management. Three local youths were trained in each study sites who worked as observers. The village Mukhiya had supervised the observer and all activities of monitoring of stream-flow and rainfall measurement. The objective of the research was to generate knowledge through participatory approach with capacity building of local communities. At the end of the research period, communities were enabled to gather data at the local level and, maintain and operate the equipment installed at sites. Researcher visited sites in November 2017 and found that the locals were operating equipment and using data whenever they needed.

### 3.3. Data

Data related to social and livelihood dimension were collected which are interlinked with each other. Several

field visits were carried out to conduct socio-economic surveys, key informant interviews and resource mapping together with members of the community to get detailed information about the prevailing situation.

Water resource data are obtained from two sources. The first source of data is from the described participatory monitoring. The second source of data is from the Department of Hydrology and Meteorology (DHM) of Nepal. We have used stage and discharge data of Lumbhuk stream for one year and available precipitation data of Jomsom climate station.

## 4. Study area

The case study area includes Dhakarjhong and Phalyak villages of Kagbeni VDC which lies in the central Mustang region of Nepal (Fig. 1). The study villages are located at 3,210 m and 3,145 m elevation respectively. These two villages are the adjoining watered area of a single stream called Lumbhuk. The area receives strong wind and intense sunlight. It falls in the rain shadow of the Annapurna ranges that acts as barrier for orographic rainfall resulting in less than 300 mm annual rainfall. This is five times lower than the average annual precipitation of Nepal.

There are 33 households in Dhakarjhong village and 48 households in Phalyak village with total population of 191 and 249 respectively<sup>1</sup>. The primary occupation of the people is agricultural business. The total agricultural land area is 20 hectare and 60 hectare respectively. Another 12 hectare and 15 hectare is left barren due to the insufficient water for irrigation.

The water catchment area of Lumbhuk stream is 10 km<sup>2</sup> at to the newly proposed stream gauging station, which is located 1.5 km upstream from the villages. The catchment elevation ranges from 3,257 m to 5,630 m above mean sea level (Fig. 1). The geographical structure of the catchment is rock land with little vegetation.

## 5. Setup of participatory monitoring

### 5.1. Instrumentation

Monitoring consists of a stream gauging station and a rainfall station at the research site. The stream gauging station consists of two types of stage recording instruments: Pressure level sensors (Aquistar PT2X) with data logging system are used for automatic water level monitoring. This instrument measures and records pressure, which is transformed to stream level, temperature of water, and time of recording. It has an accuracy of 0.05%. Full

<sup>1</sup> Kagbeni VDC Profile, 2011, Village Development Committee

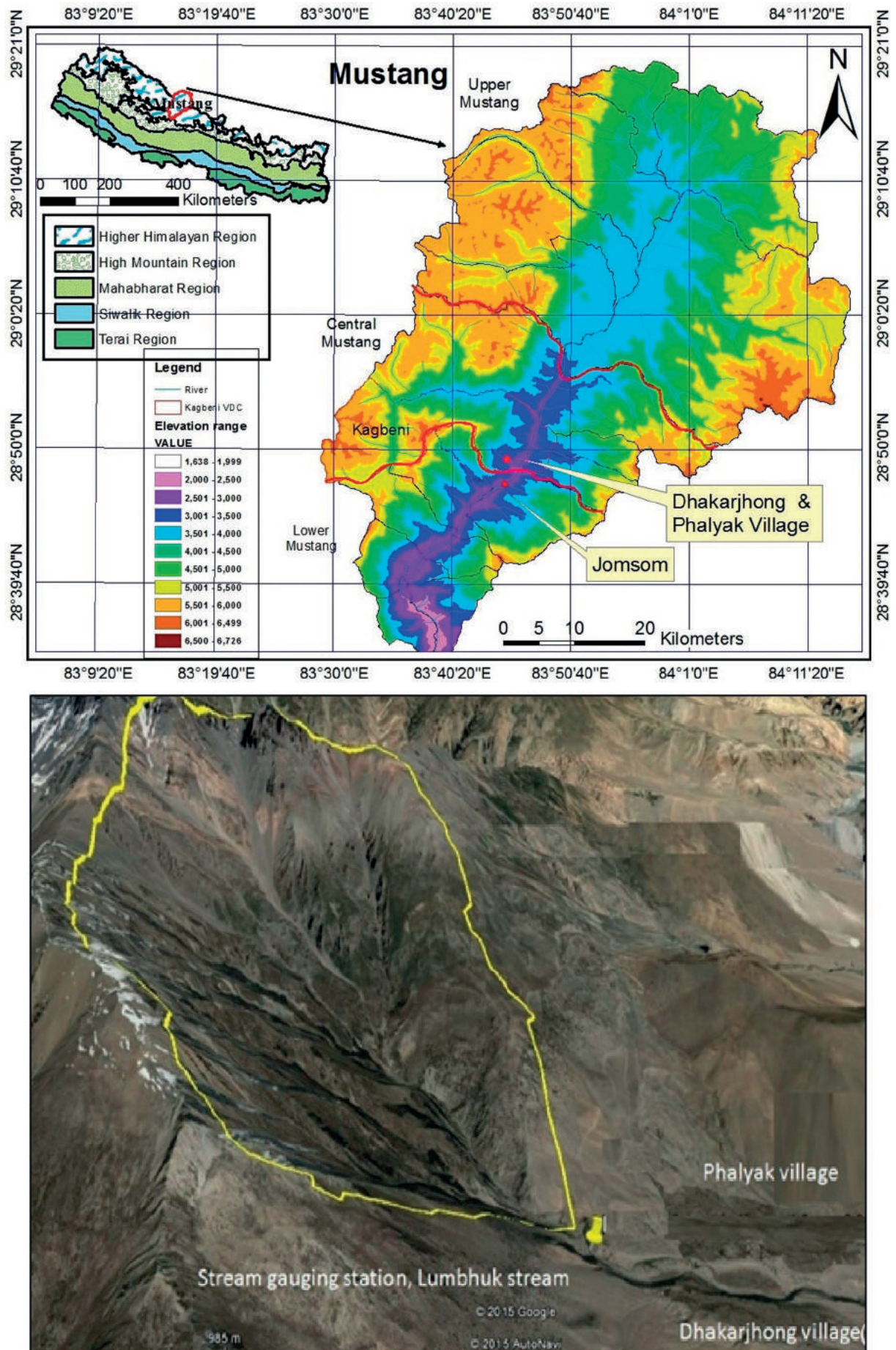


Fig. 1. The location of study area: the Dhakarjhong and Phalyak villages are located in the Kagbeni Village Development Committee jurisdiction under the Mustang District Development Committee

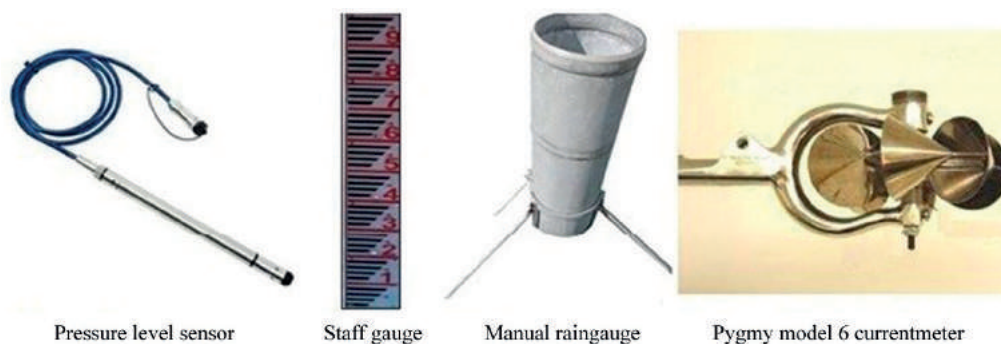


Fig. 2. Type of instruments installed for stream flow and rainfall measurement



Fig. 3. Local people's participation in monitoring started at Lumbhuk stream

scale with 4MB of data memory. The recorded data remain safe in case of power failure. The data can be easily downloaded with the help of specialized software installed in the computer. The sensor was set to records the water level data on a 15-min interval.

The manual instrument is a staff gauge made of reinforced plastic fiber. It is graduated with 1-cm scale with total length of 1 meter (Fig. 2, 3). Both the instruments are attached in the bank along with the stream. Manual instruments allow detect and correct errors in the automatic sensors, and to provide a proxy for the continuous measurements.

Each day at 08:00 AM an "observer" reads the stage of water level and cumulated rainfall and keeps these records. A general training on reading the stage data, measuring rainfall and maintenance of the instruments is provided to the observer after installation.

Water current velocity measurements in the stream were carried out to calculate the discharge. The Pygmy model 6 current meter was used for the velocity measurement of stream flow with its corresponding stage height to develop the rating curve of the stream.

An 8-inch diameter galvanized iron manual rain-gauge was installed at the research site, consisting of outer cylinder and inner cylinder. Rainfall that is collected by an outer funnel is channeled to an inner cylinder within and outer protective cylinder. The water collected in the inner cylinder is quantified with the help of a submerged measuring scale. The measuring scale is graduated in mm scale.

Additionally, hydro meteorological data from stations maintained by the Department of Hydrology and Meteorology (DHM) over that region were also collected simultaneously.

Firstly we started with the installation of monitoring instrument for stream flow measurement at Lumbhuk stream (Fig. 3). This first assessment of the stream flow is essential to understand the approximate water availability.

Local people learnt about the instruments, data collection method, use of those data and objective of installation. They guided the selection of site to install the instrument and managed the observer to carry out for the daily observation.

The youth club member also showed keen interest in these activities and take responsibility to took care of the instrument through regular inspection.

## 6. Understanding communities water requirements

People's involvement from the very beginning is important. During several field visits we sought their engagement through discussion, identifying problems and solutions. One area that local people found important was water availability for irrigation. In water scarce areas, water becomes a more limited resource than land. The crop water requirement is higher in areas which are hot, dry, windy and sunny. Lower values are found when it is cool, humid and cloudy with less wind. Surface irrigation is the common practice in the study sites. Lining canals

and preventing leaks from the distribution system have helped greatly for increasing the water use efficiency.

We observed through questionnaire, semi-structured interviews and transect walks the strong linkages between irrigation and poverty reduction in the study area. Our detail situation analysis (Regmi, Gurung 2015) shows that irrigation is understood to benefit the poor people through higher production, higher yields, lower risk of crop failure, year-round farm and also to switch from low-value subsistence production to high-value market-oriented production. For details about the work that preceded the participatory monitoring, the reader is referred to (Bhusal et al. 2017).

Irrigation canal mapping of Dhakarjhong and Phalyak village was carried out with the villagers during the field visit of the research site (Fig. 4). The main canal which starts from intake to pond is made up of concrete whereas the distribution canals are earthen. Such canals are built on demand following traditional practices, which leads to an excessive and sub-optimal number. In both villages, a storage pond is made to collect water. Generally, from 5 PM evening to 5 AM of next day, farmers store water in the pond and start irrigating their field during day time. These ponds, like the canals, have earthen beds promote to infiltration losses. The sizes of the ponds are small and not have high potential to store water during the surplus flow in the stream. Due to a decreasing water flow, farmers construct sub-terraces in the same field for a more efficient irrigation.

## 7. Results and discussion

### 7.1. Reception and management of the monitoring by the communities

The findings from the survey revealed that out of total sampled household, 100% people of Dhakarjung village and 88% people of Phalyak village are dependent in agriculture respectively for their livelihood whereas in the neighbouring villages Kagbeni and Tiri, locals have alternative for their income as business which is either by tourism or trading. A socio-economic survey concluded that the livelihood of the community is based on agricultural practices, which at the same time need water for irrigation. Yet based in the survey, water available for agricultural use is insufficient and furthermore stream-flow is decreasing. As a consequence, agricultural production is decreasing while cultivable land remains barren.

To gather evidence on this water uncertainty, the collective decision was made with local farmers to carry out measurements of stream-flow and rainfall to quantify the volume of water with respect to irrigation water need. The monitoring of stream-flow and rainfall is not easy to carry out without the participation of local people. Installation, monitoring and data collection by an appointed observer in a salary basis presented different difficulties. Basically, it might create unsustainable data collection due to lack of economic availability, no ownership of community, difficulty in protection of instruments and their

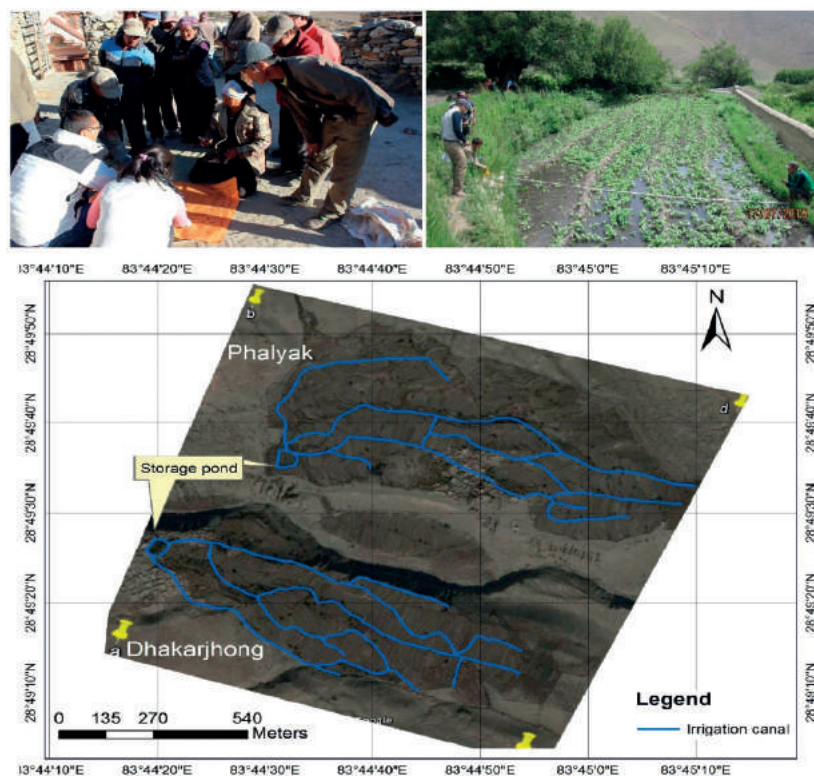


Fig. 4. Meeting with local stakeholders and member of youth club for Irrigation canal mapping (Dhakarjhong and Phalyak) and measuring the size of the field to quantify the volume of water required for irrigation per unit area of land

maintenance, lack of knowledge generation and support in decision making process to the local people. Keeping all these difficulties in mind we engaged local people in the monitoring process which made our research objective fulfilled. Participatory monitoring is the systematic recording and periodic analysis of information that has been chosen and recorded by insiders with the help of outsiders. Communities are given knowledge to collect data (example: river water level and 24 hours precipitation) with the help of developed monograph to find the amount of water they need for each crops as per season.

Participatory monitoring helps in understanding the use of local water resources and develop a sense of ownership of the information generated by concerned communities. Increased hydrological understanding further provides the basis for communities to manage their own water resources more wisely in light of increasing pressures such as climate change. The data generated from monitoring of stream flow and rainfall for example, are evidences of the challenges that communities are experiencing on a daily basis with changing pattern of river flow and rainfall. The information generated builds up their confidence and trust in their own observations as well as makes them more proactive in their communication with government agencies. This kind of participatory monitoring has been carried out in the direct involvement of local people but there are other stakeholders (VDC, DDC, local government agencies, NGOs) who have been involved indirectly.

Involvement of several stakeholders in the monitoring processes creates the basis for effective knowledge transfer between stakeholders and for local people to bridge with the government's activities. Our study also identified that strong local leadership becomes very important for participatory monitoring to ultimately succeed in the long term. While in this study, the research team had an important role in motivating the different stakeholders such as through organizing meetings and ensuring broad attendance, in the long term this has to be done by the stakeholders themselves. State institutions need to work very closely with the communities as monitoring requirements and needs are re-evaluated in light of a changing climate and livelihood requirements.

## 8. Local water allocation arrangements

Dhakarjhung and Phalyak villages share water on a daily basis. Agreeing to this, members of Dhakarjhung village get water for two days (48 hours) whereas; members of Phalyak village get water for three days (72 hours). Again the turn goes to Dhakarjhung village, which is a continuous routine not on the basis of week and season.

More than 50 years ago, each household divided the water for irrigation based on the Dhongba<sup>2</sup> or inherited area of land. In this way, each Dhongba gets 12 hours of water for irrigation. As the household property is divided into multiple Dhongba, the allocation of irrigation water get divided as well.

At present each household gets water for 3 to 18 hours depending on the size of their land (Dhongba). Each family gets their next turn of irrigation when the entire household in village is over with their turn which normally happens after 30/35 days.

One Dhongba has the right to sell their agricultural land either with allocated water hour for irrigation. This is a completely informal mechanism decided upon traditional law. Two Dhongba can share their water in return of something. For example, if one Dhongba has enough water and another has less water, the first one will provide certain hours of water to the second and in return the second has to pay back in terms of labor or water in the next season or provide Jhopa for plowing.

The study area has some aspects to be considered before implementing water use management techniques. The region is windy, sunny and arid. The soil is sandy stirring with high infiltration rate. Water collection ponds and irrigation canals are earthen, with large and sub-optimal canal networks. The size of the ponds are too small to store a sufficient amount of water during the surplus time. The region is highly vulnerable to climate change with clear symbols of changing pattern in precipitation. The intensity of precipitation is increasing with decreasing event durations. The rate of snowfall in winter season is also uneven and changing, creating the imbalance in storage of water in the catchment. Considering the above climatic and physiographic extremes and existing practices of the research site, appropriate water use management and land use management strategies should be concede.

## 9. Stream flow data analysis linked with long term temperature and precipitation trend

An analysis of temperature data from 1981-2012 of Jomsom station (DHM) shows that the annual average maximum and minimum temperature observed are 17.7°C

<sup>2</sup> Dhongba in Dhakarjhung and Phalyak (or central Mustang) are those who get ancestral property right (eg. If there is three son in family; the middle son becomes a monk and he gets one agricultural land (plot) from his parents (which is called Dhashing); the eldest and youngest sons receive the remaining properties of their parents and divide the Dhongba in two sections. For instance, if parents own one full dhongba, it will be divided into 50/50% after their separation and each sibling will get only half dhongba, if the parents own 2 dhongba, one dhongba will belong to each child after the separation.

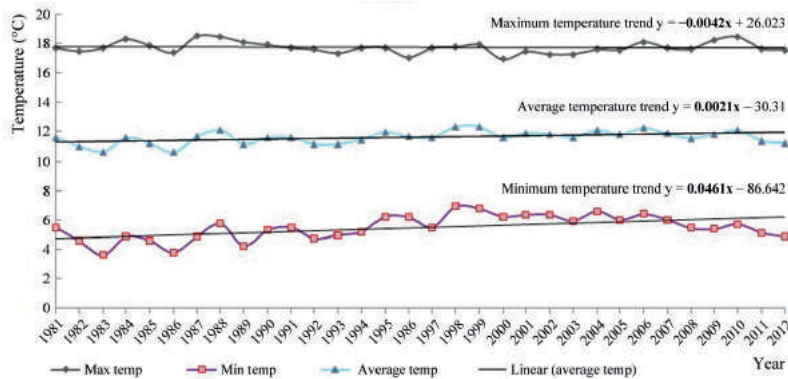


Fig. 5. Temperature trend of Jomsom station data from 1981-2012 indicates the increasing trend, particularly minimum and average temperature is increasing

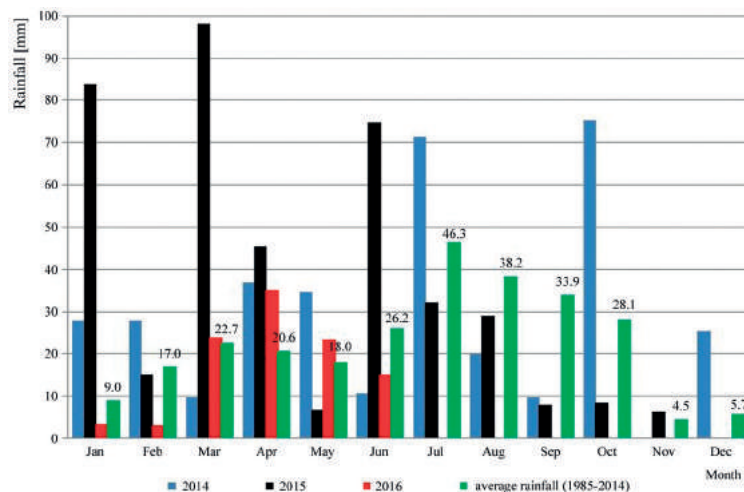


Fig. 6. Precipitation at Jomsom station of 2014, 2015 and 2016 shows the irregularity with long term average precipitation, which might be the symbol of climate change and has impact on steady stream flow

and 5.5°C, respectively (Fig. 5). The analysis showed that the temperature is in increasing trend supporting the public opinion on climate change events including reducing snow cover area, changing pattern of precipitation, unsteady stream flow and decrease in water sources.

The analysis of rainfall data from 1985 to 2014 of Jomsom station (DHM), which is the representative station for our case study site shows the average annual total rainfall as 270 mm. The case study area receives 53.5 percent of annual rainfall during the monsoon season (June, July, August, September) whereas 12.2, 11.8 and 22.5 percent during post monsoon (October, November), winter (December, January, February) and pre monsoon (March, April, May) seasons respectively (Fig. 6). The perennial flow of water in the stream depends on the accumulation of snow fall over the watershed during winter. The research (Chapagain, Bhusal 2013) on water balance of Upper Kali-gandaki Basin shows a negative trend.

The monitoring of Lumbhuk stream flow has started from July, 2015. One year recorded stage data of that stream is presented in Figure 7. The stage of the stream is continuously decreasing throughout the year except slightly

increasing in some months. The trend of stream flow with respect to rainfall shows an interesting trend. There was high precipitation (in the form of snow) on the last month of 2014 and starting months of 2015 which support the major release of water continuously up to July of 2015 (Fig. 6). After that, the precipitation decreases marking an overall decrease in water level in the stream. This provides a good evidence to support the public opinion and our assumption on the nature of stream flow. This supports that there are basically two types of precipitation; the winter precipitation in the form of snow and the summer precipitation in the form of rain that occurs in the catchment. Both play a significant role in feeding water in the stream.

Less precipitation observed in the last month of 2015 and starting month of 2016 (in the form of snow) as a result there is less storage of water in the catchment and less water flows in the stream. This could be linked to climate change but there might be other regional climatic fluctuations not captured by this study. The above scenario is also supported by the view of local youth, Mr. Govinda Bista, member of youth club in Phalyak said: »*accumulation*

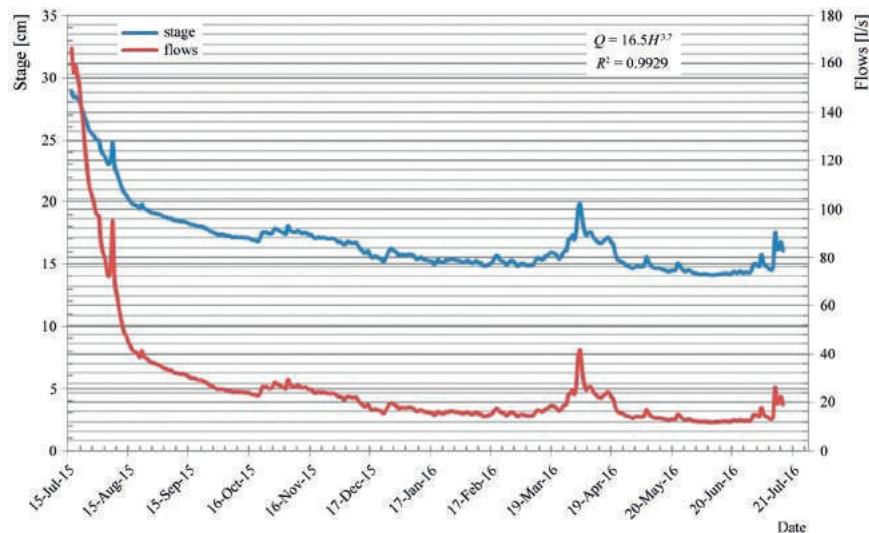


Fig. 7. Calculation of discharge based on the measured stage height with the help of rating equation developed from measured discharge with the corresponding stage height; Lumbhuk stream

of snow fall that occurs in the winter season (December, January and February) is the major source of water that discharges throughout the year».

The stage-discharge relation (rating) of the Lumbhuk stream has developed from the measured discharge and corresponding stage height. The discharge of the Lumbhuk stream at different stage height is calculated with the help of a rating equation as shown in Figure 7.

The calculated monthly discharge in the stream of the period from July 2015 to June 2016 is shown in Table 1. The higher discharge is observed in July and lower discharge in June. The calculated monthly discharge and measured monthly rainfall of the same period are used to estimate the runoff coefficient. The total monthly rainfall volume produced by average monthly rainfall (1985-2014) in the basin is multiplied with the runoff coefficient to get an average monthly runoff in the stream. The total precipitation from July 2015 to June 2016 is 193 mm was used to calculate the runoff coefficient. The calculated runoff coefficient is relatively lower in some months. Therefore, the actual runoff may potentially be larger than the calculated average runoff as shown in Table 1.

Local crop calendar was prepared in participatory approach with local farmers of the research site. The crop calendar includes different activity perform in one cropping time. Type of crop, dung transfer, land preparation, seeding, weeding, irrigation and harvesting are the main activity perform in one cropping time. Local crop calendar, guidelines of Food and Agriculture Organization of the United Nations (Brouwer, Heibloem 1986) were used to identify the information related to the types of crops, growing months, and total growing days. All these information are used to calculate crop water

need and irrigation water need for different crops which are commonly practices in our study site. The calculated values are shown in Table 2.

The available irrigation water is slightly lower for naked wheat and barley but potato has higher deficit of irrigation water. For pulses, buckwheat and apple the irrigation water is sufficient. The farmers are growing a mix of crops instead of a single crop. About 33% of agricultural land is used to cultivate apple. Cultivation of potato is carried out in the limited land and priority is given to buckwheat. This indicates that the available water in the stream is appropriate to other crops for irrigation. The available irrigation water has been calculated based on the average precipitation (Fig. 5) that occurs in the basin which may not be same in all the year.

## 10. Conclusions

The study was mainly focused in two facets, participatory monitoring of water resources and analysis of the data obtained from participatory monitoring. Participatory monitoring has established mutual advantage to both the researchers and local people. For the researcher, it is one of the easiest way for site selection, installation of instruments, protection of the instruments and data collection because presence of local people are vital in all steps. For the local people, it develops ownership, know their resources and get involve with scientists in scientific experiment to be a part of citizen science for knowledge generation that supports decision making processes.

The analysis of the stream flow data indicates that the flow of water can meet the irrigation water needs for the crops that are in practice in the available agricultural

Table 1. Average runoff in the Lumbhuk stream

Stream-flow monitored (month and year)	Calculated monthly discharge [m <sup>3</sup> ]	Calculated monthly discharge [mm]	Rainfall [mm]	Runoff coefficient	Month	Average rainfall (1985-2014) [mm]	Rainfall volume [m <sup>3</sup> ]	Average runoff Runoff coefficient × Rainfall volume [m <sup>3</sup> ]
Jul-15	195,579	19.6	32.2	0.61	July	46.3	463,467	281,504
Aug-15	140,978	14.1	29.1	0.48	August	38.2	382,367	185,242
Sep-15	78,892	7.9	8.1	0.98	September	33.9	338,533	329,722
Oct-15	66,984	6.7	8.4	0.80	October	28.1	281,300	224,318
Nov-15	65,915	6.6	6.2	1.06	November	4.5	44,667	47,487
Dec-15	51,901	5.2	5.7	0.91	December	5.7	57,233	52,113
Jan-16	44,065	4.4	3.3	1.33	January	9.0	89,667	119,731
Feb-16	38,832	3.9	3.2	1.22	February	17.0	169,600	205,809
Mar-16	46,542	4.7	23.8	0.20	March	22.7	227,367	44,463
Apr-16	58,523	5.9	35.2	0.17	April	20.6	206,100	34,266
May-16	36,712	3.7	23.3	0.16	May	18.0	179,567	28,293
Jun-16	31,736	3.2	15.2	0.21	June	26.2	261,833	54,668

Table 2. Calculation of crop water need and irrigation water need

Type of crops	Growing months	Total growing period [days]	Crop water need [mm]	Irrigation water need [mm]	Available volume of water [m <sup>3</sup> ]	Agricultural land area [ha]	Available irrigation water [mm]	Time of irrigation
Naked wheat, Barley	Nov/Dec-April/May	180	644	637	494,272	80	618	5
Potato	Mid April-Mid Aug	120	732	695	474,218	80	593	4
Pulses, Buckwheat	June-Oct	150	968	914	1075,453	80	1 344	4
Apple	Sep-Aug	several years	853	798	1607,615	80	2 010	throughout the year

land of the research site. Volume of stream flow mainly depends on the amount of precipitation fall in the basin. The winter precipitation (in the form of snow) has a crucial role in recharging and storing the water in the basin that is released in the summer months.

Considering the changing pattern of precipitation, geographic, climatic and social factor, appropriate water use and land use managements strategies should be concede to increase the agricultural production and so forth enhance the economic status of local farmers. This includes construction of large pond to store the water during surplus time, management of irrigation canal network, introducing of modern tools and techniques and adoption of adaptive and advance cropping practices. Drip irrigation technique was recommended during summer and daytime due to cold climate. Sprinkle irrigation is not feasible because of strong winds and scattered plot ownerships.

## 11. Limitations and challenges

Mainly data scarcity are the limitations for this study. One year stream flow data was used to calculate the runoff

coefficient for this study, which is not sufficient. To validate and upgrade the runoff coefficient, continuous measurement is required. Sustainability in operating of monitoring instruments, data collection, further analysis of the data and sharing and dissemination of the results are major challenges ahead.

## Acknowledgement

Data for this paper have come from the UK ESPA funded project *Adaptive Governance of Mountain Ecosystem Services for Poverty Alleviation Enabled by Environmental Virtual Observatories* (Mountain EVO UK NERC grant NE-K010239-1). We express our gratitude to Mountain EVO research programme.

## Bibliography

Aryal A., Brunton D., Pandit R., Rai R.K., Shrestha U.B., Lama N., Raubenheimer D., 2013, Rangelands, conflicts, and society in the Upper Mustang region, Nepal, Mountain Research and Development, 33 (1), 11-18, DOI: 10.1659/MRD-JOURNAL-D-12-00055.1

- Baidya S.K., Shrestha M.L., Sheikh M.M., 2008, Trends in daily climatic extremes of temperature and precipitation in Nepal. *Journal of Hydrology and Meteorology*, 5 (1), 38-51
- Bandyopadhyay J., Gyawali D., 1994, Himalayan water resources: ecological and political aspects of management, *Mountain Research and Development*, 14 (1), 1-24, DOI: 10.2307/3673735
- Beniston M., 2003, Climate change in mountain regions: a review of possible impact, *Climatic Change*, 59 (1-2), 5-31, DOI: 10.1023/A:1024458411589
- Beniston M., 2005, Mountain climates and climatic change: an overview of processes focusing on the European Alps, *Pure and Applied Geophysics*, 162 (8-9), 1587-1606, DOI: 10.1007/s00024-005-2684-9
- Bhusal J.K., Subedi B.P., 2014, Climate change induced water conflict in the Himalayas: a case study from Mustang, Nepal, *Ecopersia*, 2, 585-595
- Bhusal J.K., Chapagain P.S., Regmi S., Gurung P., Zulkafli Z., Karpouzoglou T., Pandeya B., Buytaert W., Clark J., 2017, Mountains under pressure: evaluating ecosystem services and livelihoods in the Upper Himalayan region of Nepal, *International Journal of Ecology and Environmental Sciences*, 42, 217-226
- Brouwer C., Heibloem M., 1986, *Irrigation Water Management: Training Manual No. 3: Irrigation water needs*, Food and Agriculture Organization of the United Nations, available at <http://www.fao.org/3/S2022E/S2022E00.htm> (data access 03.04.2019)
- Buytaert W., Friesen J., Liebe J., Ludwig R., 2012, Assessment and management of water resources in developing, semi-arid and arid regions, *Water Resources Management*, 26 (4), 841-844, DOI: 10.1007/s11269-012-9994-3
- Buytaert W., Zulkafli Z., Grainger S., Acosta L., Alemie T., Bastiaansen J., De Bièvre B., Bhusal J., Clark J., Dewulf A., Foggin M., Hannah D.M., Hergarten C., Isaeva A., Karpouzoglou T., Pandeya B., Paudel D., Sharma K., Steenhuis T., Tilahun S., Van Hecken G., Zhumanova M., 2014, Citizen science in hydrology and water resources: opportunities for knowledge generation, ecosystem service management, and sustainable development. *Frontiers in Earth Science*, 2 (26), 1-21, 10.3389/feart.2014.00026
- Chapagain P.S., Bhusal J., 2013, Changing water regime and adaptation strategies in Upper Mustang Valley of Upper Kaligandaki Basin in Nepal, *Sciences in Cold and Arid Regions*, 5 (1), 133-138, DOI: 10.3724/SP.J.1226.2013.00133
- Constantino P., Carlos H., Ramalho E., Rostant L., Marinelli C., Teles D., Fonseca Fonseca-Junior S., Batista Fernandes R., Valsecchi J., 2012, Empowering local people through community-based resource monitoring: a comparison of Brazil and Namibia, *Ecology and Society*, 17 (4), 22, DOI: 10.5751/ES-05164-170422
- Danielsen F., Burgess N., Balmford A., 2005, Monitoring matters: examining the potential of locally-based approaches, *Biodiversity and Conservation*, 14 (11), 2507-2542, DOI: 10.1007/s10531-005-8375-0
- Danielsen F., Burgess N., Balmford A., Donald P., Funder M., Jones J., Alviola P., Balette D.S., Blomley T., Brashares J., Child B., Enghoff M., Fjeldså J., Holt S., Hübertz H., Jensen A.E., Jensen P.M., Massao J., Mendoza M.M., Ngaga Y., Poulsen M.K., Rueda R., Sam M., Skielboe T., Stuart-Hill G., Topp-Jørgensen E., Yonten D., 2009, Local participation in natural resource monitoring: a characterization of approaches, *Conservation Biology*, 23 (1), 31-42, DOI: 10.1111/j.1523-1739.2008.01063.x
- Deng X.-P., Shan L., Zhang H., Turner N., 2015, Improving agricultural water use efficiency in arid and semiarid areas of China, *Agricultural Water Management*, 80 (1-3), 23-40, DOI: 10.1016/j.agwat.2005.07.021
- Duns R., 2011, *Vulnerability of livelihoods in Kagbeni Mustang district*, Master Thesis, University Utrecht
- Elsawah S., Guillaume J., Filatova T., Rook J., Jakeman A., 2015, A methodology for eliciting, representing, and analysing stakeholder knowledge for decision making on complex socio-ecological systems: from cognitive maps to agent-based models, *Journal of Environmental Management*, 151, 500-516, DOI: 10.1016/j.jenvman.2014.11.028
- Eriksson M., Jianchu X., Shrestha A.B., Vaidya R.A., Nepal S., Sandström K., 2009, The changing Himalayas – impact of climate change on water resources and livelihoods in the Greater Himalayas, *International Center for Integrated Mountain Development*, ICIMOD, 23 pp.
- Fraser E.D.G., Dougill A.J., Mabee W.E., Reed M., McAlpine P., 2005, Bottom up and top down: analysis of participatory processes for sustainability indicator identification as a pathway to community empowerment and sustainable environmental management, *Journal of Environmental Management*, 78 (2), 114-127, DOI: 10.1016/j.jenvman.2005.04.009
- García C.R., Brown S., 2009, Assessing water use and quality through youth participatory research in a rural Andean watershed, *Journal of Environmental Management*, 90 (10), 3040-3047, DOI: 10.1016/j.jenvman.2009.04.014
- Gautam M., Timilsina G., Acharya K., 2013, *Climate change in the Himalayas: current state of knowledge*, Policy Research Working Paper WPS6516, The World Bank, 47 pp., available at <http://documents.worldbank.org/curated/en/421301468350108330/pdf/WPS6516.pdf> (data access 03.04.2019)
- Gomani M.C., Dietrich O., Lischeid G., Mahoo H., Mahay F., Mbilinyi B., Sarmett J., 2010, Establishment of a hydrological monitoring network in a tropical African catchment: An integrated participatory approach, *Physics and Chemistry of the Earth, Part A/B/C*, 35 (13-14), 648-656, DOI: 10.1016/j.pce.2010.07.025

- Hollow B., Roetman P.E.J., Walter M., Daniels C.B., 2015, Citizen science for policy development: the case of koala management in South Australia, *Environmental Science and Policy*, 47, 126-136, DOI: 10.1016/j.envsci.2014.10.007
- Johnson N., Alessa L., Behe C., Danielsen F., Gearheard S., Gofman-Wallingford V., Kliskey A., Krümmel E.-M., Lynch A., Mustonen T., Pulsifer P., Svoboda M., 2014, The contributions of community-based monitoring and traditional knowledge to Arctic observing networks: reflections on the state of the field. *Arctic*, 68 (5), 28-40, DOI: 10.14430/arctic4447
- Kotru R., Choudhary D., Fleiner R., Khadka M., Pradhan N., Dhakal M., 2014, Adapting to climate change for sustainable agribusiness in high mountain watersheds: a case study from Nepal, ICIMOD Working Paper 2014/1, International Centre for Integrated Mountain Development, 48 pp., available at <http://lib.icimod.org/record/30105> (data access 03.04.2019)
- Manandhar S., Pandey V.P., Kazama F., 2013, Assessing suitability of apple cultivation under climate change in mountainous regions of western Nepal, *Regional Environmental Change*, 41 (2), 743-756, DOI: 10.1007/s10113-013-0531-6
- Ministry of Agricultural Development, 2013, Statistical information on Nepalese agriculture 2012/2013, Ministry of Agricultural Development, Agri-Business Promotion and Statistic Division, Statistics Section, Singha Durbar, Kathmandu, available at <http://moad.gov.np/public/uploads/1009021694-YearBook%202013.pdf> (data access 03.04.2019)
- ODOT, 2005, Appendix F – Rational method, [in:] *Hydraulic Manuals*, Oregon Department of Transportation – Highway Division, Engineering and Asset Management Unit, Geo-Environmental Section, available at [https://www.oregon.gov/ODOT/GeoEnvironmental/Docs\\_Hydraulics\\_Manual/Hydraulics-07-F.pdf](https://www.oregon.gov/ODOT/GeoEnvironmental/Docs_Hydraulics_Manual/Hydraulics-07-F.pdf) (data access 03.04.2019)
- Overdevest C., Orr C.H., Stepenuck K., 2004, Volunteer stream monitoring and local participation in natural resource issues, *Human Ecology Review*, 11 (2), 177-185
- PANO, 2009, Temporal and spatial variability of climate change over Nepal (1976-2005), Practical Action Nepal Office, 67 pp., available at [https://practicalaction.org/file/region\\_nepal/ClimateChange1976-2005.pdf](https://practicalaction.org/file/region_nepal/ClimateChange1976-2005.pdf) (data access 03.04.2019)
- Pant D., Thapa S., Bhattarai M., Molden D., 2005, Integrated management of water, forest and land resources in Nepal: opportunities for improved livelihood, CA Discussion Paper, no. 2, International Water Management Institute. Comprehensive Assessment Secretariat, 27 pp., available at [http://www.iwmi.cgiar.org/assessment/files\\_new/publications/Discussion%20Paper/CADiscussionPaper2.pdf](http://www.iwmi.cgiar.org/assessment/files_new/publications/Discussion%20Paper/CADiscussionPaper2.pdf) (data access 03.04.2019)
- Pocock M.J.O., Chapman D.S., Sheppard L.J., Roy H.E., 2014, A strategic framework to support the implementation of citizen science for environmental monitoring, final report to SEPA, Scottish Environment Protection Agency, Center for Ecology and Hydrology, Wallingford, Oxfordshire, 65 pp., available at [https://www.ceh.ac.uk/sites/default/files/hp1114final\\_5\\_complete.pdf](https://www.ceh.ac.uk/sites/default/files/hp1114final_5_complete.pdf) (data access 03.04.2019)
- Reed M.S., 2008, Stakeholder participation for environmental management: a literature review, *Biological Conservation*, 141 (10), 2417-2431, DOI: 10.1016/j.biocon.2008.07.014
- Regmi S., Gurung P., 2015, A report on detail situation analysis of the research site "Dhakarjhong and Phalyak village of Kagbeni VDC", unpublished
- Shrestha A.B., Wake C.P., Mayewski P.A., Dibb J.E., 1999, Maximum temperature trends in the Himalaya and its vicinity: an analysis based on temperature records from Nepal for the period 1971-94, *Journal of Climate*, 12, 2778-2785, DOI: 10.1175/1520-0442(1999)012<2775:MTTITH>2.0.CO;2
- Sutherland A., 1998, Participatory research in natural resources, *Socio-economic Methodologies. Best Practice Guidelines*, Natural Resource Institute, The University of Greenwich, 19 pp., available at <http://www.fao.org/docs/eims/upload/agrotech/1911/BPG03.pdf> (data access 03.04.2019)
- Viviroli D., Archer D.R., Buytaert W., Fowler H.J., Greenwood G.B., Hamlet A.F., Huang Y., Koboltschnig G., Litaor M.I., López-Moreno J.I., Lorentz S., Schädler B., Schreier H., Schwaiger K., Vuille M., Woods R., 2011, Climate change and mountain water resources: overview and recommendations for research, management and policy, *Hydrology and Earth System Sciences*, 15 (2), 471-504, DOI: 10.5194/hess-15-471-2011
- Viviroli D., Dürr H.H., Messerli B., Meybeck M., Weingartner R., 2007, Mountains of the world, water towers for humanity: Typology, mapping, and global significance, *Water Resources Research*, 43 (7), DOI: 10.1029/2006WR005653
- Walker D., Forsythe N., Parkin G., Gowing J., 2016, Filling the observational void: scientific value and quantitative validation of hydrometeorological data from a community-based monitoring programme, *Journal of Hydrology*, 538, 713-725, DOI: 10.1016/j.jhydrol.2016.04.062
- WRI, 2003, *Ecosystems and human well-being: a framework for assessment*, Millennium Ecosystem Assessment, World Resources Institute, Island Press, 245 pp. available at [http://pdf.wri.org/ecosystems\\_human\\_wellbeing.pdf](http://pdf.wri.org/ecosystems_human_wellbeing.pdf) (data access 03.04.2019)



# Long-term seasonal characterization and evolution of extreme drought and flooding variability in northwest Algeria

Kouidri Sofiane, Megnounif Abdesselam, Ghenim Abderrahmane Nekkache

*EOLE Laboratory, Tlemcen University, Tlemcen 13000, Algeria, e-mail: sofihydro@gmail.com*

**Abstract.** A three decade-long study on the variability of drought in relation to the contribution of rainfall was conducted at the Wadi Mekerra watershed, located in northwest Algeria, covering the period from 1973 to 2005. The runoff and rainfall data were analyzed using the Mann-Kendall test, the double mass curve method and the *SPI* index. A rupture of the studied series appeared during the 1980s. The rainfall and runoff trends and contributions were in general, sharply reduced. The region experienced extreme drought between 1981 and 1989, and between 1993 and 2001, rainfall contributions were greater than 60%. This increase, which was recorded in August, September and October for all the parameters studied, shows the importance of the superficial runoff component when combined with decreased infiltration. These climatic conditions reduce the natural recharging of groundwater, and cause an increased susceptibility to soil erosion, reduced agricultural production and an increased risk of floods.

**Keywords:** runoff, trend, contribution, drought

**Submitted** 8 July 2018, **revised** 31 December 2018, **accepted** 1 April 2019

## 1. Introduction

In recent years, the occurrence of prolonged, severe drought and extreme flooding has increased, affecting many regions around the world. This has led to significant social, economic and environmental losses (Zhang et al. 2017; Selek et al. 2018; Warwade et al. 2018). In recent decades, the Mediterranean region has experienced intense and severe drought (WMO 2009; Medejerab, Henia 2011; Nassopoulos 2012; Kablouti 2014; Nouaceur, Laignel 2014). Variability in rainfall from a deficit to excess has resulted in an increase in floods affecting this region (Michiels et al. 1992; Meddi et al. 2010; Coscarelli, Caloiero 2012). Recently, northwest Algeria experienced a drought characterized as severe by its magnitude (Medejerab, Henia 2011) and spatial extent (Meddi, Toumi 2013). Since the 1980s, this region has recorded many occurrences of short-term precipitation alternating with long dry periods that lead to deadly floods (Abdelhalim 2012; Baouab, Cherif 2014).

The objectives of this study were: (1) to analyze runoff and rainfall parameters with their contribution to monthly time steps, in order to detect trends and years when there was a loss of homogeneity using the Kendall test and the double mass curve method; (2) to determine dry periods using the *SPI* index, taking into account the monthly contribution of rainfall inputs; and (3), to assess the relationship between drought and flood and to detect monthly lags between rainfall and runoff.

## 2. Data and area of study

### 2.1. Area of study

The watershed of Wadi Mekerra is located in western Algeria between the latitudes  $0^{\circ}$  and  $-1^{\circ}$  and longitudes  $34^{\circ}50'$  and  $35^{\circ}50'$  (Fig. 1). It is bounded on the north by the mountain range of Tassala, on the south by the Ras El Ma highlands, on the east by the Telagh plateau and the Saïda Mountains, and on the west by the Tlemcen Mountains. The main stream, Wadi Mekerra, originates in the high steppe valleys at an altitude of 1,250 m. It drains an elongated area of approximately 3,000 km<sup>2</sup> and flows from south to north with a slope of 5.5%.

Following the 1994 flood that affected the study area, the authorities decided to set up large-scale hydraulic developments that were supposed to protect the Sidi Bell Abbes city in the medium term (Nadir 2009). Key objectives of the development included:

- The development of the upstream watershed by the construction of banquettes in areas with steep slopes (Bachi 2011).
- The creation of spraying areas on two of the main tributaries of Wadi Mekerra, namely Wadi Mouzen, with a spreading area of 2 million m<sup>3</sup> of capacity, and Wadi Mellah, with a capacity of 2.4 million m<sup>3</sup> (Nadir 2009).
- The creation of a water diversion structure from upstream of Sidi Bel Abbes that allows the evacuation of a maximum runoff of 150 m<sup>3</sup>/s (Nadir 2009; Bachi 2011).

## 2.2. Data

Rainfall and runoff data were provided by the National Hydraulic Resources Agency (ANRH). Twenty-four rainfall stations could have been used in this study, but the quality of the results may have been compromised. Quality control relied on the significant criteria of continuity and homogeneity over a long and common period, allowing for the investigation of the spatial and temporal evolution of precipitation. This, fifteen rainfall stations covering the common period from September 1973 to August 2005 were maintained in this study, with 12 stations located at the watershed of Wadi Mekerra and 3 outside (Fig. 1, Table 1). The remaining stations exhibited gaps in the data or were too low for statistical purposes.

The rainfall data (mm) used in the study was the ( $P_{month}$ ) monthly rainfall and ( $P_{day\ max}$ ) annual maximum daily rainfall. The runoff data ( $m^3\ s^{-1}$ ) was made up of the maximum annual daily runoff ( $Q_{day\ max}$ ) and the monthly runoff ( $Q_{month}$ ).

From a geomorphological point of view, this basin can be subdivided into three parts:

- Upper Mekerra (drained part 01): Extends from the south of Ras El Ma to Sidi Ali Benyoub. This drained part of the basin is analyzed from the monthly data of the rainfall station No 1 and the runoff station No 01-01 (Fig. 1).
- Middle Mekerra (drained part 02): Between Sidi Ali Benyoub and Sidi Bel Abbes. This drained part of the basin is analyzed from the monthly data of the rainfall stations No 1, 2 and 15, and the runoff station N. 02-01 (Fig. 1).
- Lower Mekerra (drained part 03): Corresponds to all the part of the basin located downstream of the city of Sidi Bel Abbes. This drained part of the basin is analyzed from the monthly data of all the rainfall stations and the runoff station No 3 (Fig. 1) (Nadir 2009; Bachi 2011).

## 3. Methods

Fluctuations in rainfall and discharge were analyzed daily, monthly and annually, using the mean value of the  $P_{days}$ ,  $P_{day\ max}$  and  $P_{month}$  on the separate parts of the catchment area defined above in Section 2.2. The analysis of the rainfall-runoff data and the determination of the trends was performed using the XLStat software at a 95% confidence level. The calculation of the tau parameter,  $\tau$ , of Kendall (Mann 1945; Kendall 1975) was used to detect possible changes in trends (Chen et al. 2007; Shadmani et al. 2012; Trambly et al. 2013; Yanon, Ndiaye 2013; Zelenáková et al. 2013; Faye 2014;

Table 1. Rainfall and runoff stations (Z: altitude; D.mer: distance to the sea)

No	Type	Name of Station	Z [m]	D.mer [km]
1	Rainfall	Ras El Ma	1,097	128
2		El Hacaiba	950	113
3		Hassi Zahana	630	77
4		Sidi Ali Boussidi	610	67
5		Tessala	580	52
6		SBA	485	61
7		Tabia	620	83
8		Hassi Dahou	650	76
9		M Ben Brahim	590	70
10		Ain Trid	530	47
11		Sidi Lahcen	501	62
12		Telagh	877	104
13		Ain Frass	424	68
14		Sfissef	545	77
15		Sidi Ali Benyoub	635	85
01-01	Runoff	El Hacaiba	950	113
02-01		Sidi Ali Benyoub	635	85
03-01		SBA	485	61

Benhamrouche et al. 2015; Sohoulane Djebou 2015). In particular, the Mann-Kendall test was used to detect trends in monthly rainfall-runoff variables for the different stations. In addition, the monthly contributions of rainfall and runoff were estimated respectively by the ratios  $P_{day\ max}/P_{month}$  and  $Q_{day\ max}/Q_{month}$ .

### 3.1. Stationarity of the series

The stationarity of the series was studied using the double mass curve method, which is simple, visual and practical. It is widely used in studies of long-term changes in hydrometeorological data (Mu et al. 2010). This method was used to analyze the maximum daily rainfall series ( $P_{day\ max}$ ) and maximum daily water runoff ( $Q_{day\ max}$ ).

### 3.2. Variability and series trends

In order to study the variability of precipitation ( $P_{month}$ ) and monthly runoff ( $Q_{month}$ ), box plots was introduced for a schematic representation of the distribution of these two variables where extremes and quartiles diagrams were constructed and processed.

### 3.3. Occurrence and magnitude of dry and wet sequences

Deficit and excess rainfall are assessed with the *SPI* index (WMO 2012) at 3 months (*SPI-3*), 9 months (*SPI-9*),

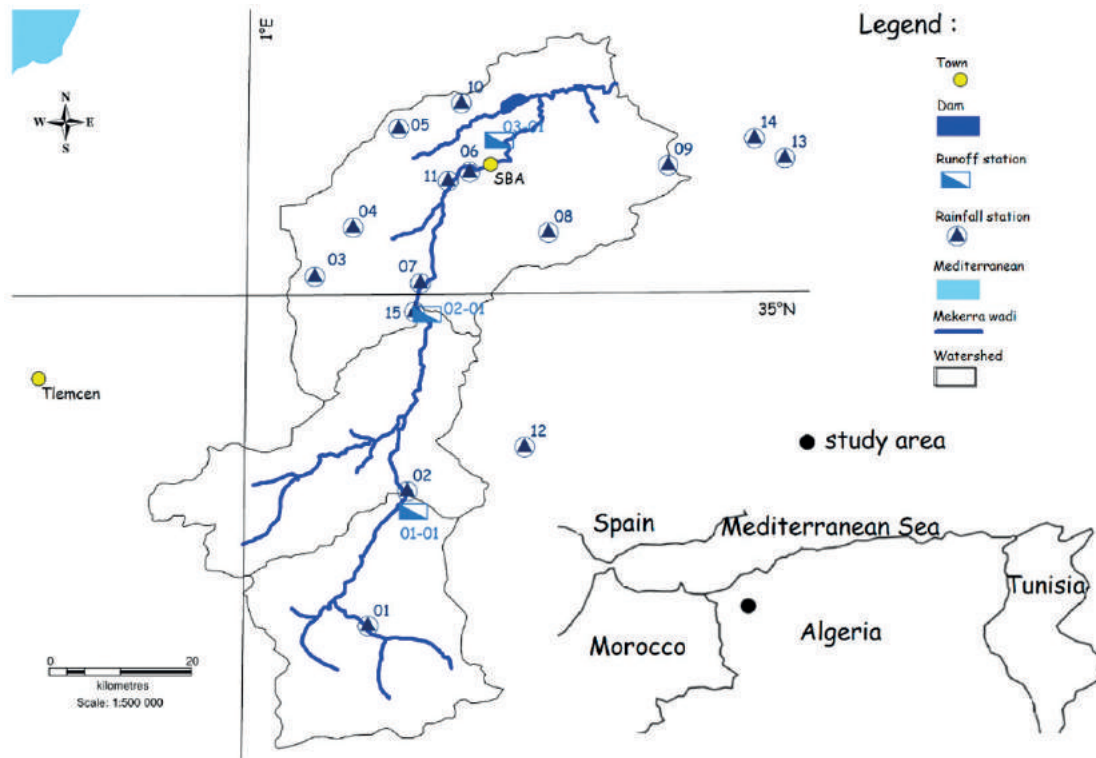


Fig. 1. Rainfall and runoff stations in the study area

Table 2. Classification of sequences by *SPI* index (WMO 2012)

2,0 and more	EW	Extremely wet
1,5 to 1,99	VW	Very wet
From 1,0 to 1,49	MW	Moderately wet
From -0,99 to 0,99	CN	Close to normal
From - 1,0 to -1,49	MD	Moderately dry
From -1,5 to -1,99	VD	Very dry
-2 and less	ED	Extremely dry

To analyze the results of *SPI* for the 32-year study, we distributed the data into eight 4-year intervals (Table 3). The choice of the interval length was determined according to the following: allowing for a reasonable number of characteristic values, making it possible to attenuate the strong inter-annual irregularity of the *SPI* indices while maintaining the overall temporal trend; distributing as evenly as possible, the high flooding events (observed during the years 1986, 1990, 1994, 1995, 1997, 2000, 2002 and 2003) across the selected intervals.

Table 3. Time intervals over the study period (1973-2005)

Period	Start Date	End Date
P 1	September 1973	August 1977
P 2	September 1977	August 1981
P 3	September 1981	August 1985
P 4	September 1985	August 1989
P 5	September 1989	August 1993
P 6	September 1993	August 1997
P 7	September 1997	August 2001
P 8	September 2001	August 2005

#### 4. Results and discussion

##### 4.1. Stationarity of series

12 months (*SPI*-12) and 24 months (*SPI*-24). *SPI* values range from extreme drought to extreme wet (Table 2).

After defining the EW, VD, VD and ED sequences, the contribution of rainfall inputs was introduced to assess whether rains were concentrated or spread out during each period.

The analysis of  $P_{day\ max}$  and  $Q_{day\ max}$  by the double mass curve method is presented in Figure 2. The analysis of the stationarity between  $P_{day\ max}$  and  $Q_{day\ max}$  by the double mass curve method showed a loss of homogeneity during the year 1986. After this date, the slope of the adjustment line increased significantly. In agreement with other published reports (Meddi et al. 2009; Talia et al. 2011), there were many years of rainfall deficit during the 1980s and 1990s. An increase in rainfall-runoff extremes was recorded at the three drained parts of the watershed; 27% for the first, 148% for the second and 800% for the third drained part of the basin. In addition, accumulations of  $P_{day\ max}$  and  $Q_{day\ max}$  at the three drained portions, 01, 02 and 03, were observed as 750, 1,200 and 1,950 mm, respectively, for the maximum daily

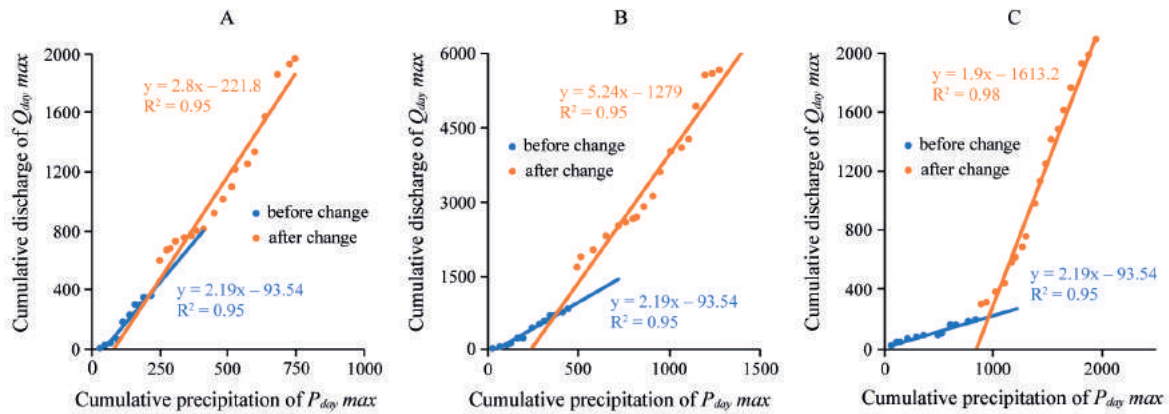


Fig. 2. Double mass curve of  $P_{day\ max}$  and  $Q_{day\ max}$  during 1973-2005 at Wadi Mekerra (A: drained part 01, B: drained part 02, C: drained part 03)

rainfall, and 1,900, 5,600 and 2,000  $m^3/s$ , for maximum daily runoff.

Extreme values of rainfall demonstrated an increasing trend since the first part drained at the outlet, while the extreme values of runoff increased from the first to the second drained parts. On the other hand, cumulative  $Q_{day\ max}$  decreased significantly in drained part 03. This decrease can be attributed to the protective installations constructed in order to minimize the flooding risks of the Sidi Bel Abess city. Indeed, discharges that reach the threshold of 150  $m^3/s$  are controlled by redirecting the water to diversion structures. However, before the rupture date, the threshold was exceeded only once in 1979, with a peak discharge of 197  $m^3/s$ . Whereas after 1986, 12 events occurred with a peak discharge greatly exceeding the threshold, with 4 peaks exceeding 500  $m^3/s$ , and a maximum of 808  $m^3/s$ . These events caused 8 major flooding actions with considerable damage to the villages upstream of the Sidi Bel Abess city (Abdelhalim 2012): October 1986: 1 dead and 200 homeless; April 1990: 2 dead and 130 homeless; September 1994: 1 dead and 22 homeless; September 1997: 1 dead; December 1997: 1 dead and 5 homeless; July 2000: 100 homeless and significant damage in rural areas during 1995, 2002 and 2003. As a result of the diversion structures, more than 60% of the drained water did not reach the gaging station controlling part 3.

## 4.2. Variability and trends of series

### 4.2.1. Drained part No 01

Monthly precipitation varied from 0 to 110 mm (Fig. 3A). The lowest values (3 mm on average) were recorded in the month of July. During the months of June and August, however, the average recorded values were 10 mm, while we found average monthly values of 20 mm

during the other months. In spite of that, a big difference between Q3 and Q4 was noticed, meaning that there were several extreme values. The areas experiencing flooding during the months of August, September and October (Fig. 3B) had very high runoff values between 141-290  $m^3/s$ , while values for the other months were  $<150\ m^3/s$ .

The analysis depicted in Figure 3C showed two periods: the first from November to July, during which there was a considerable decline in runoff and precipitation; the second period encompassed the months of August, September and October, where there was a marked increase in the parameters studied.

### 4.2.2. Drained part No 02

Monthly precipitation values ranged from 0 to 155 mm (Fig. 4A). The three months of summer June, July and August recorded the lowest values with an average of 7 mm, while during the other months of the year the average value was 25 mm. There were large differences between Q3 and Q4 during the months of February, March and September.

Floods occurred during the months of August, September and October (Fig. 4B) with very high runoff values between 403 and 808  $m^3/s$ . During the other months, the maximum runoff varied between 0 and 300  $m^3/s$ . The runoff contribution decreased considerably during all the months of the year except for October and November, when there was a remarkable increase in precipitation and runoff (Fig. 4C).

### 4.2.3. Drained part No 03

For the third part, the monthly precipitation values varied between 0 and 137 mm (Fig. 5A). During the months of June to September, the average minimum value was 10 mm, while the other months had an average

of 30 mm. A large difference between Q3 and Q4 rainfall was observed during the months of March, April, November and December. Floods occurred during the months of August, September, October and November (Fig. 5B) with very high values between 142 and 215 m<sup>3</sup>/s. The other months have values <140 m<sup>3</sup>/s. The trend of rainfall, runoff and their contribution (Fig. 5C) generally decreased throughout the year with the exception of September, October and November. The month of September was characterized by a sharp rise in rainfall and corresponding contribution of runoff. The two months of October and November were marked by an increase in both rain and runoff; however, the overall trend of the runoff was declining.

When comparing the three parts of the watershed, the intra-annual rainfall distribution was similar. The rainy season occurred from September to May and declined in summer season (June, July and August). The extreme events may occur at any time of the year. However, the annual runoff was mainly done during the fall season with the occurrence of the strongest extreme events. At the upstream watershed, part 1, eight months of the year shown an increase trend of the monthly rainfall. Similar behavior has been observed for six months when regarding the ratio trend of  $P_{day\ max}/P_{month}$ . For all months of the year, the ratio trend remains lower than the monthly rainfall trend. The highest increases are close for both tendencies and recorded during the month of August. The monthly runoff trends were declining except for the months of the fall season with the highest trend observed in August. Taking into account the rainfall recorded downstream, parts 2 and 3, the spatial average rainfall trend has changed considerably. During the spring season, the monthly precipitation trends, positive in Part 1, have declined and become negative in the Parts 2 and 3 of watershed. Further, the positive rainfall trend observed during the month of December, Part 1, was shifted to January in parts 2 and 3 of the watershed. Similarly, for runoff measured, the positive trend recorded during the fall season, in the gaging station no 1, decreased significantly at gaging stations no 2 and no 3. Globally, the increase of the ratio trend of  $Q_{day\ max}/Q_{month}$  in comparison with the runoff trend, attests that runoff are more and more concentrated in time.

After the rupture date, the decrease in annual rainfall was significant, as confirmed by the analysis of the previous Kendall tau results. Trends detected for our study area are consistent with other studies of the Mediterranean region, particularly in North Africa (Brunetti et al. 2004; Costa, Soares 2009; Reiser, Kutiel 2009; Meddi et al. 2010; Caloiero et al. 2011).

The Kendall test for the  $P_{month}$ ,  $Q_{month}$  series, with their contribution from northwest Algeria, demonstrated a change in the trend of the parameters studied. An increase in runoff was seen during August, September and October, outside the winter season where the rainfall-runoff elements are usually most important. During the remaining months, a decrease in rainfall contribution was recorded with a very strong drop in the runoff.

### 4.3. Occurrence and magnitude of dry and wet sequences

The temporal evolution of *SPI* (at 3, 9, 12 and 24 months) in 4-year periods is presented in Figure 6. Based on the *SPI*-3, *SPI*-9 and *SPI*-12 results, drought affected the study area for the periods of P3 (1981-1985) and P7 (1997-2001). In contrast, the wet sequences occurred during the periods P1 (1973-1977) and P6 (1993-1997), with precipitation contributions averaging at 35%. A high average rainfall contribution of approximately 66% was observed for the periods of P3 (1981-1985) and P7 (1997-2001). *SPI*-24 demonstrated a rainfall contribution of 45% during P1, while for the other dry sequence periods, very high contributions were recorded (greater than 60%). Since 1981, the ED and VD sequences for *SPI*-24 have maintained rainfall contributions between 30 and 60%. In contrast, the EW and VW sequences were observed during the period P1 (1973-1977), indicating that rainfall decreased to a contribution of less than 40%.

During the study period, a sharp rise in rainfall-runoff parameters was recorded for the three months of August, September and October. At the same time, very large floods affected our study area. In addition, from 1981, a severe drought affected this region, generating several phenomena as follows. Soil degradation and erosion measured over 12 years ranged from 4,217 to 124,384 t/km<sup>2</sup> per year at the Sidi Bel Abbes station, with an average of 44,048 t/km<sup>2</sup> per year (Yamani et al. 2014). This corresponds to an annual average concentration of approximately 4.52 g/L. Secondly, a drop in agricultural production was observed, with only 7,150 ha irrigated out of 30,000 ha of irrigable potential land, due to a lack of water resources (Slimani, Aidoud 2004). Thirdly, the risk of floods that severely damage property increased, as well as the loss of agriculture and industry (Abdelhalim 2012). It should also be noted that this region has also experienced human casualties. The flood of SBA (04/10/86) left 1 dead and 200 injured, while the flood of Moulay Slissen (17/08/97) claimed 1 dead and 34 injured (Abdelhalim 2012).

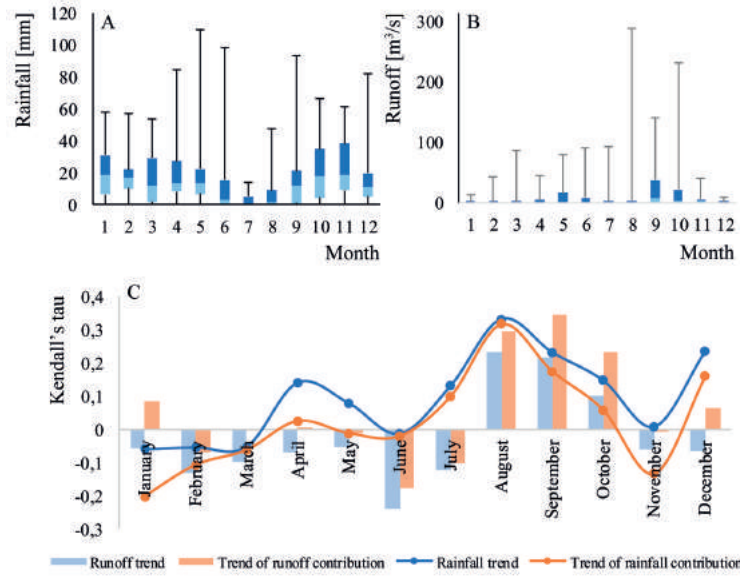


Fig. 3. Monthly rainfall (A), runoff (B) and Kendall's tau (C) in the drained part 01 of Wadi Mekkera

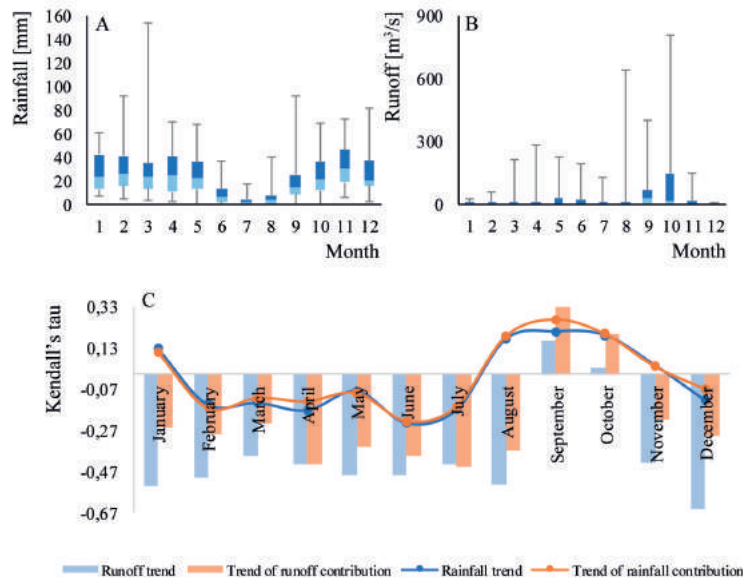


Fig. 4. Monthly rainfall (A), runoff (B) and Kendall's tau (C) in the drained part 02 of Wadi Mekkera

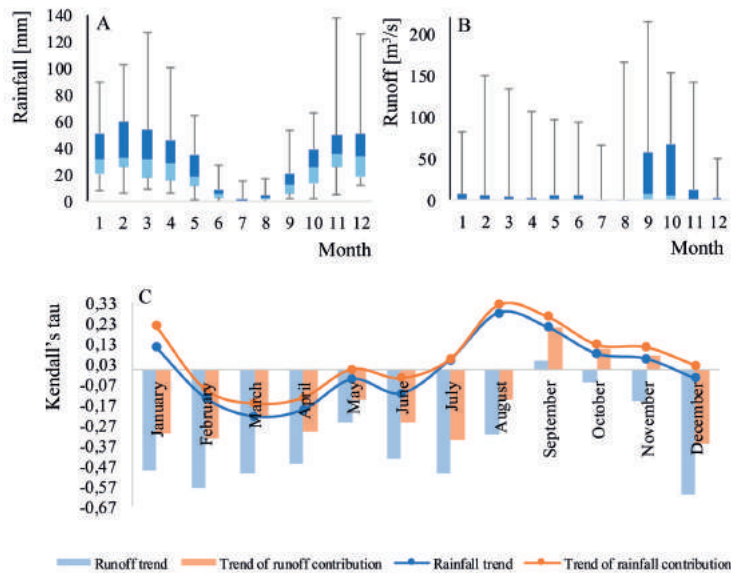


Fig. 5. Monthly rainfall (A), runoff (B) and Kendall's tau (C) in the drained part 03 of Wadi Mekkera

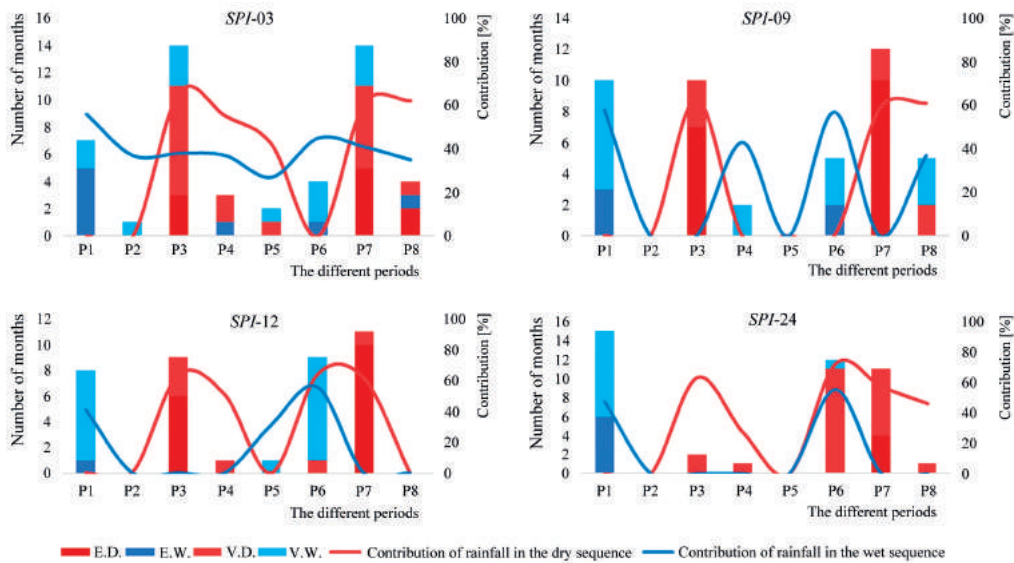


Fig. 6. Number of months and rainfall contribution in a given humidity class (Table 1) in the 4-year periods

## 5. Conclusions

The time series analysis and the statistical tests indicated a loss of homogeneity during the year of 1986. Following this, the slope of the adjustment line increased significantly. Compared to the second drained section, there was an observed decrease in cumulative  $Q_{day\ max}$ . Despite protective work, devastating floods still affected our study area. During the study period, the Mekerra watershed experienced a decline in rainfall and discharge. However, increases in the studied parameters were recorded during August, September and October, with a strong variability in the runoff series. This indicates that several extreme values were present. In general, there were two distinct periods. The first extended from November to July, during which there was a considerable reduction in runoff and precipitation. The second period encompassed the months of August, September and October, when there was a sharp rise in all parameters. Analysis of *SPI* results from the study area showed that the region experienced both Extreme Drought (ED) and Very Dry (VD) sequences. The latter was recorded since 1981, with a rainfall contribution of between 30 and 60%. In contrast, EW and VW sequences were observed in the P1 period (1973-1977), indicating that rainfall contributions dropped to less than 40%.

During the dry season, there was a sharp increase in rainfall-runoff parameters, with very large floods affecting our study area. Because of this, the soil will eventually become saturated, such that any increase in the volume of rain will result in an equivalent increase in the volume of water discharged by the river at its outlet. Under these conditions, any amount of rain that falls will contribute to flooding, soil degradation and erosion. Seasonal rainy

periods that occur during the fall generate significant runoff, usually causing flooding. The study area was found to have two distinct seasonal periods with different rainfall-runoff patterns. The first was from November to July and was characterized by precipitation, with a small runoff contribution, while the second, from August to October, manifested intense rainfall accompanied by a strong contribution from runoff.

## Bibliography

- Abdelhalim Y., 2012, Inondations torrentielles cartographie des zones vulnérables en Algérie du Nord cas de l'oued Mekerra, Wilaya de Sidi Bel Abbès (Torrential floods mapping of vulnerable zones in Northern Algeria case of Wadi Mekerra, Sidi Bel Abbès Wilaya), PhD thesis, Ecole Nationale Polytechnique, Algeria
- Bachi M., 2011, Problématique du risque inondation en milieu urbain. Cas de l'agglomération de Sidi Bel Abbès (Flood risk issue in the urban environment. Agglomeration of Sidi Bel Abbès), Memory of Magister, University of Aboubakr Belkaid, Tlemcen, Algeria
- Baouab M.H., Cherif S., 2014, Tendances, Fluctuations et Projection pour un Cas d'Etude de l'Eau Potable en Tunisie (Trends, fluctuations and projection for a case study of drinking water in Tunisia), [in:] Proceedings of 3<sup>rd</sup> International Conference Water-Climate'2014: Water Resources and Climate Change in the Mediterranean Region
- Benhamrouche A., Boucherf D., Hamadache R., Bendahmane L., Martin-Vide J., Teixeira Nery J., 2015, Spatial distribution of the daily precipitation concentration index in Algeria, *Natural Hazards and Earth System Sciences*, 15 (3), 617-625, DOI: 10.5194/nhess-15-617-2015

- Brunetti M., Buffoni L., Mangianti F., Maugeri M., Nanni T., 2004, Temperature, precipitation and extreme events during the last century in Italy, *Global and Planetary Change*, 40 (1-2), 141-149, DOI: 10.1016/S0921-8181(03)00104-8
- Caloiero T., Coscarelli R., Ferrari E., Mancini M., 2011, Trend detection of annual and seasonal rainfall in Calabria (Southern Italy), *International Journal of Climatology*, 31 (1), 44-56, DOI: 10.1002/joc.2055
- Chen H., Guo S., Xu C., Singh V.P., 2007, Historical temporal trends of hydro-climatic variables and runoff response to climate variability and their relevance in water resource management in the Hanjiang basin, *Journal of Hydrology*, 344 (3-4), 171-184, DOI: 10.1016/j.jhydrol.2007.06.034
- Coscarelli R., Caloiero T., 2012, Analysis of daily and monthly rainfall concentration in Southern Italy (Calabria region), *Journal of Hydrology*, 416-417, 145-156, DOI: 10.1016/j.jhydrol.2011.11.047
- Costa A.C., Soares A., 2009, Homogenization of climate data: review and new perspectives using geostatistics, *Mathematical Geosciences*, 41 (3), 291-305, DOI: 10.1007/s11004-008-9203-3
- Faye C., 2014, Variability and trends observed in monthly, seasonal and annual average flows in the Falémé basin (Senegal), *Hydrological Sciences Journal*, 62 (2), DOI: 10.1080/02626667.2014.990967
- Kablouti N., 2014, Les modelés numériques: outils d'évaluation et de gestion prévisionnelle de ressources en eau S/t et d'aide à la prise de décision : cas de la nappe Dunaire côtière de bouteldja, extrême nord est Algérien (Digital modeling: assessment and forecasting tools for S/T water resources and decision support: case of the Dunaire coastal sheet of bouteldja, extreme northeastern Algeria), *Le Journal de l'Eau et de l'Environnement*, 4 (7), 87-98
- Kendall M.G., 1975, Rank correlation methods, Griffin, London, 202 pp.
- Mann H.B., 1945, Nonparametric tests against trend, *Econometrica*, 13, 245-259
- Meddi M., Assani A.A., Meddi H., 2010, Temporal variability of annual rainfall in the Macta and Tafna catchments, Northwestern Algeria, *Water Resources Management*, 24 (14), 3817-3833, DOI: 10.1007/s11269-010-9635-7
- Meddi M., Talia A., Martin C., 2009, Évolution récente des conditions climatiques et des écoulements sur le bassin versant de la Macta (Nord-Ouest de l'Algérie), *Physio-Géo*, 3, 61-84, DOI: 10.4000/physio-geo.686
- Meddi M., Toumi S., 2013, Study of the interannual rainfall variability in northern Algeria, *LJEE*, 23, 40-59
- Medejerab A., Henia L., 2011, Variations spatio-temporelles de la sécheresse climatique en Algérie nord-occidentale, *Courrier du Savoir*, 11, 71-79
- Michiels P., Gabriels D., Hartmann R., 1992, Using the seasonal and temporal Precipitation concentration index for characterizing the monthly rainfall distribution in Spain, *CATENA*, 19 (1), 43-58, DOI: 10.1016/0341-8162(92)90016-5
- Mu X., Zhang X., Peng G., Wang F., 2010, Theory of double mass curves and its applications in hydrology and meteorology, *Journal of China Hydrology*, 30, 47-51
- Nadir B., 2009, Etude de crues et localisation des zones inondables (Flood study and location of flood areas), PhD thesis, Agricultural hydraulics, National School of Agronomy El Harrach Algiers, Algeria
- Nassopoulos H., 2012, The impacts of climate change on water resources in the Mediterranean, PhD thesis, Economic science, University Paris-Est, France
- Nouaceur Z., Laignel B., 2014, Changements climatiques et inondations urbaines au Maghreb central Maroc, Algérie, Tunisie (Climate change and urban flooding in Central Maghreb Morocco, Algeria, Tunisia), [in:] Proceedings of 3<sup>rd</sup> International Conference Water-Climate'2014: Water Resources and Climate Change in the Mediterranean Region
- Reiser H., Kutiel H., 2009, Rainfall uncertainty in the Mediterranean: definitions of the daily rainfall threshold (DRT) and the rainy season length (RSL), *Theoretical and Applied Climatology*, 97 (1-2), 151-162, DOI: 10.1007/s00704-008-0055-z
- Selek B., Tuncok I.K., Selek Z., 2018, Changes in climate zones across Turkey, *Journal of Water and Climate Change*, 9 (1), 178-195, DOI: 10.2166/wcc.2017.121
- Shadmani M., Marofi S., Roknian M., 2012, Trend analysis in reference evapotranspiration using Mann-Kendall and Spearman's Rho tests in arid regions of Iran, *Water Resources Management*, 26 (1), 211-224, DOI: 10.1007/s11269-011-9913-z
- Slimani H., Aidoud A., 2004, Desertification in the Maghreb: a case study of an Algerian High-Plain Steppe, [in:] Environmental challenges in the Mediterranean 2000-2050, A. Marquina (ed.), NATO Science Series: Earth and Environmental Sciences, 37, Springer, Dordrecht, 93-108, DOI: 10.1007/978-94-007-0973-7\_6
- Sohoulande Djebou D.C., 2015, Integrated approach to assessing streamflow and precipitation alterations under environmental change: application in the Niger River Basin, *Journal of Hydrology: Regional Studies*, 4 (Part B), 571-582, DOI: 10.1016/j.ejrh.2015.09.004
- Talia A., Meddi M., Bekkoussa B.S., 2011, Study of the variability of rainfall in the high plateaus and the Algerian Sahara, *Sécheresse*, 22 (3), 149-158, DOI: 10.1684/sec.2011.0314
- Tramblay Y., El Adlouni S., Servat E., 2013, Trends and variability in extreme precipitation indices over maghreb countries, *Natural Hazards and Earth System Sciences*, 13 (12), 3235-3248, DOI:10.5194/nhess-13-3235-2013

- Warwade P., Tiwari S., Ranjan S., Chandniha S.K., Adamowski J., 2018, Spatio-temporal variation of rainfall over Bihar State, India, *Journal of Water and Land Development*, 36 (1), 183-197, DOI: 10.2478/jwld-2018-0018
- WMO, 2009, WMO Bulletin. World Climate Conference-3, 58 (3), 223 pp., available at [https://library.wmo.int/pmb\\_ged/bulletin\\_58-3.pdf](https://library.wmo.int/pmb_ged/bulletin_58-3.pdf) (data access 24.05.2019)
- WMO, 2012, Standardized Precipitation Index. User guide, WMO-No. 1090, Geneva, Switzerland, 16 pp.
- Yamani K, Sekkoum M., Hazzab A., Atallah M., 2014. Étude du transport solide en suspension dans les régions semi arides méditerranéennes : cas du bassin versant de l'oued Mekerra nord-ouest Algérien, [in:] 6<sup>ème</sup> Conférence Internationale (WATMED 6): Ressources En Eau Dans Le Bassin Méditerranéen, Sousse, Tunisie
- Yanon G., Ndiaye A., 2013, Diminution observée des ressources en eau, une conséquence de la variabilité climatique? Étude basée sur une approche participative à Bambey (Sénégal), *Geo-Eco-Trop*, 37 (1), 149-156
- Zeľňáková M., Purcz P., Gargar I., Hlavatá H., 2013, Comparison of precipitation trends in Libya and Slovakia, *WIT Transactions on Ecology and the Environment*, 172, 365-374, DOI: 10.2495/RBM130301
- Zhang Z., Yu X., Jia G., Liu Z., Wang D., Hou G., 2017, Characteristics of rainfall and runoff in different extreme precipitation events in the Beijing mountain area, *Hydrology Research*, 49 (2), 363-372, DOI: 10.2166/nh.2017.011



## Homogeneous regionalization via L-moments for Mumbai City, India

Amit Sharad Parchure, Shirish Kumar Gedam

*Indian Institute of Technology (IIT), Centre of Studies in Resources Engineering, Bombay 400076, India,  
e-mail: amit231279@gmail.com*

**Abstract.** This study identified homogeneous rainfall regions using a combination of cluster analysis and the L-moments approach. The L-moments of heavy rainfall events of various durations (0.25, 1, 6, 12, 24, 48, 72, 96, and 120 h) were analysed using seasonal (June-September) rainfall measurements at 47 meteorological stations over the period 2006-2016. In the primary phase of this study, the homogeneity of Mumbai as a single region was examined by statistical testing (based on L-moment ratios and variations of the L-moments). The K-means clustering approach was applied to the site characteristics to identify candidate regions. Based on the most appropriate distribution, these regions were subsequently tested using at-site statistics to form the final homogeneous regions. For durations above 1h, the regionalisation procedure delineated six clusters of similarly behaved rain gauges, where each cluster represented one separate class of variables for the rain gauges. However, for durations below 1h, the regionalisation procedure was not efficient in the sense of identifying homogeneous regions for rainfall. Furthermore, the final clusters confirmed that the spatial variation of rainfall was related to the complex topography, which comprised flatlands (below or at mean sea level), urban areas with high rise buildings, and mountainous and hilly areas.

**Keywords:** regional analysis, L-moments, tests for homogeneity, K-means clustering, principal components analysis

**Submitted** 12 September 2018, **revised** 2 April 2019, **accepted** 4 June 2019

### 1. Introduction

Rainfall flooding is one of the most dangerous natural hazards as it affects the economy, environment, and population. Some recent studies indicate that heavily urbanized megacities in low-lying coastal areas are hotspots for flooding (Hallegatte 2010). In Mumbai, which is one of the megacities along the coast of India, severe floods occur almost every year. Furthermore, the extreme rainfall event that occurred on July 26<sup>th</sup>, 2005 demonstrated the high spatio-temporal variability of rainfall events in different areas over a 24-h period (Lokanadham et al. 2012). Therefore, it is vital to assess the regionalization of hydroclimatic variables such as flooding, evapotranspiration, and rainfall in order to optimize efficiency in design and reduce uncertainties.

Regionalization is generally used when rain gauge data are not available at a target site or to improve at-site (single) estimates, especially for short data records (Malekinezhad, Zare-Garizi 2014; Sun et al. 2015; Halbert et al. 2016; Requena et al. 2016). This approach involves “trading time for space” by pooling observations for stations with similar behavior. Various rainfall regionalization techniques have been developed and applied by researchers worldwide, for example, in Pakistan (Khan et al. 2017), Slovakia (Gaál et al. 2009), the Brazilian Amazon (Santos et al. 2015), Jeju Island, Korea (Kar et al. 2017), and mid-Norway (Hai-

legeorgis, Alfredsen 2017). In India, rainfall regionalization techniques that have been developed and applied include principal components analysis (Nair et al. 2013), correlation analysis (Sinha et al. 2013), cluster analysis (Ahuja, Dhanya 2012; Bharath, Srinivas 2015), neural networks (Saha et al. 2017), and shared nearest neighbor (Kakade, Kulkarni 2017). However, most of these applications have been on a national rather than regional scale. In addition, most of these cluster analysis studies have been conducted using a top-down approach, which explains the top-down control of the large-scale climatic attributes (e.g., mean annual precipitation, temperature, wind velocity, wind direction, and specific humidity) over regional hydrological processes and patterns (Hessburg et al. 2005). Based on these attributes, homogeneous regions are identified, which are expected to be reflected in the records of the hydrometeorological variables of interest. In this context, the L-moments approach is a promising technique, and is a well-known and widely used procedure for regionalization (Hosking, Wallis 1997; Ngongondo et al. 2011; Rahman et al. 2013). This method is relatively insensitive to outliers, and the parameter estimates are more reliable than conventional moment estimates, especially for small samples. Furthermore, the estimators of the L-moments are virtually unbiased (Smithers, Schulze 2001). In this study, the L-moments algorithm with site characteristics (objective) and site statistical (subjective, process-based) pooling techniques were used to cluster

rain gauges within the region into groups, thus augmenting the comparability of the rain gauges.

The research presented in this paper was motivated by the fact that most of the studies in this region have used data from two Indian Metrological Department (IMD) stations (Colaba and Santacruz) to investigate the formation and prediction of extreme events and estimation of design rainfall amounts. Furthermore, the July 26<sup>th</sup>, 2005 event drove the local authorities (the Municipal Corporation of Greater Mumbai (MCGM)) to install a dense network of rain gauges to measure continuous and consistent rainfall. As a result, 60 rain gauges were installed that provided more than five years of steady, coherent observations. These rain gauges were installed without prior studies on the selection of optimal sites. Moreover, Parchure and Gedam (2018) used a priori knowledge of rainfall events, and considering the advantage of Self-Organising Maps (SOMs) for (e.g.), abstraction of attributes, displayed the distribution of each component, and for effective visualisation, analysed the clustered rain gauges in groups (regions). However, this is a time-consuming method when compared with the L-moment approach. Hence, the primary intent of this study is to identify homogeneous rainfall regions at the local scale using the L-moments approach.

The specific objectives of this study are as follows:

- To perform a regionalization of heavy rainfall (of 0.25, 1, 6, 12, 24, 48, 72, 96, and 120 h duration) using the L-moments approach.
- To check whether the study area behaves as a single homogeneous region.
- To identify homogeneous rainfall regions by combining the results obtained from the site characteristics and site statistics pooling techniques.
- To evaluate the performance of the top-down approach, i.e. the L-moments approach

## 2. Study area and data description

Mumbai is situated on the western coast of India and extends between 18.00°-19.20°N and 72.00°-73.00°E. The region has a humid, tropical climate, with monsoons that move in from the southwestern Indian Ocean from June to September. Initially, Mumbai was composed of a group of islands that have now been reclaimed to meet the demand for land. This reclamation has resulted in the region having a complex topography that comprises flatlands (below or at mean sea level), urban areas, and mountainous and hilly areas (for instance, the Sanjay Gandhi National Park that is located in the northern part has an elevation of up to 450 m above mean sea level). Sub-hourly precipitation data (at 15 min intervals) were

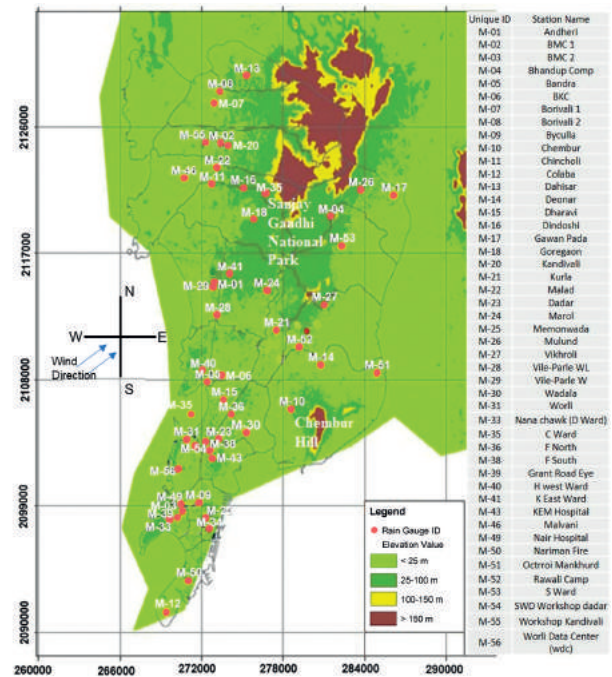


Fig. 1. Names, unique codes, and locations of rain gauge stations throughout Mumbai (on SRTM elevation map)

acquired from the MCGM. These data were collected from 60 rain gauges for the southwest monsoon period (June-September) from 2006 to 2016. However, after accounting for missing data, newer installations, as well as the reliability, consistency, and operational period of each rain gauge, this study considered data from 47 of these gauges. Figure 1 shows the names, unique codes, and locations of these gauges on a Shuttle Radar Topography Mission (SRTM) elevation map.

## 3. Methodology

This section describes the methodology used to achieve the objectives of this study.

### 3.1. Screening of data

Continuous rainfall data from the rain gauges were analyzed, and a validation method was used to ensure the reliability of the data and identify suspect or incorrect values. The suspect or incorrect data were not modified but instead were flagged appropriately (e.g., as 'suspect' or 'missing'). A range test (Estévez et al. 2015) and double mass curve were applied subsequently. Only stations with more than three years of data were screened. This procedure resulted in the inclusion of 47 stations. A series of maximum rainfall amounts for durations of 0.25, 1, 3, 6, and 12 h and 1-5 d was acquired using a movable time window method.

Table 1. Threshold values used to identify heavy storms from sub-hourly data

Duration [h]	0.25	1	12	24	48	96
Threshold [mm]	10	25	52	64.5	90	118

Furthermore, because the threshold value affects the number of data points that are extracted (Pham, Lee 2015), the threshold values proposed by IMD for identifying heavy storms were used (Table 1). The discordancy test was used to identify and remove outliers; this test was also used to identify the appropriate datasets for regionalization. If a vector:

$$u_i = [t^{(i)}, t_3^{(i)}, t_4^{(i)}]^T \quad (1)$$

controls the L-moment ratio for the site  $i$ , then the discordancy measure may be characterized as:

$$D_i = \frac{1}{3} (u_i - \bar{u})^T S^{-1} (u_i - \bar{u}) \quad (2)$$

where  $u_i$  is the vector of L-CV, L-Skewness, and L-Kurtosis,  $S$  is the covariance matrix of  $u_i$ , and  $\bar{u}$  is the mean vector of  $u_i$ .

### 3.2. Homogeneous rainfall region

The algorithm by Hosking and Wallis (1997) has been used to identify homogeneous rainfall regions in various countries, including Korea (Kar et al. 2017), Brazil (Carvalho et al. 2016), and Jakarta (Liu et al. 2015). The first step involves formation of candidate regions using cluster analysis of the site characteristics and testing the homogeneity of these proposed regions using at-site statistics (Castellarin et al. 2008; Malekinezhad, Zare-Garizi 2014). Site characteristics and site statistics are defined as follows (Gaál et al. 2009):

- Site characteristics are either quantities that are determined from the long-term climate of the site, (e.g., the mean yearly precipitation) or quantities that are known even before rainfall measurements are obtained (e.g., location, elevation, and other site physiographic properties).
- Site statistics are the measurements or any results of statistical processing of the rainfall data observed at the site.

#### 3.2.1. Site characteristics

The site characteristics (or variables) were prepared for each rain gauge station. The first three variables (latitude, longitude, and elevation) are geographical characteristics. The next 10 variables represent the long-term precipitation regime; these include the mean annual precipitation, mean monthly precipitation, maximum monthly precipitation,

and mean annual number of wet days (i.e., with daily precipitation of 4 mm or more). The remaining seven variables describe the distance from the coast along different wind directions (0, 15, 30, 45, 60, 75, and 90° from the west, as shown in Figure 1). To reduce the number of variables, a principal component analysis (PCA) technique was applied with minimal loss of information. The PCA method identifies the most critical relationship structures among several variables. As a result, a few linear combinations of the original variables are used to describe the significant part of the overall variance. These optimized variables were used as inputs to the K-means cluster algorithm (MacQueen 1967), which uncovered the inherent structures in the data. The cluster algorithm starts by computing the centroid of each cluster and then calculates the distances between the current data vector and each of these centroids. The current vector is assigned to the cluster with the closest centroid. Because this is a dynamic method, vectors can change clusters after being assigned. This process is repeated until all the vectors have been assigned to a cluster, and the members of every cluster are closer to the centroid of their assigned cluster than to the mean of the other clusters (Genolini et al. 2016; Dullo et al. 2017). There is no specific technique for optimizing the number of clusters; therefore, the following coefficients were used:

- Connectivity (Handl et al. 2005) is the degree to which the observations are kept in the same group as their closest neighbors in the data space. The connectivity value ranges from zero to infinity and should be minimized.
- Dunn Index (Dunn 1973) consolidates the divergence among clusters and their measurements to gauge the most substantial number of clusters. A higher Dunn Index implies better grouping.
- Silhouette width (Rousseeuw 1987) measures the closeness of a data vector to the assigned cluster rather than a different one. The average dissimilarity between points demonstrates the structure of the data and consequently its possible groups (Rao, Srinivas 2008). Silhouette width values close to 1.0 indicate unusual groupings.

Rao and Srinivas (2008) noted that the Dunn Index is very sensitive to outliers; hence, in this study, the silhouette width was used first, followed by the Dunn Index, and finally the connectivity index. The optimal selection also maximized the quality of the clusters obtained.

#### 3.2.2. Site statistics

The L-moments method works as a linear function of probability weighted moments that are defined by the general form:

$$\lambda_r = \frac{1}{r} \sum_{k=0}^{r-1} (-1)^k \binom{r-1}{k} E \{X_{r-k:r}\} \quad (3)$$

where  $\lambda_r$  is the straight capacity of the  $r^{\text{th}}$  L-moment of a distribution  $X$ , and  $r$  is a non-negative integer with values 1-3. Using equation (3), the first four L-moments are composed as follows:

$$\lambda_1 = EX \quad (4)$$

$$\lambda_2 = \frac{1}{2} E(X_{2:2} - X_{1:2}) \quad (5)$$

$$\lambda_3 = \frac{1}{3} E(X_{3:3} - 2X_{2:3} + X_{1:3}) \quad (6)$$

$$\lambda_4 = \frac{1}{4} E(X_{4:4} - 3X_{3:4} + 3X_{2:4} - X_{1:4}) \quad (7)$$

The L-moment ratios are defined as:

$$\tau_2 = \frac{\lambda_2}{\lambda_1}, \tau_3 = \frac{\lambda_3}{\lambda_2}, \tau_4 = \frac{\lambda_4}{\lambda_2} \quad (8)$$

where:  $\tau_2$  is the measure of covariance (scale);  $\tau_3$  is the measure of skewness (with range 0-1);  $\tau_4$  is the measure of kurtosis (peakedness). These ratio estimators and their respective graphical charts are especially significant for identifying the distributional properties of skewed data.

### 3.2.3. Heterogeneity test

A homogeneous region is a set of sites whose probability distributions are approximately identical after rescaling their respective site variables. To project a homogeneous region, a statistical comparison of the site distributions of L-moment samples was performed. Hosking and Wallis (1993) recommended a statistical test of the heterogeneity ( $H$ ) of a proposed homogeneous region. Accordingly, the heterogeneity was computed as:

$$H = \frac{V_{obs} - \mu_v}{\sigma_v} \quad (9)$$

Here,  $\mu_v$  and  $\sigma_v$  are the mean and standard deviation of the simulated data, respectively.  $V_{obs}$  was obtained from the regional data, based on three V Statistics ( $V_1, V_2, V_3$ ) defined as follows:

$$V = \left\{ \frac{\sum_{i=1}^N n_i (\tau_2^i - \tau_2^R)^2}{\sum_{i=1}^N n_i} \right\}^{\frac{1}{2}} \quad (10)$$

The region is sensibly homogeneous if  $H < 1$ , potentially homogeneous if  $1 \leq H < 2$ , and definitely heterogeneous if  $H \geq 2$  (Hosking, Wallis 1993).

### 3.3. Goodness of fit of the regionalisation algorithm

To evaluate the performance of the L-moment approach, we compared it with an SOM regionalisation method (Parchure, Gedam 2018) using two regionalisation efficiency measures, namely, regionalisation efficiency ( $RE$ ) and allocation efficiency ( $AE$ ) (Núñez et al. 2016):

$$RE = \frac{HR}{TR} \times 100$$

$$AE = \frac{SAHR}{TS} \times 100$$

where:  $HR$  – number of homogeneous ( $H1 < 2.0$ ) subregions ( $n$ );  $TR$  – total number of subregions (homogeneous + heterogeneous) ( $n$ );  $SAHR$  – stations allocated in homogeneous subregions ( $n$ );  $TS$  – total number of stations available in the regionalisation process ( $n$ ).

Once the subregions have been delineated, the homogeneity analysis is performed on these subregions using Hosking and Wallis's (1997)  $H1$  heterogeneity measure. The  $H1$  and regionalisation efficiency measures were analysed using the rainfall depths of various durations.

Most of the statistical analyses and graphical illustrations of the results of this study were developed with the statistical program R-3.2.0, Orange Canvas 3.7.1 software, and MS Excel version 2007.

## 4. Results and discussion

This section presents the results of this study.

### 4.1. Mumbai as a single region

Mumbai was inspected as a single homogeneous region. The homogeneity test results, shown in Table 2, indicate that Mumbai could be regarded as a single homogeneous region for precipitation amounts of 1-4 d durations but not for those of less than 1 d duration. This distinction could be due to the occurrence of intense one-day duration storms. As such, these heavy storms are very unlikely to last for one or more consecutive days. This may be the explanation for the homogeneity of the other multiday precipitation amounts. Table 2 also shows another fascinating part of the heterogeneity investigation. The definitely heterogeneous ( $H > 2.0$ ) behaviour occurs once again for the 5-day duration precipitation, perhaps due to changes in climatic parameters.

Table 2. Summary of homogeneity tests for the Mumbai region as a whole

Rainfall time period [h]	H Test		
	H1	H2	H3
0.25	12.7	12.88	9.77
1	12.03	13.35	11.71
6	5.33	0.24	-2.58
12	3.39	-0.82	-2.64
24	1.47	-1.51	-2.93
48	-0.47	-2.32	-2.52
72	-1.43	-2.99	-3.33
96	-1.5	-2.78	-2.77
120	12.88	14.77	12.31

## 4.2. Homogeneous rainfall regions

### 4.2.1. Site characteristics

The PCA method was used to optimize the input variables; this resulted in nine components that captured about 95% of the variance in the total input variables (Fig. 2).

The input variables for the cluster analysis determined by the PCA results are as follows:

- Longitude and Latitude: these variables describe the location of the gauges.
- Five wind direction angles: these angles are in the range 195°-255°, indicative of the southwesterly winds from the Arabian Sea that blow over the study area.
- Two precipitation variables: these are the mean annual precipitation and mean July precipitation (July is the wettest month of the year).

The optimum number of clusters was derived using the K-means cluster technique, the nine principal components, and the three internal indices described in section 3.2.1. Table 3 shows the values obtained

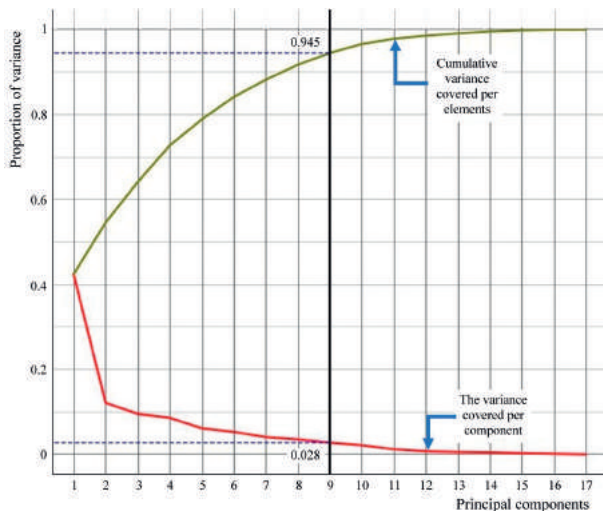


Fig. 2. Nine principal components captured about 95% of the variance in the total variables

Table 3. Results obtained from 2 to 8 cluster stages with K-means clustering method

Internal measures	Connectivity	Dunn	Silhouette
2	21.72	0.17	0.24
3	23.44	0.2	0.25
4	23.75	0.22	0.26
5	40.88	0.2	0.17
6	41.15	0.12	0.22
7	41.48	0.14	0.23
8	45.67	0.15	0.22

from the cluster stages 2-8 with the K-means cluster technique. Four candidate precipitation regions were identified. The homogeneity of each region was inspected for all of the selected durations. Figure 4 (left) shows the location and composition of each region (cluster). A compact overview of the most relevant variables of the regions is shown in Table 5. Another intriguing insight from Table 4 is that the dominant part of the region did not pass the homogeneity test. Figure 4 also shows that a few sites are scattered in the geographical space. These results were the bases for our conclusion that a combination of the site characteristics and site statistics must be used for homogeneous regional analysis. The specific outcomes of this analysis are as follows:

- Region SC#1 (region #1 for site characteristics) consists of 16 stations located in the area near the Arabian Sea, mainly in the southwestern part of Mumbai. Table 4 indicates that this region is heterogeneous for precipitation durations up to 6 h, which might be due to the effect of air masses from the territory of the Arabian Sea. Also, the detailed analysis of the data highlighted the extraordinary amount of rainfall measured at Worli (57.4-89.14 mm) and Wadala (55.12 mm) for 15 min events.
- Region SC#2 is the largest among the regions studied based on site characteristics. This region, which comprises 18 sites covering the southwestern part and extending further inland, represents low land, urban areas with high-rise buildings, and parts of the windward side of the Sanjay Gandhi National Park. The rain gauge cluster for this region consists of a few sites having minimum and maximum mean annual precipitation and mean July precipitation (Table 5). The region was identified as homogeneous according to the *H* test except for 15-min precipitation amounts.
- Region SC#3 is located in the eastern part of Mumbai and consists of five sites covering the leeward side of the Sanjay Gandhi National Park. The sites are fairly scattered at various altitudes; however, the mean

elevation is the highest among the four regions (Table 5). The cluster analysis isolated these sites principally because they have the highest station altitudes, which resulted in the heterogeneity of the region for rainfall durations up to 3 d (Table 4). The detailed analysis of the data also indicates significant variation in rainfall amount, which may be due to the funnelling action by the Chembur and Sanjay Gandhi National Park hills.

- Region SC#4 consists of 8 sites located predominantly in the western part of the city between the Arabian Sea and windward side of the Sanjay Gandhi National Park. This region was identified as homogeneous according to the  $H$  test (Table 4).

The L-moments graphs shown in Figure 3 indicate that three distinct groups of sites comprise the region SC#2 (top graph). These sites are located in two different geographical regions. The first group is made up of 4 sites from the southeastern parts (the lowlands) of Region SS#5: Kurla, Rawali camp, Deonar, and Octroi Mankhurd. The second group consists of 4 stations located near the foot of the Sanjay Gandhi National Park hills on the windward side (Region SS#6). The third group includes 10 sites from the lowland and urban parts of Region SS#2. The L-moments diagram (Fig. 3) of region SC#3 suggested moving the Vikhroli station to Region SS#5.

Therefore, based on the L-moments diagram, a further subdivision of Regions SC#2 and SC#3 was performed using site statistics. This analysis excluded the unusually wet sites (Worli and Wadala) from Region SC#1. The results indicate that the region becomes homogeneous for the one-hour precipitation amount, while the  $H$  value decreases from 3.87 to 3.18 for the 15-min rainfall amount.

#### 4.2.2. Site statistics

The final precipitation regionalization was created using the site statistics and the results of the site characteristics analysis as inputs. The primary intent was to reflect the characteristics of the individual geomorphological units and consider an objective measure of similarity within the regions. Six regions were obtained from combining the best features of the two pooling strategies. The composition and geographical locations of these regions are shown in Figure 4 (right), and a synopsis of their physical and climatological characteristics is given in Table 5. In addition, Table 4 shows the heterogeneity measures for the selected rainfall durations. The specific outcomes of this analysis are as follows:

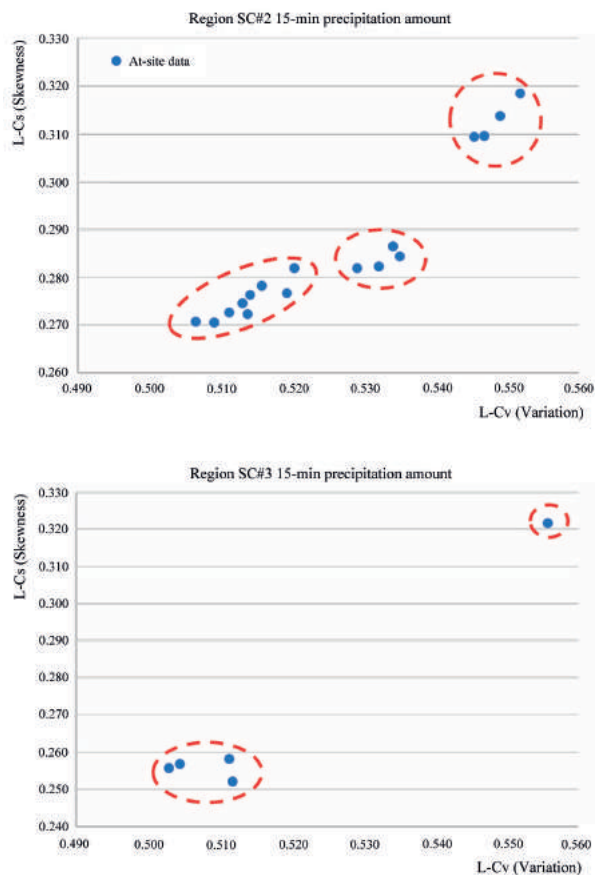


Fig. 3. L-moments graph for Regions SC#2 and SC#3 for 15 min precipitation duration

- Region SS#1 consists of 14 stations in the area near the Arabian Sea, mainly covering the southwestern area of Mumbai. This region is identical to Region SC#1, except for the two stations (Worli and Wadala) that recorded extraordinary rainfall events. The  $H$  test results for rainfall durations of 1 h and above suggested that this region is homogeneous.
- Region SS#2 comprises 10 sites, the majority of which are also in Region SC#2; the stations that are located near the mountain area and leeward side of Chembur Hill are excluded from Region SC#2. This region was identified as homogeneous except for the 15-min precipitation.
- Region SS#3 comprises four sites and stretches through the leeward side of the Sanjay Gandhi National Park hills to the east of Mumbai. This region was identified as homogeneous for most of the durations probably due to the shadowing effect of the hills, which reduces the rainfall.
- Region SS#4 is similar to Region SC#4 because of its high level of homogeneity.
- Region SS#5 consists of five sites located between the Sanjay Gandhi National Park and Chembur hills. These stations are grouped together due to the funnelling action of the hills. The  $H$  test results indicated

Table 4. Summary of homogeneity ( $H$ ) test values of sites identified based on site statistics and site characteristics (in parentheses) for each region and rainfall duration

Rainfall duration [h]	$H$ Test	Region SS#1 (SC#1)	Region SS#2 (SC#2)	Region SS#3 (SC #3)	Region SS#4 (SC#4)	Region SS#5	Region SS#6
0.25	$H_1$	3.65 (3.87)	2.64 (5.59)	5.1 (6.27)	-0.72 (-0.72)	2.08	5.65
1	$H_1$	0.94 (3.88)	-0.01 (0.8)	1.42 (1.19)	-0.26 (-0.26)	1.22	1.51
6	$H_1$	0.25 (0.15)	-1.19 (-1.71)	0.79 (1.24)	-1.16 (-1.16)	-0.53	-0.85
12	$H_1$	-1.06 (-0.89)	-1.54 (-1.98)	1.29 (1.81)	-0.35 (-0.35)	-1.26	-0.68
24	$H_1$	-1.95 (-1.76)	-1.45 (-2.28)	0.9 (1.86)	0.03 (0.03)	-1.6	-0.8
48	$H_1$	-3.12 (-2.97)	-1.52 (-2.04)	1.1 (1.42)	-0.63 (-0.63)	-1.17	-0.57
72	$H_1$	-2.58 (-2.64)	-0.98 (-2)	0.26 (0.84)	-0.66 (-0.66)	-0.85	-1
96	$H_1$	-2.8 (-2.62)	-1.63 (-2.04)	0.93 (0.93)	-0.33 (-0.33)	-0.66	-0.5
120	$H_1$	-1.03 (-1.12)	-0.63 (-0.63)	-0.69 (1.25)	0.48 (0.48)	-0.13	0.37

Table 5. Summary of relevant characteristics of sites identified based on site statistics and site characteristics (in parentheses) for each region

Relevant characteristics	Region SS#1 (SC#1)	Region SS#2 (SC#2)	Region SS#3 (SC#3)	Region SS#4 (SC#4)	Region SS#5	Region SS#6
Number of stations	14* (16)	10 (18)	4 (5)	8 (8)	5	4
Range of $H$ [m]	11.66-1.28 (11.66-31.28)	12.31-37.2 (8.84-50.09)	10.71-85.68 (10.71-85.68)	13.86-24.99 (13.86-24.99)	8.84-29.61	28.26-50.09
Average of $H$ [m]	21.77 (21.88)	22.52 (23.96)	40.71 (39.12)	20.63 (21.6)	16.93	37.3
Range of Mean Annual Precipitation [mm]	1791.68-2228.02 (1791.68-2429.21)	1601.8-2393.33 (1601.8-2598.32)	2137.4-2594.28 (1940.39-2594.28)	1793.35-2616.77 (1793.35-2616.77)	2218.32-2598.32	1905.05-2227.82
Median of Mean Annual Precipitation [mm]	1997.49 (2039.57)	2181.02 (2219.2)	2435.06 (2099.13)	2132.66 (2227.76)	2429.21	2102.46
Range of Mean July Precipitation [mm]	651.7-930.89 (651.7-947.86)	637.37-954.51 (637.37-1139.48)	824.11-1139.48 (675.73-1090.6)	675.73-1090.6 (765.48-896.75)	746.51-1034.15	725.77-922.36
Median of Mean July Precipitation [mm]	778.83 (797.7)	845.58 (866.42)	949.15 (853.88)	803.16 (804.32)	917.98	853.73

that this region is homogeneous for rainfall durations of 1 h and above except for the 15-min rainfall duration.

- Region SS#6 includes four sites on the windward side of Sanjay Gandhi National Park and covers the area west of Mumbai near the foot of the hills.

These results confirmed the effect of the complex topography of the study area on the spatial variation of rainfall.

The topography includes the flatland near the Arabian Sea, the urban areas with high-rise buildings, and the mountains and hilly areas (particularly the Sanjay Gandhi National Park). In addition, the intense precipitation recorded over Region SS#2, which is located in the urban pocket, supports the findings of Paul et al. (2018) that associates extreme precipitation with urbanization.

4.2.3. Heterogeneity test

The six regions that were identified by the site statistics were also identified as potentially homogeneous regions according to the *H* test for rainfall durations of 1 h and above (Table 4). However, the spatial variation in the 15-min rainfall data resulted in the heterogeneity of the regions. The rapid reduction in spatial variation as the rainfall duration increases explains why the regions were identified as homogeneous for rainfall durations of 1 h and above. Because the *H* test is a somewhat subjective process, unusual sites may be removed and the sites regrouped to improve the homogeneity of the identified regions. However, further removal and regrouping of the sites was not performed for the following reasons:

- To avoid loss of valuable information on precipitation in the analysis of dissimilar sites.
- To avoid the unnecessary burden of evaluating extraordinary events, especially where removal of such sites produces minimal change in the *H* Value.

4.3. Goodness of fit of the regionalisation algorithm

Figure 5a shows the box-whisker plot of the *H1* heterogeneity values of the two regionalisation methods (L-moment and SOM) for the rainfall with 0.25 h duration. The SOM method showed the lowest *H1* dispersion; all of its values were below the critical value

(*Hc* = 2). These results highlighted that the direct application of cluster analysis by itself does not guarantee an automatic delimitation of homogeneous regions, which supports the findings of Hosking and Wallis (1997), Ilorime and Griffis (2013) and Wazneh et al. (2015).

Similarly, Figure 5b shows the efficiency values (*RE* and *AE*). SOM showed higher *RE* (*AE*) efficiency (100%) as compared to the L-moment approach (20%). This method was based on the predefined region sizes and a function of MAP, which depicts consistency in the strong relationships between precipitation variability, L-moment-ratios, and MAP (Wallis et al. 2007; Núñez et al. 2011).

These results support the findings of Clarke (2010) and Núñez et al. (2016), highlighting the limitations of the L-moment approach: (a) Meteorological networks cannot fully represent the spatial continuum of the large-scale variables and attributes; (b) Cluster analysis has been used in general with the expectation of identifying homogeneous regions, but in physical terms, it remains to be established why such regions should be considered homogeneous. Hence, a subjective judgement in the regionalisation process is warranted, owing to a possibility of dissociation between the expression of Mother Nature (to paraphrase J.R. Wallis) and how the monitoring station networks and the associated statistical analysis procedures capture this expression (Hosking, Wallis 1997; Wazneh et al. 2015).

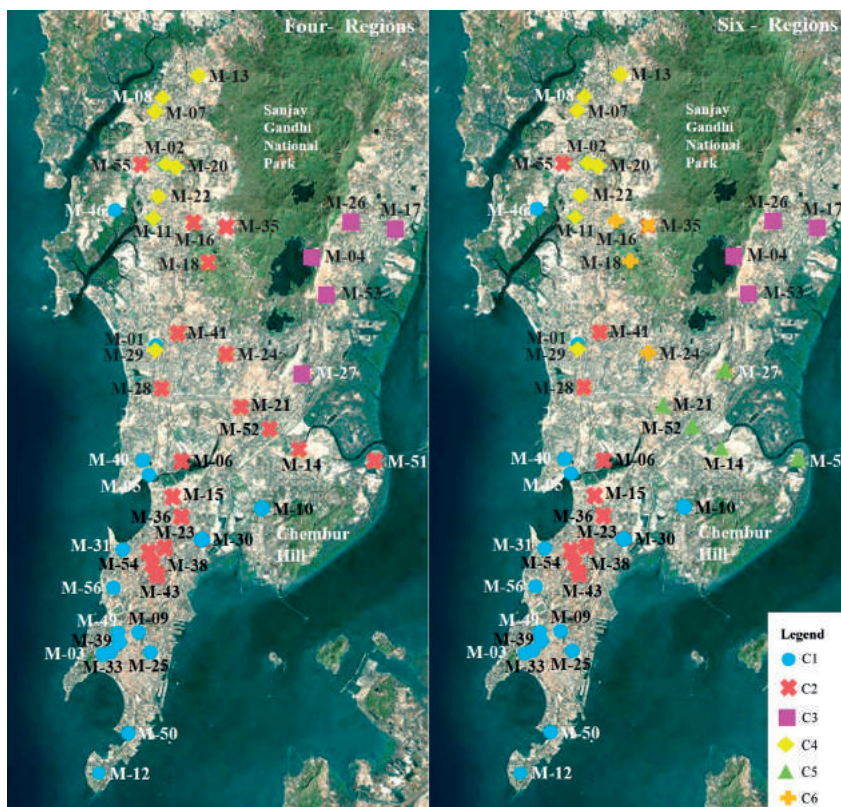


Fig. 4. Composition and location of regions using site characteristics (left) and refinement using site statistics (right)

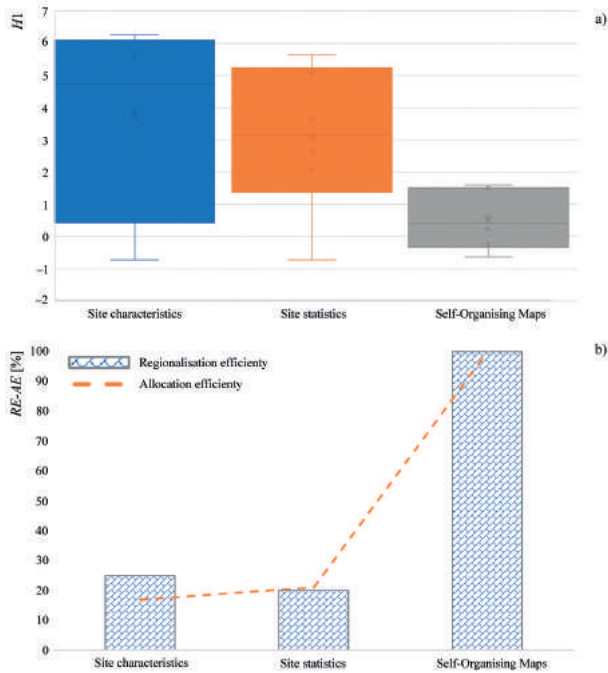


Fig. 5. Representations of efficiency evaluation: (a)  $H1$  boxplots for various regionalisation methods; (b) regionalisation and allocation efficiency bar plots for various regionalisation methods

## 5. Conclusions

The main objective of this research was to identify the homogeneous rainfall regions of Mumbai based on a combined analysis of site characteristics and site statistics. The study also focused on the climatological conditions of the city using rainfall amounts of various durations (0.25, 1, 6, 12, 24, 48, 72, 96, and 120 h). The main results and conclusions are as follows:

1. Mumbai can be considered as a single homogeneous region for precipitation events of 1-4 d durations but not for those of less than one day duration. This could be due to the occurrence of intense storms of one day or shorter duration.
2. To obtain the homogeneous regions, it is advisable to evaluate the variance in the homogeneous sub-regions obtained via L-moment regarding changes in the temporal scale of the response variable.
3. The combination of two techniques, namely cluster analysis (objective) and site statistical pooling (subjective) for identification of homogeneous region support the findings of Clarke (2010) and Núñez et al. (2016) and highlighted the limitations of these approaches.
4. The regions based on the site statistics approach were identified as potentially homogeneous according to the  $H$  Test for rainfall durations of 1 h and above. However, spatial variation in the 15-min rainfall data resulted in the heterogeneity of the regions. The rapid reduction in spatial variation as the rainfall duration

increases explains why the regions were identified as homogeneous for rainfall durations of 1 h and above. Because the  $H$  Test is a somewhat subjective process, unusual sites may be removed, and the sites regrouped to improve the homogeneity of the identified regions. However, further removal and regrouping of the sites was not performed. These results support the SOM approach adopted by Parchure and Gedam (2018) to cluster rain gauges in groups (regions).

5. The six clusters of rainfall gauges obtained confirm that the spatial variation of rainfall is a result of the complex topography of Mumbai, which includes the flatland near the Arabian Sea, the urban areas with high-rise buildings, and the mountainous and hilly areas (particularly the Sanjay Gandhi National Park located in the northern part).

The limitations of the study are the following:

1. This study only identified homogeneous rainfall regions. A potential topic of future research would be the computation of appropriate probability distribution functions and design rainfall quantities along with their return periods.
2. Further research is needed to test the hypothesis of clusters using other climatological data (such as temperature, wind speed, and wind direction) that are measured by MCGM at the 47 stations and radar data obtained by the IMD.
3. The discussions of this study have alluded to possible influences from the complex orography and coastal proximity of Mumbai. The significance of these influences needs to be confirmed through future studies of multiple cases across different cities.

## Acknowledgments

The authors thank the MCGM for providing rain gauge data and the Indian Metrological Department, Mumbai, for their comments and suggestions, which significantly contributed to improving the clarity of the paper.

## Bibliography

- Ahuja S., Dhanya C.T., 2012, Regionalization of rainfall using RCDA cluster ensemble algorithm in India, *Journal of Software Engineering and Applications*, 5 (8), 568-573, DOI: 10.4236/jsea.2012.58065
- Bharath R., Srinivas V.V., 2015, Regionalization of extreme rainfall in India, *International Journal of Climatology*, 35 (6), 1142-1156, DOI: 10.1002/joc.4044
- Carvalho J.R.P. de, Nakai A.M., Monteiro J.E.B.A., 2016, Spatio-temporal modeling of data imputation for daily rainfall series

- in homogeneous zones, *Revista Brasileira de Meteorologia*, 31 (2), 196-201, DOI: 10.1590/0102-778631220150025
- Castellarin A., Burn D.H., Brath A., 2008, Homogeneity testing: how homogeneous do heterogeneous cross-correlated regions seem?, *Journal of Hydrology*, 360 (1-4), 67-76, DOI: 10.1016/j.jhydrol.2008.07.014
- Clarke R., 2010, On the (mis)use of statistical methods in hydroclimatological research, *Hydrological Sciences Journal*, 55 (2), 139-144, DOI: 10.1080/02626661003616819
- Dullo T.T., Kalyanapu A.J., Teegavarapu S.V., 2017, Evaluation of changing characteristics of temporal rainfall distribution within 24-hour duration storms and their influences on peak discharges: case study of Asheville, North Carolina, *Journal of Hydrologic Engineering*, 22 (11), DOI: 10.1061/(ASCE)HE.1943-5584.0001575
- Dunn J.C., 1973, A fuzzy relative of the ISODATA process and its use in detecting compact well-separated clusters, *Journal of Cybernetics*, 3 (3), 32-57, DOI: 10.1080/01969727308546046
- Estévez J., Gavilán P., García-Marín A.P., Zardi D., 2015, Detection of spurious precipitation signals from automatic weather stations in irrigated areas, *International Journal of Climatology*, 35 (7), 1556-1568, DOI: 10.1002/joc.4076
- Gaál L., Kyselý J., Szolgay J., 2008, Region-of-influence approach to a frequency analysis of heavy precipitation in Slovakia, *Hydrology and Earth System Sciences*, 12 (3), 825-839, DOI: 10.5194/hess-12-825-2008
- Gaál L., Szolgay J., Lapin M., Faško P., 2009, Hybrid approach to the delineation of homogeneous regions for regional precipitation frequency analysis, *Journal of Hydrology and Hydromechanics*, 57 (4), 226-249, DOI: 10.2478/v10098-009-0021-1
- Genolini C., Ecochard R., Benghezal M., Driss T., Andrieu S., Subtil F., 2016, kmlShape: An efficient method to cluster Longitudinal data (time-series) according to their shapes, *PLOS One*, 11 (6), DOI: 10.1371/journal.pone.0150738
- Hailegeorgis T.T., Alfredsen K., 2017, Regional flood frequency analysis and prediction in ungauged basins including estimation of major uncertainties for mid-Norway, *Journal of Hydrology: Regional Studies*, 9, 104-126, DOI: 10.1016/j.ejrh.2016.11.004
- Halbert K., Nguyen C.C., Payrastre O., Gaume E., 2016, Reducing uncertainty in flood frequency analyses: a comparison of local and regional approaches involving information on extreme historical floods, *Journal of Hydrology*, 541 (Part A), 90-98, DOI: 10.1016/j.jhydrol.2016.01.017
- Hallegatte S., 2010, Flood risks, climate change impacts and adaptation benefits in Mumbai. An initial assessment of socioeconomic consequences of present and climate change induced flood risks and of possible adaptation options, *OECD Environment Working, Papers*, 27, DOI: 10.1787/5km4hv6wb434-en
- Handl J., Knowles J., Kell D.B., 2005, Computational cluster validation in post-genomic data analysis, *Bioinformatics*, 21 (15), 3201-3012, DOI: 10.1093/bioinformatics/bti517
- Hessburg P.F., Kuhlman E.E., Swetnam T.W., 2005, Examining the recent climate through the lens of ecology: inferences from temporal pattern analysis, *Ecological Applications*, 15 (2), 440-457
- Hosking J.R.M., Wallis J.R., 1993, Some statistic useful in region frequency analysis, *Water Resources Research*, 29 (2), 271-281, DOI: 10.1029/92WR01980
- Hosking J.R.M., Wallis J.R., 1997, *Regional frequency analysis: an approach based on L-moments*, Cambridge University Press, Cambridge, UK, 224 pp.
- Ilorme F., Griffis V.W., 2013, A novel procedure for delineation of hydrologically homogeneous regions and the classification of ungauged sites for design flood estimation, *Journal of Hydrology*, 492, 151-162, DOI: 10.1016/j.jhydrol.2013.03.045
- Kakade S.B., Kulkarni A., 2017, Seasonal prediction of summer monsoon rainfall over cluster regions of India, *Journal of Earth System Science*, 126 (34), DOI: 10.1007/s12040-017-0811-5
- Kar K.K., Yang S.-K., Lee J.-H., Khadim F.K., 2017, Regional frequency analysis for consecutive hour rainfall using L-moments approach in Jeju Island, Korea, *Geoenvironmental Disasters*, 4 (18), DOI: 10.1186/s40677-017-0082-0
- Khan S.A., Hussain I., Hussain T., Faisal M., Muhammad Y.S., Shoukry A.M., 2017, Regional frequency analysis of extremes precipitation using L-moments and partial L-Moments, *Advances in Meteorology*, DOI: 10.1155/2017/6954902
- Liu J., Doan C.D., Liang S.-Y., Sanders R., Dao A.T., Fewtrell T., 2015, Regional frequency analysis of extreme rainfall events in Jakarta, *Natural Hazards*, 75 (2), 1075-1104, DOI: 10.1007/s11069-014-1363-5
- Lokanadham B., Gupta K., Nikam V., 2012, Characterization of spatial and temporal distribution of monsoon rainfall over Mumbai, *ISH Journal of Hydraulic Engineering*, 15 (2), 69-80, DOI: 10.1080/09715010.2009.10514941
- MacQueen J.B., 1967, Some methods for classification and analysis of multivariate observations, [in:] *Proceedings of the Fifth Berkeley Symposium on Mathematical Statistics and Probability. Volume 1: Statistics*, L.M. Le Cam, J. Neyman (eds.), University of California Press, Berkeley, 281-297
- Malekinezhad H., Zare-Garizi A., 2014, Regional frequency analysis of daily rainfall extremes using L-moments approach, *Atmósfera*, 27 (4), 411-427, DOI: 10.1016/S0187-6236(14)70039-6

- Nair A., Mohanty U.C., Acharya N., 2013, Monthly prediction of rainfall over India and its homogeneous zones during monsoon season: a supervised principal component regression approach on general circulation model products, *Theoretical and Applied Climatology*, 111 (1-2), 327-339, DOI: 10.1007/s00704-012-0660-8
- Ngongondo C.S., Xu C.Y., Tallaksen L.M., Alemaw B., Chirwa T., 2011, Regional frequency analysis of rainfall extremes in Southern Malawi using the index rainfall and L-moments approaches, *Stochastic Environmental Research and Risk Assessment*, 25 (7), 939-955, DOI: 10.1007/s00477-011-0480-x
- Núñez J.H., Hallack- Alegría M., Cadena M., 2016, Resolving regional frequency analysis of precipitation at large and complex scales using a bottom-up approach: The Latin America and the Caribbean Drought Atlas, *Journal of Hydrology*, 538, 515-538, DOI: 10.1016/j.jhydrol.2016.04.025
- Núñez J.H., Verbist K., Wallis J.R., Schaefer M.G., Morales L., Cornelis W.M., 2011, Regional frequency analysis for mapping drought events in north-central Chile, *Journal of Hydrology*, 405 (3-4), 352-366, DOI: 10.1016/j.jhydrol.2011.05.035
- Parchure A.S., Gedam S.K., 2018, Precipitation regionalization using Self-Organizing Maps for Mumbai City, India, *Journal of Water Resource and Protection*, 10 (9), 939-956, DOI: 10.4236/jwarp.2018.109055
- Paul S., Ghosh S., Mathew M., Devanand A., Karmakar S., Niyogi D., 2018, Increased spatial variability and intensification of extreme monsoon rainfall due to urbanization, *Scientific Reports*, 8 (3918), DOI: 10.1038/s41598-018-22322-9
- Pham V.H., Lee B.R., 2015, An image segmentation approach for fruit defect detection using k-means clustering and graph-based algorithm, *Vietnam Journal of Computer Science*, 2 (1), 25-33, DOI: 10.1007/s40595-014-0028-3
- Rahman M., Sarkar S., Najafi M.R., Rai R.K., 2013, Regional extreme rainfall mapping for Bangladesh using L-moment technique, *Journal of Hydrologic Engineering*, 18 (5), DOI: 10.1061/(ASCE)HE.1943-5584.0000663
- Rao A.R., Srinivas V.V., 2008, Regionalization of watersheds. An approach based on cluster analysis, *Water Science and Technology Library Series*, 58, Springer Netherlands, 245 pp.
- Requena A.I., Chebana F., Mediero L., 2016, A complete procedure for multivariate index-flood model application, *Journal of Hydrology*, 535, 559-580, DOI: 10.1016/j.jhydrol.2016.02.004
- Rousseeuw P.J., 1987, Silhouettes: a graphical aid to the interpretation and validation of cluster analysis, *Journal of Computational and Applied Mathematics*, 20, 53-65, DOI: 10.1016/0377-0427(87)90125-7
- Saha M., Mitra P., Nanjundiah R.S., 2017, Deep learning for predicting the monsoon over the homogeneous region of India, *Journal of Earth System Science*, 126 (54), DOI: 10.1007/s12040-017-0838-7
- Santos E.B., Lucio P.S., Silva C.M.S., 2015, Precipitation regionalization of the Brazilian Amazon, *Atmospheric Science Letters*, 16 (3), 185-192, DOI: 10.1002/asl2.535
- Sen S., Vittal H., Singh T., Singh J., Karmakar S., 2013, At-site design rainfall estimation with a diagnostic check for nonstationary: an application to Mumbai rainfall datasets, [in:] *Proceedings of HYDRO 2013 INTERNATIONAL*, 4-6 December 2013, Madras, India, 14 pp.
- Sherly M.A., Karmakar S., Chan T., Rau C., 2015, Design rainfall framework using multivariate parametric-nonparametric Approach, *Journal of Hydrologic Engineering*, 21 (1), DOI: 10.1061/(ASCE)HE.1943-5584.0001256
- Singh J., Sekharan S., Karmakar S., Ghosh S., Zope P.E., Eldho T.I., 2017, Spatio-temporal analysis of sub-hourly rainfall over Mumbai, India: is statistical forecasting futile?, *Journal of Earth System Science*, 126 (38), DOI: 10.1007/s12040-017-0817-z
- Sinha P., Mohanty U.C., Kar S.C., Dash S.K., Robertson A.W., Tippett M.K., 2013, Seasonal prediction of the Indian summer monsoon rainfall using canonical correlation analysis of the NCMRWF global model products, *International Journal of Climatology*, 33 (7), 1601-1614, DOI: 10.1002/joc.3536
- Smithers J.C., Schulze R.E., 2001, A methodology for the estimation of short duration design storms in South Africa using a regional approach based on L-moments, *Journal of Hydrology*, 241 (1-2), 42-52, DOI: 10.1016/S0022-1694(00)00374-7
- Sun X., Lall U., Merz B., Nguyen V.D., 2015, Hierarchical Bayesian clustering for nonstationary flood frequency analysis: application to trends of annual maximum flow in Germany, *Water Resources Research*, 51 (8), 6586-6601, DOI: 10.1002/2015WR017117
- Wallis J.R., Schaefer M.G., Barker B.L., Taylor G.H., 2007, Regional precipitation-frequency analysis and spatial mapping for 24-hour and 2-hour durations for Washington States, *Hydrology and Earth System Sciences*, 11 (1), 415-442, DOI: 10.5194/hess-11-415-2007
- Wazneh H., Chebana F., Ouarda T.B.M.J., 2015, Delineation of homogeneous region for regional frequency analysis using statistical depth function, *Journal of Hydrology*, 521, 232-244, DOI: 10.1016/j.jhydrol.2014.11.068



## **After COP24 Conference in Katowice – the role of the Institute of Meteorology and Water Management – National Research Institute in connection of hydrological and meteorological measurements and observations with climate change adaptation actions**

During the night of the 14<sup>th</sup> December 2018, the difficult but extremely important 24<sup>th</sup> Conference of the Parties to the United Nations Framework Convention on Climate Change (COP 24) came to an end. The aim of the UN climate summit in Katowice was to develop a Rulebook, i.e. a “road map”, for the implementation of the Paris Agreement of 2015, which aimed at limiting the global rise in temperature.

The main objective of the Paris Agreement is to strengthen the global response to the threat of climate change by maintaining a global temperature rise in this century much less than 2°C above pre-industrial levels, and to continue efforts to limit the temperature rise to 1.5°C. To achieve these goals, appropriate mobilization and funding, a new technological framework and strengthened capacity building must be established. This acts to support the activities of developing and vulnerable countries, in accordance with their own national goals. The agreement also provides for an improved transparency framework for the actions taken and the provided support.

In order for the Paris Agreement to become fully operational, a work program for the development of principles, procedures and guidelines for a wide range of issues was launched in Paris. In 2016, the Parties began to cooperate with each other within subsidiary bodies (APA – Ad Hoc Working Group on the Paris Agreement, SBSTA – Subsidiary Body for Scientific and Technological Advice and SBI – Subsidiary Body for Implementation) and in various bodies. The COP, the official conference of the Parties of the Paris Agreement (CMA), took place for the first time in 2016 in connection with the COP 22 in Marrakech and adopted the first two decisions. One of them - the work program, in accordance with the assumption, was completed in 2018 during COP 24 in Katowice, and the second one which aimed at developing a mechanism for the exchange of experiences in the field of adaptation.

One of the fundamental elements of the Paris Agreement is the group of activities undertaken in the area of adaptation. The implementation of these activities at the national level would not be possible without meteorological and hydrological monitoring carried out by the Institute of Meteorology and Water Management – National Research Institute (IMGW-PIB), under the Water Law Act, as a national hydrological and meteorological survey.

The lack of a common position of experts emphasizes the importance and necessity of conducting regular analysis of the state of the environment, based on a unified methodology. Conducting measurements and observations by the IMGW-PIB covers all physical processes taking place in the atmosphere and hydrosphere. In particular, these processes are important in planning activities that slow down the processes of climate change, for the adaptation to existing changes. The methodology used for meteorological and hydrological analysis is reflected in the international schemes that create an integrated system of data collection, transmission and processing.

Coherent systems and methods for conducting measurements and observations, as well as independent analysis conducted in many countries, allow for the creation of scenarios and models of climate change, the determination of trends and reveal the need to immediately implement measures of the Paris Agreement. As a result of the work of scientists in the field of climate change, on the basis of long-term measurements and observation sequences, from Member countries of the World Meteorological Organization (WMO), a Special Report on the impact of climate change on 1.5°C (SR15) was adopted. It states that global warming is likely to increase to 1.5°C above pre-industrial levels between 2030 and 2052, if no action is undertaken and the insulation will continue to grow at the currently observed rate. SR15 summarizes the impact of 1.5°C warming (equivalent to 2.7°F) on the functioning of the planet, and outlines the necessary steps to limit global warming.

A positive evaluation of the system for monitoring climate change and its effectiveness will be possible only when it will be possible to plan the appropriate adaptation, elimination or reduction of risks by all countries. To carry out such an assessment, it is necessary to obtain historical, current and forecasted hydrological and meteorological information on the changing environmental conditions. This is provided by the national survey, which is cooperating with the crisis management sector in the country.

Currently, the IMGW-PIB continuously provides government authorities, the society and the national economy with up-to-date information within three main systems: the measurement and observation system (approximately 1750 hydrological and meteorological measurement stations); the data transfer system; and the data processing, forecasting and warning system.

IMGW-PIB performs regular measurements carried out in accordance with the WMO guidelines throughout Poland, based on the network of hydrological and meteorological measurement stations. These measurements contribute to the development of methods of warning against dangerous phenomena, and also allows for the development of science in the area of unprecedented or unrecognized processes and phenomena.

The implementation of the Paris Agreement and the Katowice Climate Package in Poland would not be possible without the proper mobilization and allocation of key resources in the decision-making process. In the case of extreme phenomena, which have demonstrated a significant increase in recent, the hydrological and meteorological protection system play the key role in the interaction with the crisis management system. Experiences with meteorological and hydrological hazards that have hit Poland in the 21<sup>st</sup> century have demonstrated the need to strengthen activities in the area of adaptation, as well as the possibilities of their detection in order to effectively use information by entities responsible for the security of the society.

Measurement data collected, processed and made available by IMGW-PIB significantly improve the ability of the early identification and assessment of potential risks through the usage of modern tools, thus developing new solutions for the detection of extreme weather phenomena.

Correct and reliably performed tasks of the national hydrological and meteorological survey provide public administration bodies, as well as the whole society, with up-to-date data on the state of the atmosphere and hydrosphere, forecasts and warnings in both daily and threat situations.

Conducting constant, reliable, unified monitoring using the hydrological and meteorological survey and services is one of the basic tools that provide data and information on the environmental impact of forecasted climate change for Poland. This leads to the planning of activities that minimize the negative effects of climate change and paves the way to the full implementation of the Paris Agreement.

Marta Barszczewska, Ksawery Skąpski

*Institute of Meteorology and Water Management – National Research Institute*

## Bibliography

- Dz.U. 2005 Nr 187, poz. 1568, Ordinance of the Council of Ministers of September 13<sup>th</sup>, 2010 on granting the Institute of Meteorology and Water Management in Warsaw the status of a national research institute, (in Polish), ISAP, Sejm RP
- Dz.U. 2008 Nr 225, poz. 1501, Ordinance of the Minister of the Environment of November 6<sup>th</sup>, 2008 on standard procedures for collecting and processing information by the national hydrological and meteorological survey and national hydrogeological survey, (in Polish), ISAP, Sejm RP
- Hoegh-Guldberg O., Jacob D., Taylor M., Bindi M., Brown S., Camilloni I., Diedhiou A., Djalante R., Ebi K.L., Engelbrecht F., Guiot J., Hijioka Y., Mehrotra S., Payne A., Seneviratne S.I., Thomas A., Warren R., Zhou G., 2018, Impacts of 1.5°C global warming on natural and human systems, [in:] Global warming of 1.5°C. An IPCC Special Report on the impacts of global warming of 1.5°C above pre-industrial levels and related global greenhouse gas emission pathways, in the context of strengthening the global response to the threat of climate change, sustainable development, and efforts to eradicate poverty, V. Masson-Delmotte, P. Zhai, H.-O. Pörtner, D. Roberts, J. Skea, P.R. Shukla, A. Pirani, W. Moufouma-Okia, C. Péan, R. Pidcock, S. Connors, J.B.R. Matthews, Y. Chen, X. Zhou, M.I. Gomis, E. Lonnoy, T. Maycock, M. Tignor, and T. Waterfield (eds.), Intergovernmental Panel on Climate Change, 175-311, in press
- IPCC, 2007, Climate change 2007: Impacts, adaptation and vulnerability. Contribution of Working Group II to the Fourth Assessment Report of the Intergovernmental Panel on Climate Change, M.L. Parry, O.F. Canziani, J.P. Palutikof, P.J. van der Linden, C.E. Hanson (eds.), Cambridge University Press, Cambridge, UK, 976 pp.
- Kozłowska-Szczęśna T., Limanówka D., Niedźwiedz T., Ustrnul Z., Paczos S., 1993, Thermal characteristic of Poland, (in Polish), Zeszyty Instytutu Geografii i Przestrzennego zagospodarowania PAN, 18, 81 pp.
- Kurowska-Łazarz R., Szulc W., Woźniak B., Piotrowska M., Drożdżyńska J., 2015, Vademecum Meteorological measurement and observations, IMGW-PIB, Warsaw, 69 pp.
- Szumiejko F., Wdowikowski M., 2016, IMGW-PIB Monitor as a source of information on dangerous meteorological and hydrological phenomena for crisis management needs, Obronność. Zeszyty Naukowe Wydziału Zarządzania i Dowodzenia Akademii Sztuki Wojennej, 2 (18), 209-226
- UNFCCC, 2016, Report of the Conference of the Parties on its twenty-first session, held in Paris from 30 November to 13 December 2015. Addendum. Part two: Action taken by the Conference of the Parties at its twenty-first session, 1/CP.21 Adoption of the Paris Agreement, FCCC/CP/2015/10/Add.1, 21-36